Dissertation zur Erlangung des Doktorgrades

der Fakultät für Chemie und Pharmazie

der Ludwig-Maximilians-Universität München

Models for angiogenesis on micro-structured surfaces

- A novel view on endothelial cell biology -

Simon Ludwig Schuster

aus Leimen

2016

Erklärung

Diese Dissertation wurde im Sinne von § 7 der Promotionsordnung vom 28. November 2011 von Herrn Prof. Dr. Stefan Zahler betreut.

Eidesstattliche Versicherung

Diese Dissertation wurde eigenständig und ohne unerlaubte Hilfe erarbeitet.

München, den

_____

Simon Ludwig Schuster

Dissertation eingereicht am: 12.01.2016

1. Gutachter: Prof. Dr. Stefan Zahler

2. Gutachter: Prof. Dr. Angelika Vollmar

Mündliche Prüfung am: 15.02.2016

für Jonas

Content

1. Abstract

Endothelial cell (EC) migration is an essential process in angiogenesis as ECs sprout from preexisting vessels, following chemotactic gradients. However, most of the data obtained about EC migration has been acquired in artificial two dimensional (2D) cell culture environments. Recent reports showed that migration in fibrillary environments can be mimicked by spatial confinement, achieved by micro patterning techniques (Doyle et al. 2009). In the first part of this work it was investigated whether a model system based on linearly structured surfaces allows to draw conclusions about the migration of ECs in fibrillary 3D collagen matrices. In order to estimate the cellular behavior of ECs on linearly structured surfaces, a comprehensive cell biological analysis was performed. ECs on narrow 3 µm wide tracks (also termed 1D in the following) migrated less efficient in comparison to ECs on broader tracks in regard to mean velocity, persistence, and run velocity. Additionally, ECs in 1D displayed a distinct actin cytoskeleton architecture, compressed nuclei, and different orientation of the centrosome in comparison to ECs on wider tracks. The frequent directional changes of ECs on narrow tracks were accompanied by pronounced membrane blebbing, while migrating and elongated cells displayed a lamellipodium as cellular protrusion. This behavior was contractility-dependent as both modes were provoked by using Blebbistatin or Calyculin A, respectively. The comparison between 1D and 3D migrating cells revealed a striking similarity in actin cytoskeleton architecture and in switching between two morphological modes. Cells migrating in 3D moved slower but more persistent after Blebbistatin treatment, which was likewise the case for cells migrating in 1D. In contrast to this, cells in the 2D system migrated faster but less persistent after Blebbistatin treatment. A Rac1 inhibitor used in this study showed the tendency to influence the migratory potential similarly in 1D and 3D, in contrast to 2D. However, a microtubule disrupting agent displayed different effects in 1D and 3D. These experiments demonstrated that the 1D system allows to draw conclusions about certain aspects of 3D migration. Thus, using this 1D migration system, important aspects of 3D migration can be mimicked in a highly controlled setting.

In the second part of this work, a system for artificial tip cell formation was investigated. For the analysis of tip and stalk cells specifically structured surfaces were designed. These structures provided areas allowing only a restricted number of cell-cell contacts and areas allowing a high number of cell-cell contacts. ECs with a low number of cell-cell contacts displayed increased VEGFR2 expression levels in comparison to cells with a high number of cell-cell contacts, a phenomenon which was inhibited by using a Notch signaling inhibitor. This system will be a useful tool in the future to decipher tip and stalk cell competition within a defined cellular population and a defined microscopic frame.

2. Introduction

2.1 Angiogenesis in health and disease

Angiogenesis is defined as the formation of new blood vessels derived from a preexisting vascular network, and plays an important role in physiological processes like tissue growth, development, and wound healing (Tonnesen et al. 2000). However, the process of angiogenesis gained most attention in medicine and cancer biology due to its important role in numerous pathological conditions and its potential as a therapeutic target (Folkman 1995; Carmeliet and Jain 2000). Angiogenesis is functionally divided into two sub-forms: sprouting angiogenesis (Ribatti and Crivellato 2012) and intussusceptive angiogenesis (Makanya et al. 2009). Sprouting angiogenesis is the scientifically more examined form of angiogenesis and is defined as the formation of new blood vessels by endothelial sprouts from a pre-existing vessel towards a specific stimulus. For the formation of sprouts the endothelial cells (ECs) need to fulfill several requirements e.g. the degradation of the basement membrane (a thin fibrous layer separating the ECs from the connective tissue) *via* the action of matrix metalloproteases (Davis and Senger 2005), as well as the ability of migration and chemotactic orientation (Terranova et al. 1985; Lamalice et al. 2007). In contrast to this, intussusceptive angiogenesis is known as the formation of blood vessels by the division of a pre-existing vessel into two vessels, a process especially important during embryonic development (Djonov et al. 2000; Makanya et al. 2009). Importantly, the process of angiogenesis differs from the process of vasculogenesis, where new blood vessels are formed upon differentiation of angioblasts, endothelial progenitor cells present in the embryo (D'Alessio et al. 2015). However, the traditional distinction between these two processes, playing a crucial role in adults or embryonic development, respectively, is blurred as endothelial progenitor cells (EPCs) have been shown to be important in adult blood vessel formation (Pelosi et al. 2014) and might play a role in tumor angiogenesis as well (Spring et al. 2005).

In general, angiogenesis has gained a high importance by the pioneering work of Judah Folkman, who first described angiogenesis as a crucial process for cancer progression (Folkman 1971; Folkman 1995). Since then, an extensive search for angiogenesis regulators led to the identification of potential targets for anti-vascular treatment in cancer and other diseases. The most examined signaling pathway in this process is the vascular endothelial growth factor receptor (VEGFR) pathway, which plays a major role in vascular regulation (Olsson et al. 2006), and has been assessed to be a promising target for anti-cancer therapy. Consequently, the first drug approved for anti-angiogenic cancer treatment was the humanized monoclonal antibody Bevacizumab, interfering with VEGFR

signaling by binding to its ligand VEGF-A (Glade-Bender et al. 2003; Willett et al. 2004). Many other anti-angiogenic drugs were discovered afterwards, e.g. the multi-kinase inhibitors Sorafenib and Sunitinib (Gridelli et al. 2007), or the VEGF-neutralizing aptamer Pegaptanib (Doggrell 2005). In the following section, an overview about the underlying regulatory mechanisms of VEGFR signaling will be given.

2.2 VEGF-receptor signaling

Vascular endothelial growth factor receptors are members of the receptor tyrosine kinase (RTK) superfamily and consist of a pattern of three different receptors in mammals: VEGFR1 (Flt-1), VEGFR2 (Flk-1/KDR), and VEGFR3 (FLT4) (Olsson et al. 2006). Common to these receptors is a large extracellular domain consisting of up to seven immunoglobulin-like domains, a transmembrane domain, a juxta-membrane domain, and two intracellular kinase domains (Olsson et al. 2006) [**Fig. 2.1**]. Ligands binding to these receptors are members of the vascular endothelial growth factor (VEGF) family - VEGF-A, VEGF-B, VEGF-C, VEGF-D, the placenta growth factor (PLGF), and the corresponding splice variants. Every ligand preferentially forms homodimers and possesses diverse affinities to the various VEGFRs, reflecting the complexity of VEGFR regulation, which provides the ability to influence various essential physiological processes [**Fig. 2.1**]. Yet, the most prominent factor for angiogenesis is VEGF-A, which is strongly upregulated in hypoxic tissue due to stabilization of hypoxia-inducible factors (HIFs) (Pugh and Ratcliffe 2003). The receptor activation itself occurs by binding of VEGF-dimers, leading to homo- or hetero-dimerization and subsequent auto-phosphorylation of the receptor (Olsson et al. 2006). Subsequently, recruitment of various scaffold and signaling proteins is induced, resulting in signal amplification and translation of the signal into an adequate biological response. Inactivation of the receptor is mediated through de-phosphorylation by the two phosphatases SHP1 and SHP2 (Guo et al. 2000), or by internalization and
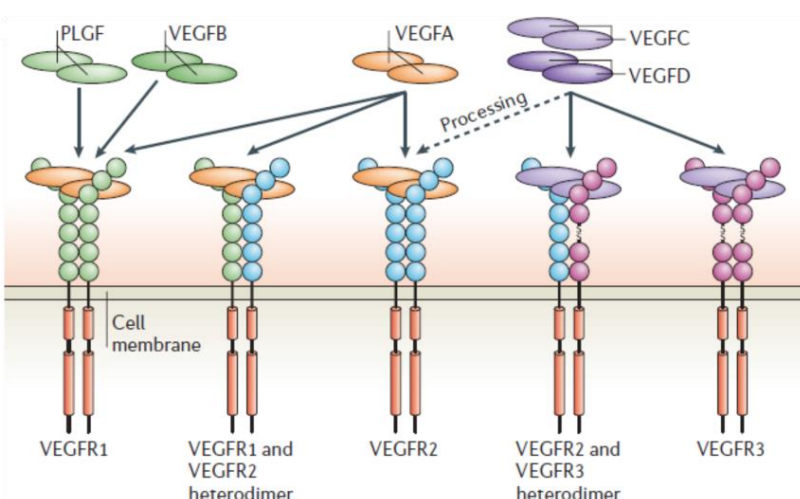
Fig. 2.1 Interaction of various VEGF-dimers with the three mammal members of the VEGF-receptor family. Receptors consist of several immunoglobulin-domains (spheres) and two intracellular kinase domains (cylinders). Arrows indicate affinities. Figure adapted and modified from Olsson et al. 2006.

degradation of the receptor (Lampugnani et al. 2006). Beside angiogenesis, VEGF-receptor signaling plays a role in various embryogenic processes like lymphatic or cardiovascular development (Kaipainen et al. 1995; Madonna and De Caterina 2009) Additionally, it is important for the stimulation of nitric oxide (NO) production and thus vasodilatation *via* Akt/PKB and eNOS in ECs (Kroll and Waltenberger 1999; Maniatis et al. 2006). In the following, VEGFR2 signaling in the context of migration and orientation will be described in more detail.

2.3 Migration of endothelial cells

2.3.1 VEGFR2 signaling and Rho GTPases as regulators of endothelial cell motility

Migration of ECs requires a highly complex orchestration of processes like orientation, protrusion, contraction, and adhesion. After sensing motogenic signals, ECs reorient and built actin-dependent cellular protrusions (e.g. lamellipodia). Subsequent attachment of these protrusion to the respective substrate *via* integrins, and stress fiber mediated contraction of the trailing edge leads to a translocation of the cell body and completion of the migration cycle (Sheetz et al. 1999; Lamalice, Le Boeuf, and Huot 2007). ECs are attracted to chemotactic stimuli (VEGF, angiopoietins, and other cytokines), haptotactic stimuli (Davis and Senger 2005), and mechanotactic stimuli (Song Li et al. 2005). For reasons of simplicity, only VEGF as a chemotactic stimulus and thus regulator of migration will be described in more detail.

VEGFR2 activation is the main intrinsic cellular signal transmitting pathway upon a VEGF-A stimulus, as VEGFR2 possesses the highest intrinsic kinase activity in comparison to the other VEGFRs (Olsson et al. 2006). As described above, receptor activation occurs by dimerization and auto-phosphorylation of the receptors at the tyrosine residues Y1214, Y1175, and Y951 which are located in protein binding motifs. These phosphorylated binding motifs provide docking sites for proteins harboring SH2 (src homology 2), or PTB (phosphor-tyrosine binding) domains (Olsson et al. 2006). The small GTPases of the Rho family (mainly Cdc42, Rac1, RhoA) are key players in EC motility and are regulated by VEGFR signaling (among many other regulatory mechanisms). In general, they are described as molecular convergence nodes of migration as they act as regulators of actin organization, adhesion assembly, and contraction (Parsons, Horwitz, and Schwartz 2010). Their regulation *via* recruitment and activation of guanine nucleotide exchange factors (GEFs) and GTPase activating proteins (GAPs) is complex. Crosstalk with other pathways (e.g. integrin signaling pathway), and also interactions between the individual GTPases of the Rho family among themselves,

leads to a close-meshed cellular signaling network. A simplified overview of Rho GTPase signaling pathways and their main tasks in actin reorganization is displayed in **Fig. 2.2**.

The small GTPase Cdc42 is known to be activated indirectly by VEGFR2 signaling as its activation is dependent of phosphorylation at tyrosine residue 1214 (Lamalice et al. 2004). The mediators known for Cdc42 activation are the adaptor protein Nck and the kinase Fyn (Lamalice et al. 2006). The most critical role of Cdc42 is the formation and regulation of filopodia. These thin actin containing protrusions are located in the cells' leading edge, playing an important role in sensing chemotactic stimuli (Mattila and Lappalainen 2008) [**Fig. 2.2**]. Moreover, Cdc42 is essential for the activation of the p38 MAPK signaling pathway, which is involved in actin remodeling and stress fiber formation *via* heat shock protein 27 (HSP27) (Huot et al. 1997). Additionally, Cdc42 has been shown to interact with members of the PAK protein family being involved in actin cytoskeletal reorganization, e.g. through activation of the LIM-kinase (Edwards et al. 1999).

In contrast to Cdc42, Rac1 is known to be mainly important for the formation of lamellipodia and membrane ruffles (Sit and Manser 2011). It has been shown that Rac1 is activated by Vav2, a GEF which is recruited to the membrane upon VEGFR2 signaling and subsequently phosphorylated and activated by Src, a direct interaction partner of VEGFR2 (Garrett et al. 2007). An important effector of Rac1 is WAVE, a member of the Wiskott-Aldrich syndrome protein (WASP) family, which regulates the activity of the Arp 2/3 complex. This Arp 2/3 complex stimulates actin polymerization by providing new
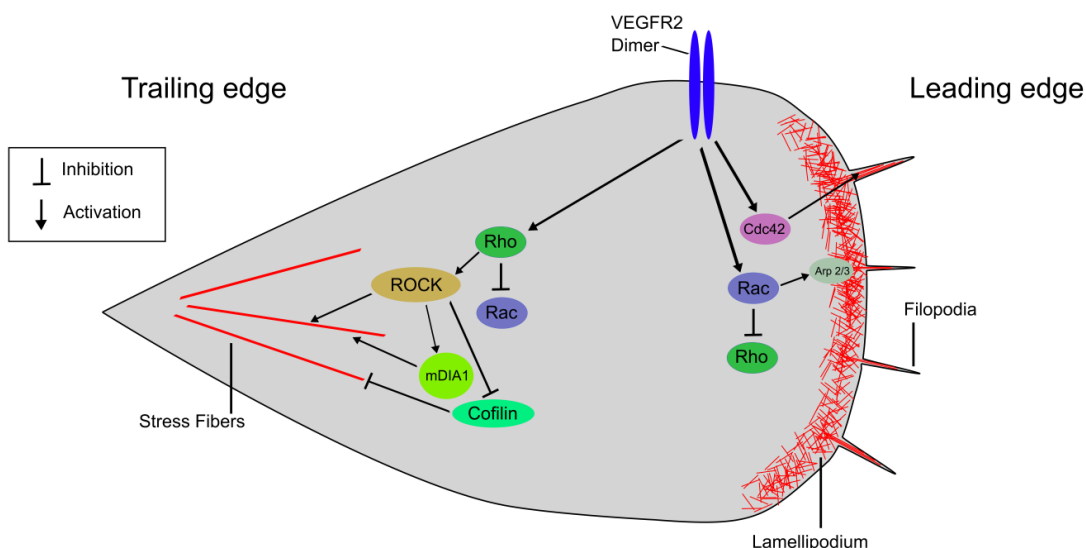
Fig. 2.2 Schematic and simplified overview of Rho GTPase signaling upon VEGFR2 dimerization and activation.
Cdc42 and Rac1 are mainly active in the leading edge of a cell, organizing lamellipodia and filopodia. RhoA activity is restricted to the trailing edge where stress fiber mediated contraction is predominantly important. The size ratios of the signaling proteins and the cell do not reflect reality. Signaling mechanisms are described in the text.

nucleation points and is thus of high importance in branched networks located in the lamellipodium for instance (Volkmann et al. 2001).

The third important GTPase regulating cellular motility is RhoA. RhoA is activated *via* VEGFR2 signaling in a HSP90-dependent manner (Le Boeuf et al. 2004). Important effectors of RhoA are the phosphoinositide-3 kinase (PI3K), as well as the Rho associated kinase (ROCK). ROCK itself has many targets which affect actin cytoskeleton reorganization e.g. the focal adhesion kinase (FAK). FAK is organized in focal adhesion clusters, where it plays a pivotal role in adhesion and cellular motility (Higuchi et al. 2013). Moreover, ROCK is a potent mediator of cellular contractility by phosphorylating the regulatory myosin light chain directly and additionally phosphorylating and thereby deactivating the myosin light chain phosphatase (Riento and Ridley 2003) [**Fig. 2.3**]. Additionally, direct activation of mDIA1 and indirect ROCK-mediated inhibition of Cofilin *via* LIM-kinase regulates actin polymerization of stress fibers (Lamalice et al. 2007) [**Fig.2.2**]. In general, RhoA can be seen as an important regulator of stress fiber maintenance.

It is mentionable, that Rac1 and Cdc42 are predominantly active in the leading edge of a cell (near lamellipodia and filopodia), while RhoA activity is more restricted to the trailing edge (where stress fiber formation and thus contraction predominantly occurs) (Parsons, Horwitz, and Schwartz 2010) [**Fig. 2.2**]. These spatially restricted activities reflect the different tasks of Rho GTPases in cellular migration and actin reorganization. For example it has been shown that Rac1 suppresses RhoA in the leading edge by activating its GTPase activating protein p190RhoGAP (Nimnual et al. 2003). In contrast to this, RhoA suppresses Rac1 activity near the trailing edge by activation of filGAP, a GTPase activating protein of Rac1 (Ohta et al. 2006; Burridge and Doughman 2006).

Beside the previously described GTPases, other essential factors exist to modulate endothelial cell migration *via* VEGFR signaling. Upon phosphorylation and activation of VEGFR, the adaptor molecule Shb binds directly to the intracellular domain of the VEGFR *via* a SH2 domain (Holmqvist et al. 2004). This results in recruitment and activation of PI3K, leading to local production of PIP_3 by phosphorylation of membrane lipids. Signaling proteins which harbor a PH (pleckstrin homology) domain can bind to PIP_3 and thus are recruited to the membrane. A prominent effector of PI3K is AKT/PKB, which is a potent mediator of actin remodeling and cellular motility in endothelial cells (Morales-Ruiz et al. 2000). Among others, AKT/PKB targets FAK, previously mentioned as an important regulator of adhesion. Likewise, the previously mentioned GEFs and GAPs often harbor PH domains. Thereby, PI3K signaling also contributes to Rho GTPase regulation (Welch et al. 2003).

2.3.2 Regulation of actin-myosin contractility in endothelial cell migration

The actin-myosin system in non-muscle cells is an evolutionary highly conserved mechanism for the creation of mechanical tension. This is important on a molecular but also on a cellular level as contractility is the central regulator of cell shape (Parsons, Horwitz, and Schwartz 2010). Contractility is crucial for cellular migration, being responsible for stress fiber-mediated trailing edge retraction (Lamalice et al. 2007). Stress fibers consist of approximately 10 to 30 actin filaments which are cross-linked by α-actinin and organized in an anti-parallel manner (Tojkander et al. 2012). Functionally they are linked to focal adhesions either solely on one side (dorsal stress fibers) or on both sides (ventral stress fibers) (Tojkander et al. 2012). Stress fibers are found all over the cell body, but are concentrated in the central and rear regions of a cell. They provide a scaffold for myosin II filaments which generate molecular tension by moving two actin filaments together and thus shorten the stress fibers (Murrell et al. 2015). Myosin II consists out of two heavy chains, two regulatory light chains (RLCs), and two essential light chains (ELCs). Myosin is organized in bipolar bundles to interact with filamentous actin (f-actin) *via* the so called head domains of the heavy chains (Vicente-Manzanares et al. 2009). Upon ATP hydrolysis, the head domain undergoes a conformational change and the actin filaments of the stress fibers are pulled towards each other in a "power stroke" mechanism (Málnási-Csizmadia et al. 2010). The regulation of myosin motor activity is mediated by phosphorylation and de-phosphorylation of Thr18 and Ser19 at the RLCs (Shen et al. 2010). An increased phosphorylation results in an increased myosin II motor activity. In endothelial cells this is achieved by two main proteins, which are displayed in **Figure 2.3**. One of these proteins is the previously described Rho associated kinase (ROCK), which directly phosphorylates the RLC, but also prevents de-phosphorylation of the RLC by inhibiting the myosin light chain phosphatase (MLCP). The second protein is the myosin light chain kinase (MLCK) which is activated by the calcium binding protein Calmodulin and also directly phosphorylates the RLC of myosin II (Shen et al. 2010).
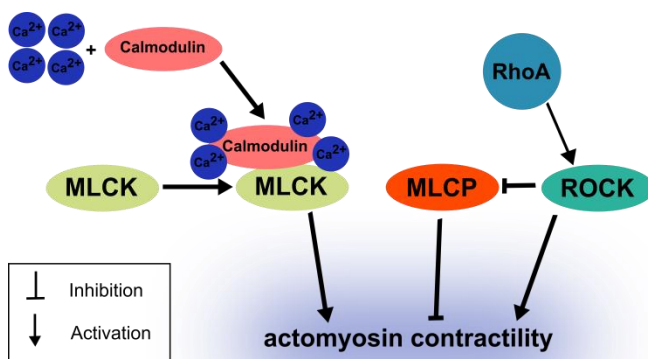
Fig. 2.3 Molecular pathways involved in the generation of tension *via* actin-myosin contractility.
MLCK is activated by binding of Calmodulin, a Ca^{2+} binding protein. Activated MLCK enhances contractility by phosphorylation of the regulatory light chain of myosin II. ROCK which is activated by RhoA, inhibits the myosin light chain phosphatase (MLCP), and directly phosphorylates the regulatory light chain of myosin II, controlling contractility in two different ways.

2.4 Tip cell formation

Regulation of the factors described in section 2.2 is tightly controlled to allow a directed migration of a cell collective towards an VEGF-A gradient during sprouting angiogenesis (Gerhardt et al. 2003). In order to coordinate the movements within a new sprout, only specialized tip cells express high levels of VEGFR2, leading the cellular collective into a hypoxic area (Gerhardt et al. 2003).

Tip cell formation is a fundamental process for sprouting angiogenesis and depends mainly on the differentiation of specialized cells, leading a new sprout towards a specific angiogenic stimulus consisting of VEGF and other cytokines. The selection of tip cells (and stalk cells) is the result of a cellular competition depending on DLL4-Notch, an evolutionary highly conserved cell-cell contact-dependent signaling mechanism (Artavanis-Tsakonas et al. 1999) [**Fig. 2.4**]. In general, a tip cell is defined by its specific set of receptors (Blanco and Gerhardt 2013; Jakobsson et al. 2010), expression or repression of characteristic genes (Siemerink et al. 2012; del Toro et al. 2010; Strasser et al. 2010), a high number of dynamic filopodia (Gerhardt et al. 2003), its front position in the sprout, and the low proliferative activity (Gerhardt et al. 2003). In contrast to this, stalk cells are highly proliferative and establish adherent and tight junctions for lumen formation and to provide vascular stability to the new sprout (Blanco and Gerhardt 2013). There are various factors involved in the process of tip and stalk cell selection, but for reasons of simplicity only the interplay of VEGFRs and Notch signaling will be described in more detail.

Initially in the sprouting process, a cell from a (re)activated preexisting vessel loses attachment to the neighboring cells, degrades the basement membrane, and starts to migrate along the VEGF gradient (Blanco and Gerhardt 2013). The initial selection of a cell to become a tip cell is presumably random and mainly dependent on the VEGFR2 expression of the cell at the time point of local VEGF level increase (Jakobsson et al. 2010). While tip cells display a high DLL4 and VEGFR2 (high kinase activity) expression level but low levels of VEGFR1 (very low kinase activity), stalk cells display low levels of VEGFR2 and DLL4, but high levels of VEGFR1 [**Fig. 2.4**]. High levels of the membrane bound delta-like ligand 4 (DLL4) in tip cells leads to an increased Notch signaling activation in neighboring cells resulting in a decrease of DLL4 and VEGFR2 expression, but an increase of VEGFR1 expression [**Fig. 2.4**]. This ensures that only single cells obtain the tip cell phenotype, while other cells are laterally suppressed and obtain a phenotype characteristic for stalk cells. As tip cells lead the sprout, they usually possess less cell-cell contacts compared to stalk cells resulting in a decreased Notch signaling and thus additional stabilization of the tip cell phenotype. Moreover, the high VEGFR2 levels in

tip cells are responsible for the high number of filopodia which are a characteristic feature of tip cells but have been shown to be dispensable for the guidance of new sprouts (Phng et al. 2013). In stalk cells, the low VEGFR2 but high VEGFR1 expression levels result in a reduced response to VEGF-A as VEGFR1 mainly acts as a decoy receptor, due to its low intrinsic kinase activity but very high affinity to VEGF-A (Jakobsson et al. 2010). As DLL4 expression is dependent on VEGFR signaling [**Fig. 2.4**], the low sensibility to VEGF ensures low levels of DLL4, hence stabilizes the stalk cell phenotype, as the cell is not capable of suppressing neighboring cells *via* Notch signaling. While tip cells ensure a coordinated movement of the cell collective, stalk cells build up the lumen and form the novel blood vessel. This whole process is highly dynamic and cells in the tip cell position of a new sprout might change frequently during sprout progression (Jakobsson et al. 2010).
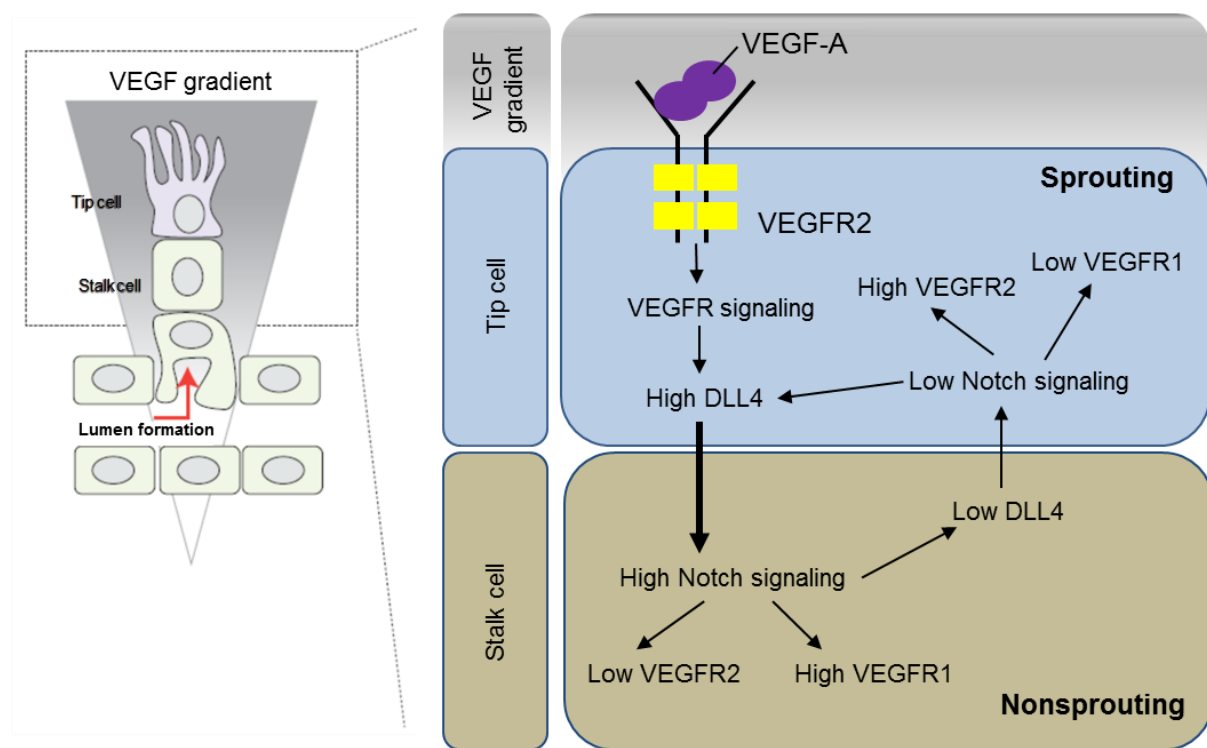
Fig. 2.4 Tip and stalk cell competition upon a VEGF-A gradient.
Initially, VEGF-A binds to VEGFR2. VEGFR2 signaling leads to increased expression of the membrane bound ligand DLL4 in tip cells, resulting in enhanced Notch signaling in neighboring stalk cells. The enhanced Notch signaling in stalk cells results in low VEGFR2 but high VEGFR1 expression, making the cell insensitive to VEGF stimulation, which in turn stabilizes the stalk cell phenotype. The low levels of DLL4 in the stalk cells results in low Notch signaling in the tip cells, stabilizing the tip cell phenotype by up-regulation of DLL4 and VEGFR2 and down-regulation of VEGFR1. Figure adapted and modified from Blanco and Gerhard, 2013.

2.5 Adhesion and contractility as regulatory mechanisms of plasma membrane blebbing

In contrast to the "classical" cell protrusions (e.g. filopodia and lamellipodia), which are regulated by the Rho GTPase protein family (described in section 2.2), membrane blebs become more and more important in cell biology, being crucial for cellular migration of leukocytes (Lämmermann et al. 2008), or as an alternative migration mode of cancer cells (Wolf et al. 2003). Importantly, membrane blebs, playing a role in migration processes, have to be distinguished from blebs observed in apoptotic processes (Coleman et al. 2001). In this section, only the formation of membrane blebs in the context of migration and spreading will be described in more detail, including many mechanistic similarities to apoptotic blebs.

Plasma membrane blebs expand as a result of intracellular hydrostatic pressure (Charras et al. 2005). This is in contrast to other cellular protrusions like lamellipodia, where actin polymerization is the driving force (Charras and Paluch 2008). Retraction of the membrane blebs occurs through polymerization of actin at the bleb cortex and subsequent retraction of the bleb towards the cell body happens in an actin-myosin contractile-dependent manner (Charras et al. 2006). To date, many molecular players associated with the actin cytoskeleton have been identified to be either essential or not important for bleb formation (reviewed in Fackler and Grosse 2008). One major regulator of membrane blebbing is the previously described Rho-ROCK signaling pathway due to its potential to provide cellular contractility. Beside the necessity of contractility in bleb retraction as mentioned before, contractility has been shown to be a critical inducer of membrane blebs due to induction of local ruptures in the cell cortex (Paluch et al. 2006; Ruprecht et al. 2015). In contrast to the knowledge about intracellular mechanism, extracellular cues which provoke bleb formation are rather unknown. To date, the best analyzed extracellular cause of plasma membrane bleb formation is the change, loss, or reduction of adhesion, for example during cell spreading. Moreover, it has been shown that leukocytes migrate in an integrin-independent and bleb-based manner (Lämmermann et al. 2008). Another study showed that softness of the substrate is critical for bleb formation of breast cancer cells (Kitzing et al. 2007). To date, plasma membrane blebbing of endothelial cell biology has been exclusively described in the context of cell spreading (Norman et al. 2011), which can be likewise seen as a temporal low adhesive state. In the first part of this study, it is demonstrated that plasma membrane blebbing is inducible in endothelial cells through spatial confinement and enhancement of contractility in a defined setup. Additionally it is shown, that blebbing plays a role in 3D migration of endothelial cells as a dynamic and important reaction to low adhesive environments.

2.6 Current models to investigate angiogenesis

The establishment of new models for the investigation of angiogenesis is of great importance and has been addressed in this study. A brief overview of existing models and assays will be given in this section. All models described can be divided into four categories – *in vitro* models (e.g. tube formation assay), *ex vivo* models (e.g. aortic ring assay), *in vivo* models (e.g. CAM assay) and *in silico* modeling. As all of them are specific to certain aspects of angiogenesis, all of them possess their advantages and disadvantages. Usually, a combination of assays is applied in laboratory routine to fully evaluate the effects of e.g. pharmacological compounds and to create a good scientific base for the *in vivo* translation.

2.6.1 *In vitro* assays

Like for other cell types, behavior of ECs upon specific stimuli can be tested using standard *in vitro* cell biological methods including assays for proliferation (e.g. cell-counting after a specific time; MTT assays) and migration (e.g. boyden chamber assay, scratch assay). As both differentiation and migration play a pivotal role in sprouting angiogenesis, these assays usually provide a good first overview on endothelial cell behavior as they are technically easy to handle and usable for large screening experiments.

Beside the standard cell assays, the most common in *vitro assay* for investigation of angiogenesis is the "tube formation assay". Here, cells are cultured under conditions where they built a capillary-like network structure. This morphogenetic process of network formation is often used as a read-out for the pro- or anti-angiogenic effects of compounds in laboratory routine. The tubule-like structures can be observed in short time experiments on a layer of a gel matrix after three to six hours (Arnaoutova and Kleinman 2010). Also 3D approaches have been experimentally addressed, where tubule-like structures are formed between two layers of gel matrices (Gagnon et al. 2002). These experiments better mimic the *in vivo* situation but are usually technically challenging and difficult to analyze.

Although the tube formation assay is the only well established system to test for the morphogenetic potential of ECs in an *in vitro* approach to date, results obtained from these experiments have to be interpreted with caution. The main reason for this is that the process is not endothelial-specific as other cell types were shown to build up networks under certain conditions - cells which do not form networks *in vivo* (Donovan et al. 2001). However, results from our laboratory proved, that conclusions drawn from tube formation

assays are in general in line with results obtained from migration assays, implying that overall migratory potential is more important than the ability of morphogenesis. In the last years multiple microfluidic setups have been established to test endothelial cells under *in vivo*-like conditions (e.g. under shear stress) (Shao et al. 2009; Abaci et al. 2014). So far, these approaches have not emerged to be accessible to a broad range of users, but harbor a huge potential for future EC-based research.

2.6.2 *Ex vivo* assays

Ex vivo assays are described as methods which allow the withdrawal and cultivation of organs or tissues from mice (or other animals) in order to elucidate the complex process of angiogenesis in an *in vivo*-like situation. One of the most common *ex vivo* assays is the "aortic ring assay". Herby, small, approximately 1 mm wide rings of a mouse (or rat) aorta are embedded into a three dimensional matrix like matrigel or type I collagen (Baker et al. 2012). After five to nine days, micro-vessels sprout from the aortic ring into the gel and can be quantified regarding their number and length. Likewise, cell coverage of the micro-vessels with pericytes can be quantified using antibody immuno-stainings for respective marker proteins like NG2 (Ozerdem et al. 2001). Moreover, micro-vessel structures and lumen formation are addressable using the 3D reconstruction capabilities of confocal microscopy. Beside the testing of pharmacological compounds on their antiangiogenic effects, cell treatment *via* siRNA transfections are feasible using this system (Baker et al. 2012). Moreover, aortas from transgenic mice are adaptable to this system, in order to compare their angiogenic potential upon knockout conditions (Baker et al. 2012). The main advantage of this assay is that ECs are in a natural-like environment, being surrounded by a three-dimensional matrix embedding other cells which are known to play a role in angiogenesis (e.g. pericytes). However, the main disadvantage of the system is the huge variability, especially between different animals, implicating the necessity of accurate quantification. Moreover, always non-human material is used which makes the translation to clinical trials even more challenging.

2.6.3 *In vivo* assays

In vivo assays for angiogenesis are numerous and are performed in various model animals like zebrafish, mouse, or rat. The most common assays are the chick chorioallantoic membrane (CAM) assay, the dorsal skinfold chamber assay, and various tumor models. Here, only the CAM assay and the tumor models will be described in more detail.

The CAM is a highly vascularized membrane which serves as a gas exchange barrier and is accessible outside the chick embryo (Staton et al. 2009). Sprouting angiogenesis in the CAM is observed between day five and day twelve after starting the incubation of the fertilized egg. A small window in the egg shell allows manipulation of the CAM inside the egg shell. Alternatively, the embryo is artificially cultured in a petri dish without the egg shell. This system allows the testing of potentially antiangiogenic substances or even the cultivation of xenografts tumors or human cancer cells (Staton et al. 2009). The advantages of the CAM assay are low costs and simplicity, making the system suitable for high-throughput screenings. The disadvantages are the non-mammalian origin, the differentiation of new vessels from preexisting ones and the occurrence of both sprouting and intussusceptive angiogenesis.

Tumor models in mice are widely used in laboratory routine as they provide the only possibility to investigate angiogenesis *in vivo* in a mammalian model system. The most common method to achieve this is the subcutaneous injection of tumor cells into the mice. Upon formation of a solid tumor, treatment with the substance of interest can be investigated. In order to estimate the antiangiogenic potential of the substance of interest, the tumor size is measured at regularly time periods, vascularization of the tumor tissue is estimated and the tumor volume is quantified at the end of the study.

2.6.4 *In silico* modeling

In silico modeling of angiogenic processes is efficient as angiogenesis relies on pattern formation based on cell-cell contact-dependent regulation of receptor expression as well as on gradients of specific stimuli as described in section 2.3. Thus, the computation of processes like tip cell formation based on existing experimental data is feasible and useful (Bentley et al. 2009). As structured surfaces provide a highly controllable environment, experimental data obtained with these novel approaches likely provide a stable and reproducible experimental basis for computational analyses of complex processes. The second part of this thesis investigates structured surfaces as a tool to model tip cell formation.

2.7 Structured surfaces in cell biology

2.7.1 Importance of structured surfaces in cell biology

Structured surfaces and other artificial systems gained more and more importance in the last years, as cell biology in the traditional 2D cell culture is artificial. Moreover 2D cell culture allows for a very undifferentiated and limited analysis of cellular behavior. Cells in a flat cell culture dish (usually consisting of rigid polystyrene) face a uniform, infinite, and stiff environment (Théry 2010) [**Fig. 2.5**]. In contrast to this, cells *in situ* face very specific microenvironments with spatial confinement, restricted space for spreading, or specific numbers of neighboring cells [**Fig. 2.5**]. With structured surfaces, it is possible to reconstitute the various micro-environments on a flat surface, and to analyze the cellular response in high quality and quantity.

In general, micro-patterns allow for the manipulation of many cellular processes. The most common reactions of cells cultured in confined environments or on micro-structures are the massive changes in actin cytoskeleton architecture (Théry et al. 2006). Cells cultured on T- or V-shape patterns form pronounced stress fibers in order to over-span the non-adhesive regions. These fibers are contractility dependent and diminish using the
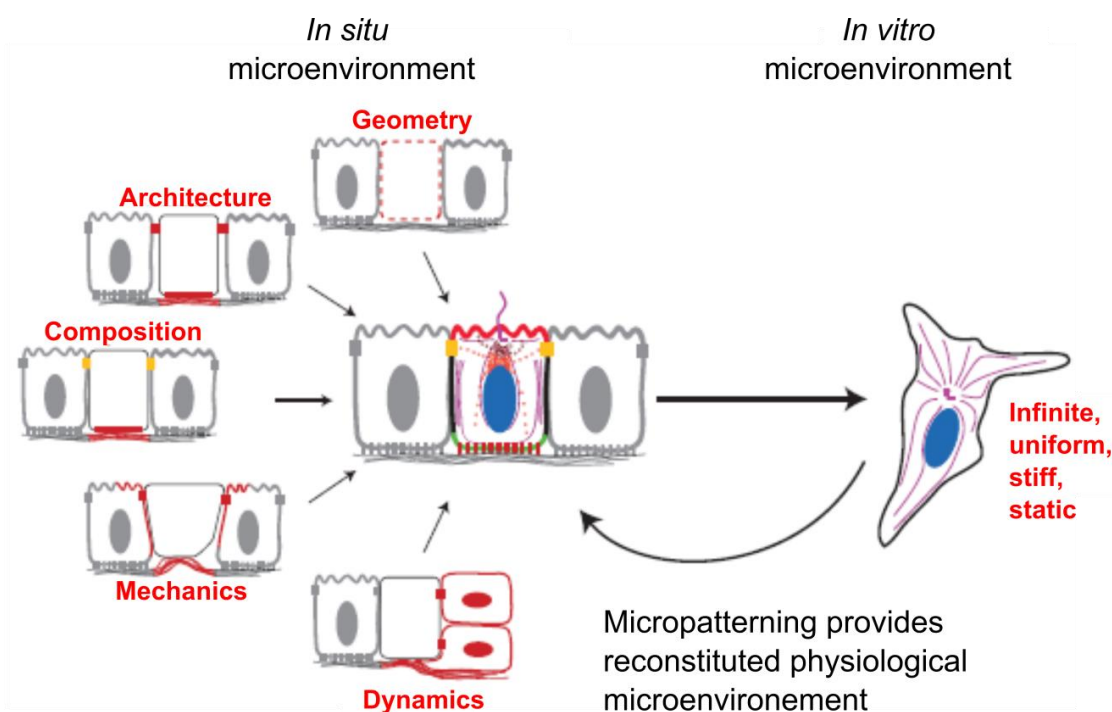
Fig. 2.5 Microstructures can be used to reconstitute cellular micro-environments.
Cells face a stiff, uniform, infinite, and static environment in an *in vitro* environment (2D cell culture). This is in contrast to their *in situ* situation where they face very specific micro-environments. Micro-patterning can be used to reconstitute the physiological micro-environments on a flat surface and to analyze cellular behavior in a high quantity and quality. Figure adapted and modified from Théry 2010.

ROCK inhibitor Y27632 (Théry et al. 2006). Furthermore, adhesion sites are only formed at the sites of highest tensional stress (Théry et al. 2006). Micrometer-sized ECM-protein dots helped to elucidate the maximal distance between adhesion sites, which is between 58-73 nm for different cell types, respectively (Arnold et al. 2004). Moreover, micro-patterns have been used to study and modify intracellular polarity. With asymmetrical patterns, it has been shown that endocytosis is dependent on extracellular cues (Grossier et al. 2014), and that directed cell migration is inducible by using tear drop shaped patterns (Jiang et al. 2005). Moreover, lamellipodium formation is controllable by asymmetric shaped micro-patterns (James et al. 2008). Other striking findings were the dependencies of centrosome and Golgi orientation in confined environments. Both cellular structures are taken as polarity markers in cell biology as they usually form an axis in the direction of migration (together with the nucleus). However, both orientation of centrosomes and Golgi apparatus have been shown to change under confined environments (Pouthas et al. 2008; Doyle et al. 2009, this study). Additionally, cellular differentiation is influenced by micro-patterning, as it has been shown that shape and contractile status determine the cell fate (Kilian et al. 2010).

Migration in combination with micro-patterning has been a central research focus, as micro-patterns are used to preset guidance cues in order to facilitate automated analysis of migration parameters (Maiuri et al. 2012; Maiuri et al. 2015) or to mimic 3D migration of fibroblasts (Doyle et al. 2009). In a very sophisticated study, Maiuri and coworkers demonstrated that speed and persistence of cells are exponentially correlated. Further it was shown that actin retrograde flow, the actin flow from the lamellipodium towards the cell center (Gardel et al. 2008) maintains migration persistence through a positive feedback loop mechanism (Maiuri et al. 2015). Moreover, thin protein adhesion cues can potentially be used as a model system to mimic 3D migration as protein tracks induces a fast and uniaxial migration behavior (Doyle et al. 2009; Doyle et al. 2012).

The previously described examples demonstrate the potential of micro-patterning approaches in cell biology. Most of these studies were carried out on plastic, glass, or polydimethylsiloxane (PDMS) surfaces as they are suitable for easy-to-handle micro-patterning techniques like micro-contact printing. However, as the field of micro-patterns progresses, new techniques are introduced, which can be used to manipulate cell behavior dynamically e.g. with the help of photo-switchable patterns (Rolli et al. 2012). Likewise, the possibility of patterning soft and sticky substrates is a great tool to decipher cellular reactions to spatial confinements and specific geometries in the future (Yu et al. 2012).

2.7.2 Structured surfaces in endothelial cell biology

As this study focuses on EC reactions to micro-patterns, some common approaches using micro-patterns with their background in angiogenesis are introduced in this section. Micro-patterns were used to create linear tracks, mimicking cell shape of ECs under fluid shear stress (Vartanian et al. 2010). Likewise, mechanical properties of endothelial cells are influenced by micro-patterns as elongated cells possessed a higher stiffness compared to control cells (Kidoaki and Matsuda 2007). Additionally, nucleus deformation of ECs has been in the focus of researchers. Versaevel and coworkers demonstrated a correlation between cell elongation and nucleus deformation resulting in an altered chromatin condensation and proliferation rate of ECs (Versaevel et al. 2012).

A question often addressed is whether tube formation on micro-patterned surfaces is possible and if so, if it is influenced by the dimension of the substratum. Lines of different widths have been used to produce cell tubes with different diameters. After a distinct time of cultivation a lumen was observed (Dike et al. 1999; Lei et al. 2012), suggesting that spatial restriction is a critical parameter for tube formation. Similarly, indirect patterning was performed by cultivation of ECs on a patterned glass slide and subsequent transfer onto a Matrigel layer. Herby, cells formed tubes in the dimensions of the preset patterns (Okochi et al. 2009). In the future, this approach will provide information about geometrical constraints of tube formation in a highly controlled setting.

Migration behavior of ECs on micro-patterns has been rudimentarily elucidated to date. It has been shown that ECs migrate faster on 15 µm wide tracks compared to 30 and 60 µm wide tracks (Li et al. 2001). This is in contrast to another study where researchers showed a decreasing velocity with decreasing tracks width (Lei et al. 2012). Another study was performed with implemented medium flow into the experimental setup. ECs migrated faster when the flow was parallel to the direction of migration. When the flow was perpendicular, the cells migrated less efficient (Lin and Helmke 2009). However, no comprehensive analysis of migration behavior of single ECs on migration tracks, was performed so far. The first part of this study focuses on EC migration on micro-patterns, elucidating differences to existing studies and to other cell types.

2.8 Aim of the study

Several models for angiogenesis are used in laboratory routine to date. However, most of the common models are technically challenging, difficult to interpret and quantify, and thus poorly predictive for the *in vivo* situation. Moreover, no reliable in *vitro assays* exist, being accessible to a broad range of laboratories. Angiogenesis is a process based on the formation of patterns, networks, and shapes. These features make angiogenesis suitable to be addressed with structured surfaces, like specific patterns can be preset in order to study morphogenetic processes and migration under spatial restriction.

To date, no comprehensive cellular characterization of ECs migrating on micro-patterns has been performed. The first part of this work focuses on a cell biological characterization of ECs on micro-tracks, following the intention to mimic 3D migration by using very thin protein guidance cues. As 2D cell culture and migration is very artificial, this migration model helps to elucidate migration behavior of ECs in a fibrillary 3D environment and provides a technically easy to handle and easy to analyze setup for large scale screening experiments.

Tip cell formation is a highly complex process which is exclusively investigated with complex animal models and assays to date. In the second part of this thesis a model for artificial tip cell formation on a flat surface is introduced. This model serves to elucidate cell-cell contact-dependent processes in a highly controllable and easy to handle setup.

The aim of this study was the creation and characterization of models based on structured surfaces to predict endothelial cell behavior in a highly controlled manner. These models are expected to lead the way to complex artificial *in vitro* systems, which have a higher predictive value than the current model systems.

3. Results

3.1 Micro-tracks as a tool to study endothelial cell migration

3.1.1 HUVECs on narrow tracks display less stress fibers and focal adhesions but pronounced cortical actin

The aim of this thesis was to mimic endothelial 3D migration with artificial guidance cues [**Fig. 3.1A**]. As a first step, the behavior of HUVECs migrating on tracks of different widths was characterized in order to study overall cellular behavior and to adjust conditions for further experiments. The lamellipodal formation was stepwise reduced with decreasing
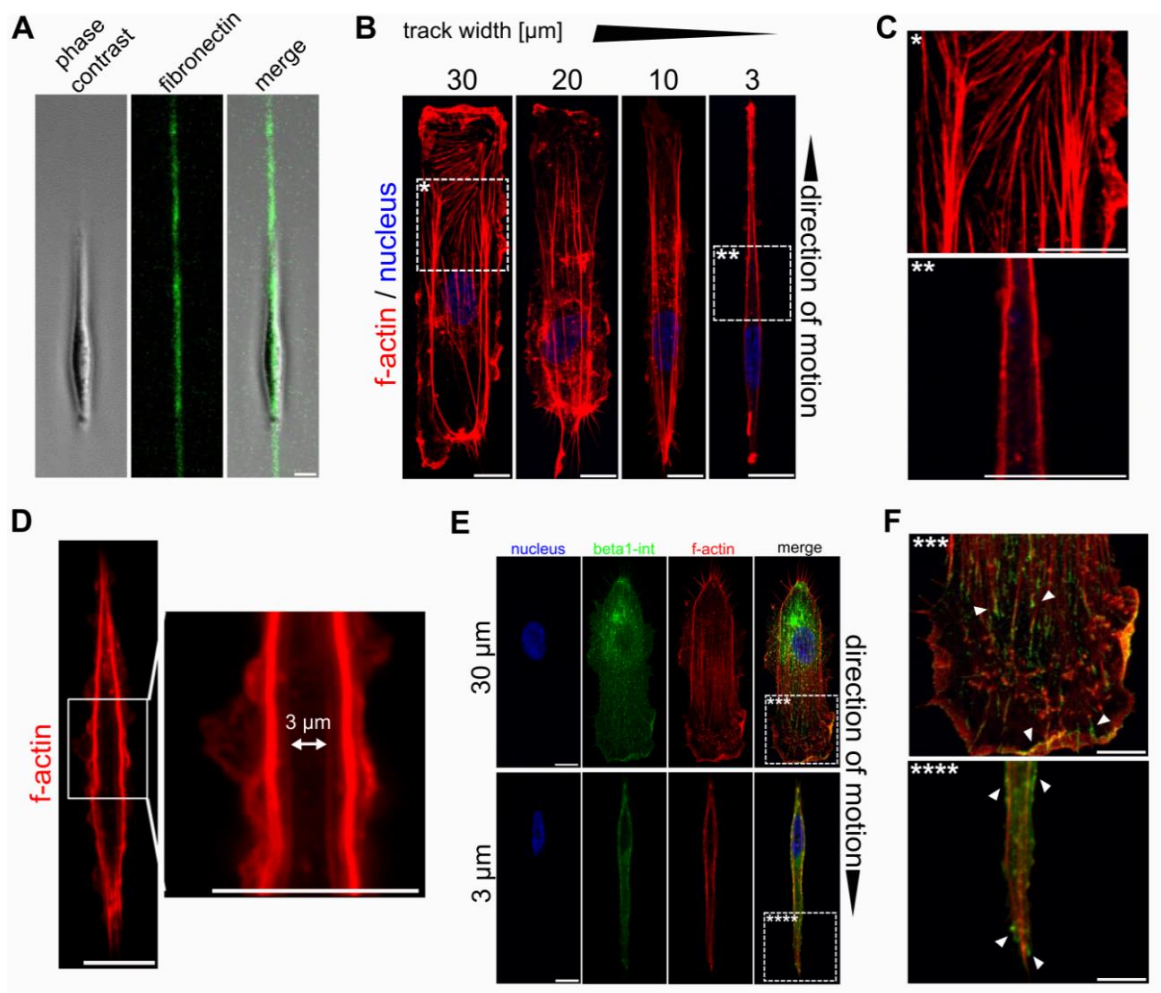
Fig. 3.1 Characterization of HUVECs migrating under confinement.
(**A**) Representative HUVEC migrating on a DyLight488-labeled fibronectin, 3 µm wide track.
(**B**) Comparison of HUVECs migrating on tracks of 3, 10, 20, and 30 µm width. Cells were fixated with 4 % pFA, 20 hours after seeding and stained for f-actin and nuclei. (**C**) Magnification of areas marked in (B) of cell migrating on a 30 µm wide track (*) and on a 3 µm wide track (**).
(**D**) Railroadfibers of HUVEC migrating on a 3 µm wide track. Cell was stained for f-actin.
(**E**) HUVECs on 3 and 30 µm wide tracks stained for nuclei (blue), beta1-integrin (green), and f-actin (red). (**F**) Magnification of areas marked in (E) of HUVEC on 30 µm wide track (***) and 3 µm wide track (****). White arrowheads mark focal adhesions at the leading edge and at the lamellum. Bars equal 10 µm.

track width as expected [**Fig. 1B**]. Furthermore, cells migrating on 30, 20, and 10 µm wide tracks showed a high amount of stress fibers being distributed over the whole cell body [**Fig. 3.1B, 3.1C**]. In contrast, cells seeded on 3 µm wide tracks exhibited pronounced bundles of cortical actin and characteristic "railroad fibers", bordering the micro-structures [**Fig. 3.1D**]. Additionally, cells on broader tracks (> 3 µm) displayed a high amount of lateral lamellipodia while cells on 3 µm wide tracks possessed a very small pseudo-lamellipodium at the leading edge and no or only few lateral lamellipodia, indicated by f-actin (fibrillary actin) staining [**Fig. 3.1B, 3.1C**]. As a reduced amount of stress fibers was observed on 3 µm wide tracks, cells were stained for focal adhesion complexes. For this purpose an antibody against β1-integrin was used. β1-integrin is responsible for fibronectin binding in complex with α5-integrin (Yang et al. 1993). Confirming our expectations, a reduced amount of focal or nascent adhesions was observed on 3 µm wide tracks compared to 30 µm wide tracks [**Fig. 3.1E, 3.1F**].

3.1.2 Golgi and centrosome localization of HUVECs is regulated independently in confined environments

As Doyle and colleagues showed a different centrosome localization for 2D migrating fibroblasts and cells migrating under confinement (Doyle et al. 2009), this was investigated for ECs. Moreover, Golgi complex orientation in cells under confinement was examined as it was done with Bsc1 cells before (Pouthas et al. 2008). To ensure better comparability, cells were seeded on both 3 µm (1D) and 30 µm wide tracks. On the wider tracks cells generally had a broad leading edge with a defined migration direction, but a morphology similar to cells in 2D environments [**Fig. 3.2**]. On 30 µm wide tracks, the Golgi was located laterally to the nucleus [**Fig. 3.2A**]. On narrow 3 µm wide tracks the Golgi complex was predominantly found laterally to the nucleus [**Fig. 3.2B**]. Only occasionally, the Golgi was located behind the nucleus, near the trailing edge. In contrast to this, centrosome orientation changed upon confinement. On 30 µm wide tracks, the centrosomes were predominantly located laterally to the nucleus [**Fig. 3.2C**] even though the values displayed a higher variance compared to the data describing Golgi orientation. On narrow 3 µm wide tracks, the centrosomes were mainly located behind the nucleus near the trailing edge. During relaxation of the cell on 3 µm wide tracks (e.g. during a directional reorientation), the cellular polarity was lost as described in section 3.1.5 in more detail. On 3 µm wide tracks this resulted in a switch of the centrosome from a posterior to a lateral position in relation to the nucleus (data not shown).

Fig. 3.2 Position of the centrosome and Golgi in confined environments. Position of the Golgi complex in relation to the nucleus center of HUVECs on (**A**) 30 µm wide tracks and (**B**) on 3 µm wide tracks. The position of the centrosomes in relation to the nucleus is shown for HUVECs migrating on (**C**) 30 µm wide tracks and (**D**) on 3 µm wide tracks. White arrowhead mark centrosome. 45 cells were analyzed per setting. Images for quantification obtained from three individual experiments. Bars equal 10 µm.
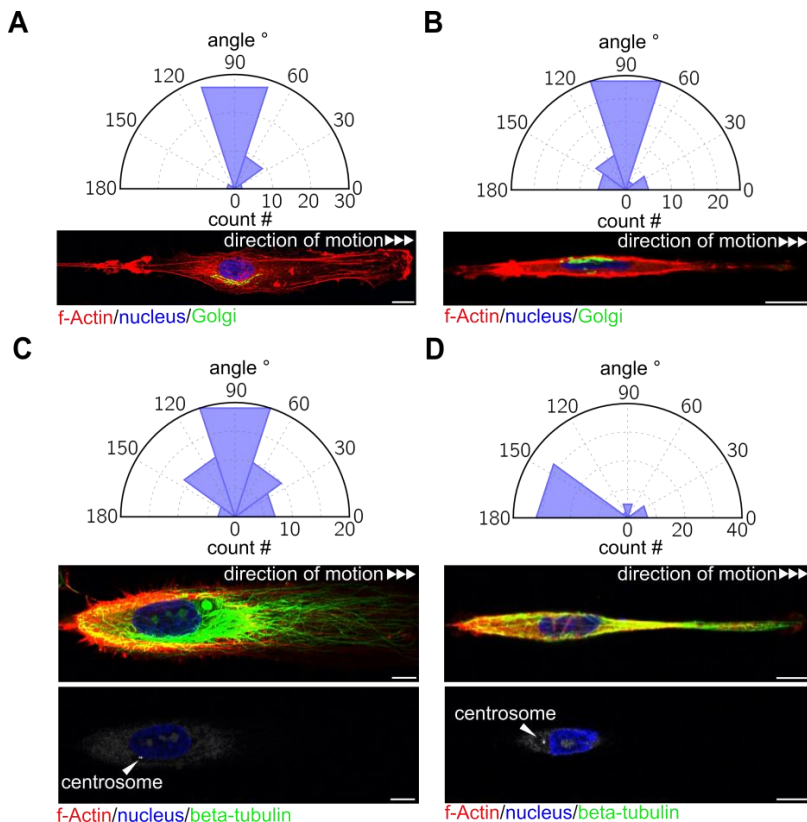
3.1.3 HUVECs on 3 µm wide migration tracks display a compressed nucleus shape

The nucleus is considered to play a pivotal role in cell migration in confined spaces as it is much stiffer compared to the residual components of the cell (Dahl et al. 2008). Consequently, the shape of the nucleus under confinement was characterized [**Fig. 3.3**]. For that purpose the shape factor of various nuclei was determined, by calculating the quotient of two diameters (d_1 and d_2) perpendicular to each other. A perfect circle possesses a shape factor of 1. Nuclei of HUVECs seeded on 3 µm wide tracks were very significantly elongated (shape factor close to 0) compared to nuclei of cells on 30 µm wide tracks [**Fig. 3.3A**]. Cells seeded on fibronectin 2D plastic surfaces showed a significantly rounded morphology compared to cells on 3 µm wide tracks [**Fig. 3.3A**]. The differences in shape of nuclei of cells on 30 µm wide tracks compared to cells in 2D were mild but robust. Additionally, an alteration of chromatin condensation in nuclei of cells on 3 µm wide tracks was observed. The characteristic "railroad fibers" carved into the nucleus, caused a local increase in chromatin condensation, visualized by Hoechst staining [**Fig. 3.3B**]. This effect has been exclusively observed in cells on 3 µm wide tracks. On broader tracks condensed chromatin was evenly distributed. Importantly, solely polarized cells which have been classified as migrating at the time point of fixation were analyzed [**Fig. 3.3**]. Conceivably, nuclear shape might additionally change on narrow 3 µm wide tracks, during relaxation of the cell e.g. being induced by a directional reorientation.
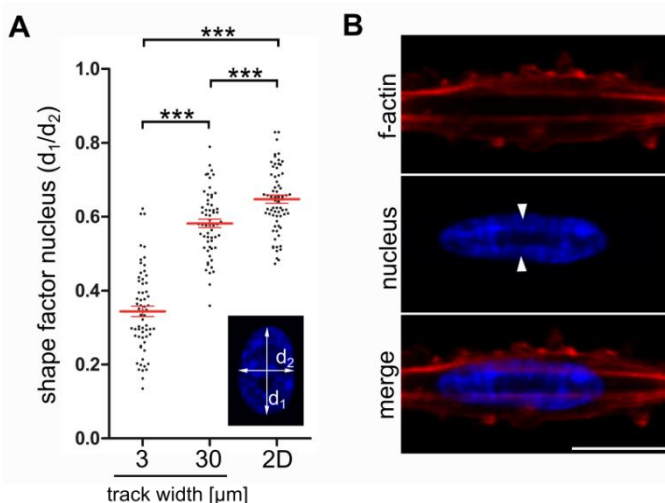
Fig. 3.3 Impact of confinement on the nucleus shape.
(**A**) Nucleus shape factor of HUVECs migrating on 3 µm wide tracks, 30 µm wide tracks, and on a fibronectin coated surface (2D). n = 3; Mean ± SEM; t-test p***< 0.001. (**B**) Railroad-fibers induce locally enhanced condensation of chromatin in the nucleus (arrowheads). Cells were stained with rhodamine-phalloidin and Hoechst 33342 for visualization of f-actin and nuclei, respectively. Bar equals 10 µm.

3.1.4 HUVECs migrate less efficient in 1D environments

As reduced lateral spreading is thought to favor a fast and directed fibroblast migration (Doyle et al. 2009), migration parameters of HUVECs migrating on tracks with different widths were analyzed. Surprisingly, cells migrating on broader tracks (20 µm and 30 µm) showed a significantly higher mean velocity compared to cells migrating on 3 µm wide tracks [**Fig. 3.4A**], even though cells on broader tracks displayed a high number of lateral lamellipodia as visualized by cortactin immuno-staining [**Fig. 3.4B**]. Additionally, directionality calculated from the quotient of total cell displacement and total trajectory length was assessed. Cells migrating on thin 3 µm and 10 µm wide tracks changed their direction more frequently during the migration process in comparison to cells on wider tracks [**Fig. 3.4C**]. As the narrow migration tracks mimic an environment with limited adhesion, the spreading area of cells on different track widths was quantified. A linear reduction of adhesion area was observed with decreasing track width [**Fig. 3.4D**]. Kymographic analysis of cells migrating on 3 µm wide tracks revealed that cells displayed a very high dynamic fluctuation in the leading and trailing edge [**Fig. 3.4E**]. In contrast cells on 30 µm wide tracks protruded and retracted very evenly over the observation time [**Fig. 3.4F**]. As both directionality and mean velocity decreased on thinner tracks, the contribution of the low directionality to the low mean velocity was assessed. This is necessary, as frequent cell stops during the migration process result in a strongly reduced mean velocity, even though the cells might not migrate slower between two reorientation phases. For this purpose a change point analysis (bimodal analysis) was performed, dissecting cell trajectories in migration phases (=run) and orientation phases (=rest) [**Fig. 3.4G**] (performed in cooperation with Prof. Joachim Rädler, LMU Munich). This allowed the calculation of run velocities comprising only the migration phases in between two orientation phases. In addition, persistence times were calculated by survival function analyses. In addition to changes in mean velocity of cells migrating on different track width, a reduction of run velocities on narrow migration tracks was observed [**Fig. 3.4H**].

Moreover, cells migrating on narrow tracks displayed a very low persistence time compared to cells migrating on wider tracks [**Fig. 3.4I**].
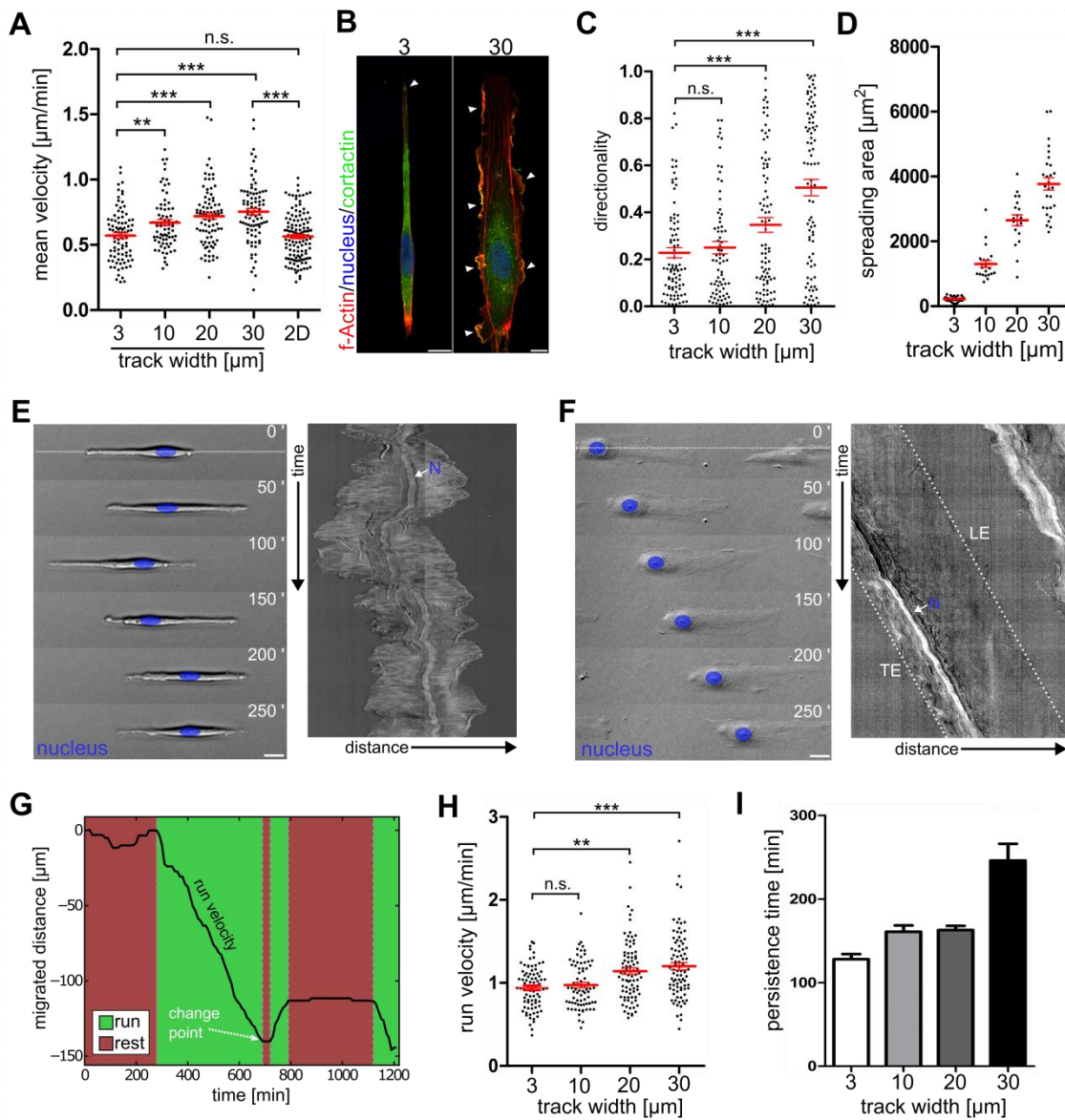
Fig. 3.4 Characterization of HUVECs migrating under confinement.
(**A**) Mean velocity of HUVECs migrating on tracks of different widths and 2D surfaces. (**B**) Confocal images of cells on tracks of 3 µm and 30 µm width stained for f-actin, nuclei, and cortactin. Bars equal 10 µm. (**C**) Directionality analysis of HUVECs migrating on different track widths. (**D**) Spreading areas of HUVECs on different track widths. (**E**) Representative HUVEC migrating on a 3 µm track at different timepoints with corresponding kymograph. Framerate: 2/min. Nucleus is marked in blue. (**F**) Representative HUVEC migrating on a 30 µm wide track at different time points with corresponding kymograph. Framerate: 2/min. LE = Leading edge; TE = Trailing edge; N = Nucleus. Nucleus is marked in blue. (**G**) Example of track analysed with the bimodal change point analysis. Green = run phases contributing to run velocity. Red = Rest phases were cells change direction and don't move. (**H**) Run velocity analysis of HUVEC migrating on different track widths. (**I**) Persistence time analysis calculated *via* survival function analysis. n = 3; Mean ± SEM. t-test p**<0.01; p***<0.001; n.s. = not significant.

3.1.5 Contractility as a fundamental regulator of motility and cell shape in 1D migrating cells – HUVECs in 1D switch between two morphological modes

The frequent changes of migration direction on 3 µm wide tracks were often accompanied by pronounced membrane blebbing. In contrast cells in the migration mode displayed a lamellipodium as cellular protrusion and only few or no blebs [**Fig. 3.5A; compare Movie S1 and Movie S2;** Movies are found on the compact disc attached to this thesis; Movie descriptions are in the appendix]. In order to visualize cytoskeletal dynamics of the differential cellular protrusions, cells were transfected with cortactin-GFP and LifeAct-RFP and seeded on 3 µm wide tracks. Cells in the migration phase showed strong membrane ruffling at the leading edge [**Movie S3**] while cells in the orientation mode displayed a common bleb expansion and retraction cycle [**Movie S4**]. As membrane blebbing is a result of high cortical contractility, contractile areas of the cytoskeleton were investigated. Therefore, cells on 3 µm wide tracks were immuno-stained with an antibody targeting the phosphorylated and thus active form of the myosin light chain (ppMLC). Cells in the orientation mode displayed a very high cortical contractility over the whole cell body. In contrast, cells in the migration mode displayed contractility exclusively at the trailing edge [**Fig. 3.5B**]. The high contractility in the orientation mode was accompanied with reduction of cell length as a strong correlation of cell length and the total number of membrane blebs was observed [**Fig. 3.5C**]. As the two modes displayed two different contractile states, cells were treated with Blebbistatin, a myosin II inhibitor (Kovács et al. 2004), and Calyculin A, a compound which enhances contractility (Ishihara et al. 1989). Subsequently, migration trajectories and cellular morphologies were analyzed and compared. Surprisingly, mean velocity of 1D migrating cells was significantly reduced after both Blebbistatin (by 34 %) and Calyculin A treatment (by 17 %) [**Fig. 3.5D**]. In line with our expectations, Calyculin A treated cells showed a reduced cell length [**Fig. 3.5E**] and enhanced cell bleb formation in comparison to control cells [**Fig. 3.5F**]. In contrast, Blebbistatin treated cells displayed a strongly elongated and polarized morphology, harboring long cellular protrusions and a relatively small cell body compared to control cells [**Fig. 3.5E, 3.5F**]. As a connection between membrane blebbing and cellular reorientation was observed, cell trajectories were analyzed with regard to directionality in more detail. In the analysis, persistence of Blebbistatin treated cells was significantly increased (by 78 %), whereas Calyculin A treated cells tended to reorient more often reflected by a non-significant directness of cell migration [**Fig. 3.5G**]. However, a high contractile and thus un-persistent cell population might have been lost by treatment with Calyculin A. One indication for this is the observation that contraction was accompanied with decreasing spreading area after Calyculin A treatment [**Fig. 3.5E**].
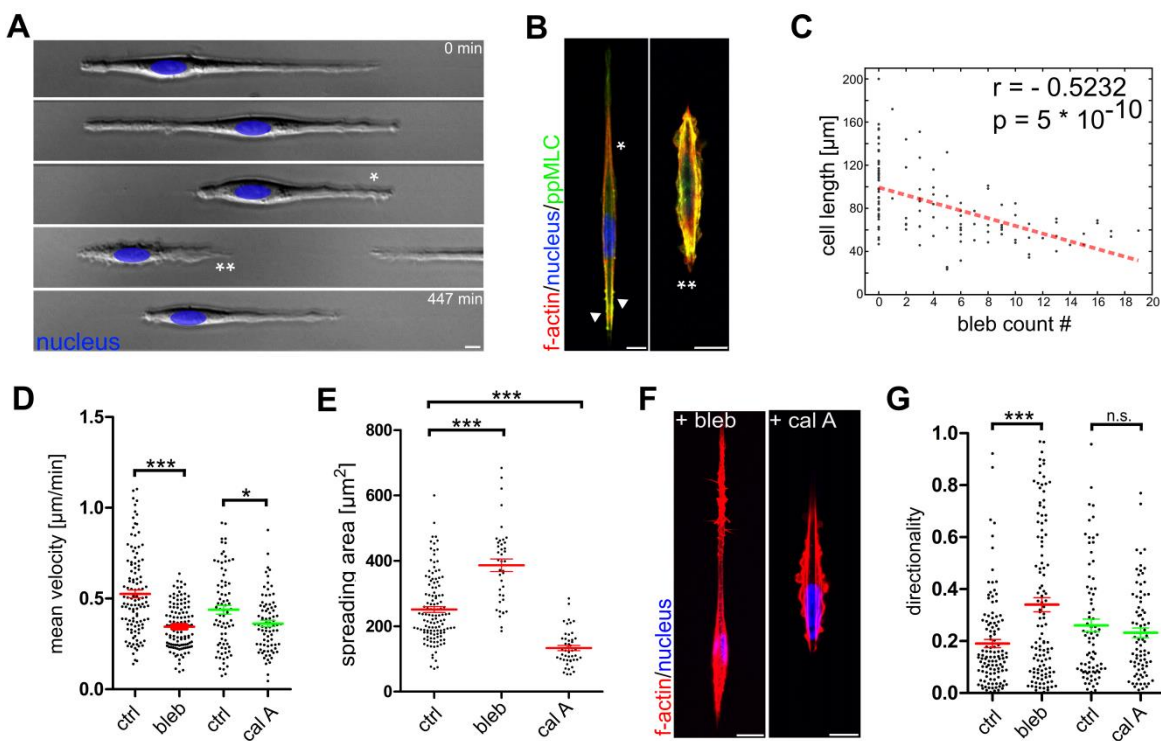
Fig. 3.5 Role of contractility for HUVECs migrating on 1D microtracks.
(**A**) HUVEC migrating on a 3 µm wide track display different morphologies: a lamellipodium based migration mode (*) and a bleb-based reorientation mode (**). (**B**) HUVEC in migration and reorientation mode immuno-stained for phosphorylated form of MLC (ppMLC), nuclei, and f-actin. (**C**) Pearson correlation of cell length and number of blebs (r = - 0.5232; p = 5 * 10⁻¹⁰). Red line indicates data trend. (**D**) Mean velocity analysis of HUVECs migrating on 3 µm wide tracks. Cells were treated with 10 µM blebbistatin (bleb) or 250 pM Calyculin A (cal A), respectively. (**E**) Spreading area of cells on 3 µm wide tracks treated with 10 µM Blebbistatin or 250 pM Calyculin A, respectively (**F**) Representative images of cells treated with 10 µM Blebbistatin or 250 pM Calyculin A, respectively. 20 hours after seeding cells were fixated with 4 % pFA and stained for nuclei and f-actin. (**G**) Directionality analysis of HUVECs migrating on 3 µm wide tracks treated with 10 µM Blebbistatin or 250 pM Calyculin A, respectively. n = 3; Mean ± SEM. t-test $p^* < 0.05$; $p^{***} < 0.001$; n.s. = not significant. Bars equal 10 µm.

3.1.6 HUVECs migrating on 2D surfaces move faster but less persistent upon contractility inhibition

To further compare aspects of the newly established 1D cell migration system to a conventional 2D system, cells migrating on fibronectin-coated plastic surfaces were treated with Blebbistatin or Calyculin A. Subsequently migration trajectories and cellular morphologies were analyzed and compared. The identification of appropriate compound concentrations was achieved by performing scratch assay analyses. Blebbistatin did not interfere with cell migration, independently of the applied concentration [**Fig. 3.6A**]. In contrast, Calyculin A inhibited cell migration in concentrations of 0.2 to 0.5 nM [**Fig. 3.6B**]. To further investigate cellular reaction of HUVECs in 2D environments to Blebbistatin and Calyculin A treatment, experiments were performed on a single cell level. Remarkably, HUVECs treated with Blebbistatin showed a very strong morphological reaction, resulting

in formation of numerous lateral protrusions and lamellipodia [**Movie S5**] in comparison to control cells [**Movie S6**; **Fig. 3.6C**]. In contrast, Calyculin A treated cells displayed a circular morphology and formed cell blebs very sporadically (data not shown). Further analysis of cells migrating in 2D revealed some striking differences in comparison to cells migrating in 1D (see section 3.1.5). In the 2D system ECs were slightly faster after Blebbistatin treatment compared to control cells (13 %) while cells treated with Calyculin A migrated slower by 48 % [**Fig. 3.6D**]. Analysis of directionality revealed that both Blebbistatin and Calyculin A treated cells migrated less persistently (34 % and
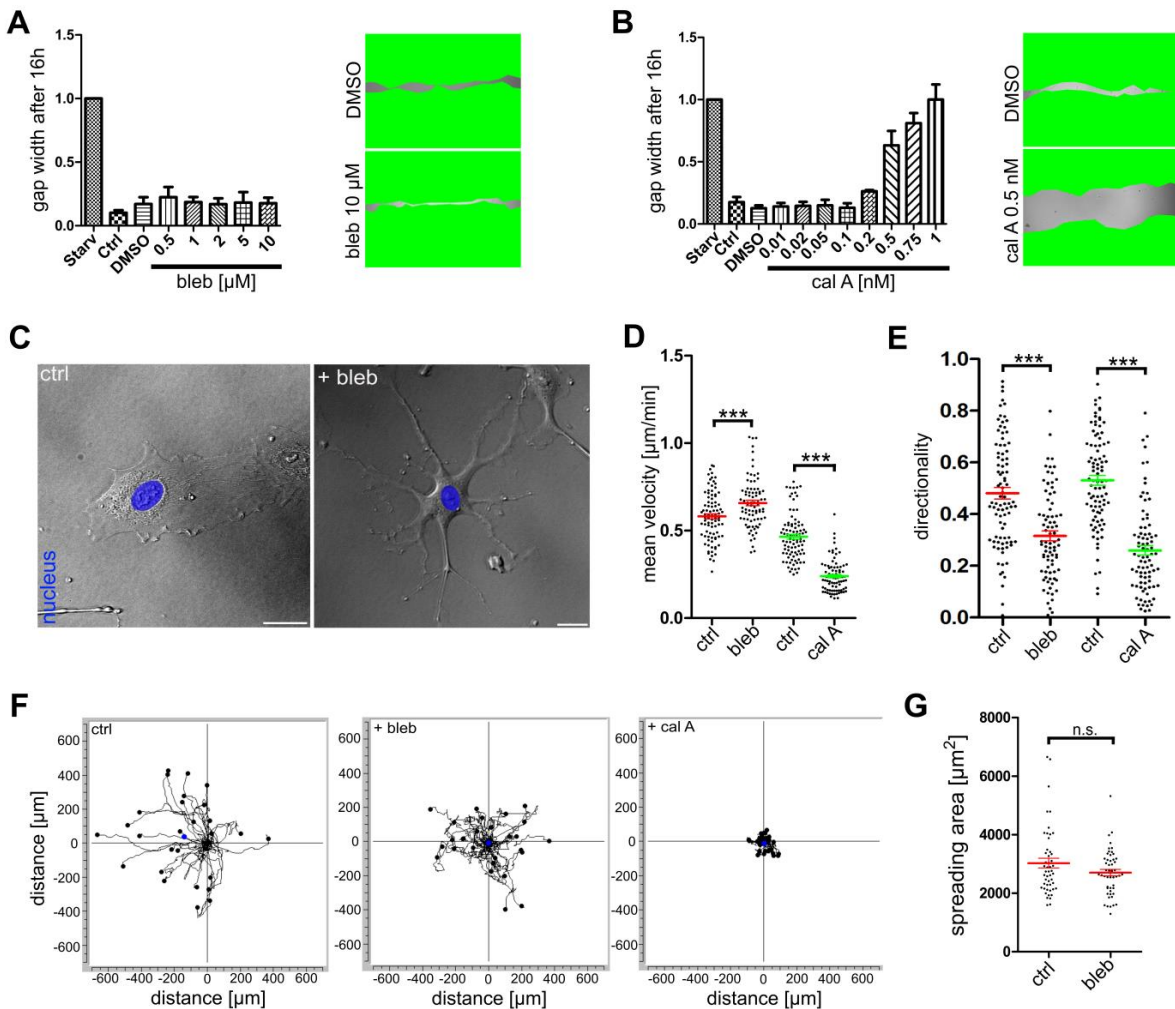
Fig. 3.6 Role of contractility for HUVECs migrating in 2D.
(**A**) Scratch assay analysis with various concentrations of Blebbistatin (bleb). Representative images for cells treated with 10 µM Blebbistatin and corresponding control. Cell covered areas are displayed in green. Starv = starvation control. (**B**) Scratch assay analysis with various concentrations of Calyculin A. Representative images for cells treated with 500 pM Calyculin A and corresponding control control. Cell covered areas are displayed in green. Starv = starvation control. (**C**) DIC images of HUVEC treated with 10 µM Blebbistatin and respective control cell (**D**) Mean velocity analysis of cells migrating on fibronectin coated 2D surfaces. (**E**) Directionality analysis of HUVECs on 2D surfaces treated with 10 µM Blebbistatin or 250 pM Calyculin A, respectively. (**F**) Trajectories of HUVECs treated with Blebbistatin or Calyculin A. (**G**) Quantification of spreading area upon Blebbistatin treatment and respective controll cells. n =3; Mean ± SEM. t-test p***<0.001. Bars equal 10 µm.

51 %, respectively) [**Fig. 3.6E**]. The corresponding trajectories of these analyses are displayed in **Fig. 3.6F.** As an increased adhesion area was observed after Blebbistatin treatment in the 1D system (see section 3.1.5), the adhesion area after treatment was investigated for cells in the 2D system. Quantification revealed no significant changes in adhesion area after Blebbistatin treatment [**Fig. 3.6G**].

3.1.7 HUVECs migrating in 1D and 3D share common morphological aspects

A switch of membrane protrusions was observed for HUVECs migrating on thin 1D micro-tracks. This raised the question whether this behavior is reflected in an *in vivo* like system. For this purpose cells were seeded in collagen I gels and their overall cytoskeletal architecture was compared to the phenotype of the cells migrating in the 1D system. For additional control, HUVECs seeded on planar, fibronectin-coated surfaces were analyzed [**Fig. 3.7**]. As described before, two main morphological phenotypes are distinguishable on 3 µm wide tracks [**Fig. 3.7A**]. On the one hand, elongated cells harboring a small lamellipodium at the leading edge were observed. On the other hand, many cells displayed a contracted and roundish phenotype, equipped with many cell blebs but no clear polarization or lamellipodium. In contrast, cells migrating on planar surfaces
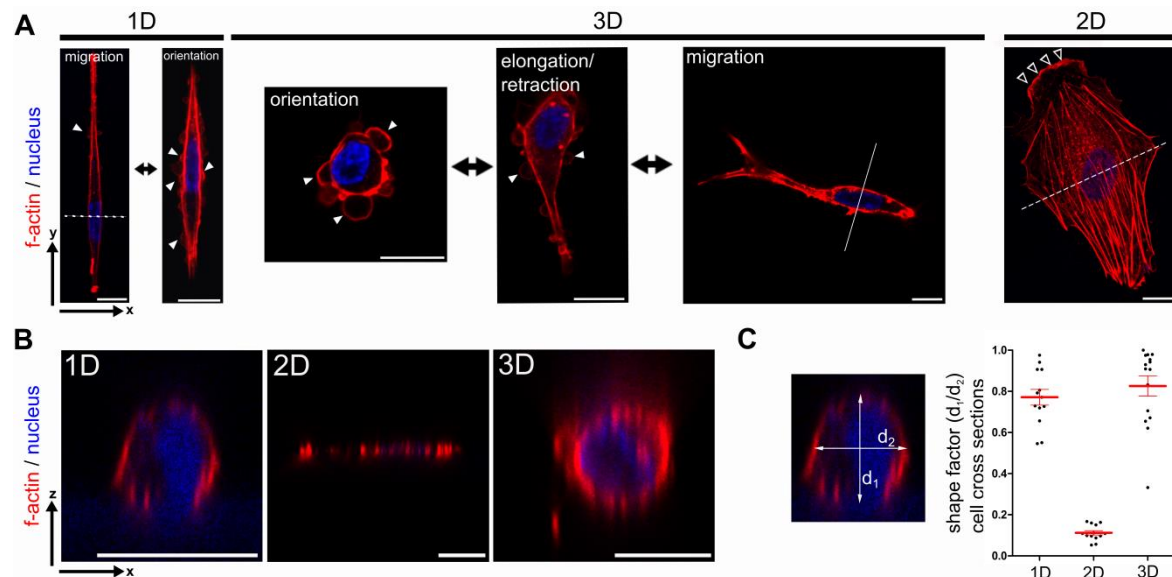
Fig. 3.7 HUVECs migrating in 1D and 3D share common morphological aspects. (**A**) Comparison of main morphologies of HUVECs migrating in 1D (3 µm wide fibronectin track), 3D (1 mg/ml Collagen I gel), and 2D (fibronectin coated plastic surface). 20 hours after seeding cells were fixated with 4 % pFA and stained with rhodamine-phalloidin and Hoechst 33342. (**B**) Cross section profiles of cells in 1D, 2D, and 3D. Cross sections were made in the area of the nucleus as indicated by dashed lines in (A). (**C**) Shape factor analysis of HUVECs in 2D and elongated cells in 1D and 3D. Mean ± SEM. 15 cross section profiles of independent cells were analysed in every setting. White arrowheads mark membrane blebs.

displayed a unimodal phenotype with a clear lamellipodium-based migration mode [**Movie S6**]. In the 3D fibrillary environment of a collagen I gel both mentioned phenotypes of cells migrating in 1D were observed [**Fig. 3.7A**]. One cell population displayed a roundish morphology without a clear cell polarization, equipped with numerous membrane blebs. A second cell population showed an elongated phenotype with only few or no cell blebs [**Fig. 3.7A**]. It is notable, that cells in both 1D and 3D settings contained no cytosolic stress fibers but very pronounced cortical actin bundles. These extreme forms of cell morphology do not reflect reality completely as intermediate cell morphologies which were elongated but still had cells blebs were detected in both 1D and 3D settings. Additionally, z-cross-section-profiles of cells in all three systems were compared to each other [**Fig 3.7B**]. Cells in the 1D system shared a similar cross-section profile compared to elongated cells in the 3D system as indicated by the shape factor analyses [**Fig. 3.7C**]. While cells in 2D displayed a flat and spread out phenotype, cells in both 1D and 3D environments shared a rounded cross-section profile. In order to visualize the contact area of cells to collagen I gels, collagen I was stained in combination with f-actin [**Fig. 3.8**]. The mean fiber width of the collagen I gel was approximately 400 to 600 nm, being six times smaller than the average track width of the described 1D system [**Fig. 3.8A-B**]. In contrast to non-migrating blebbing cells [**Fig. 3.8C**], clear actin cytoskeleton containing
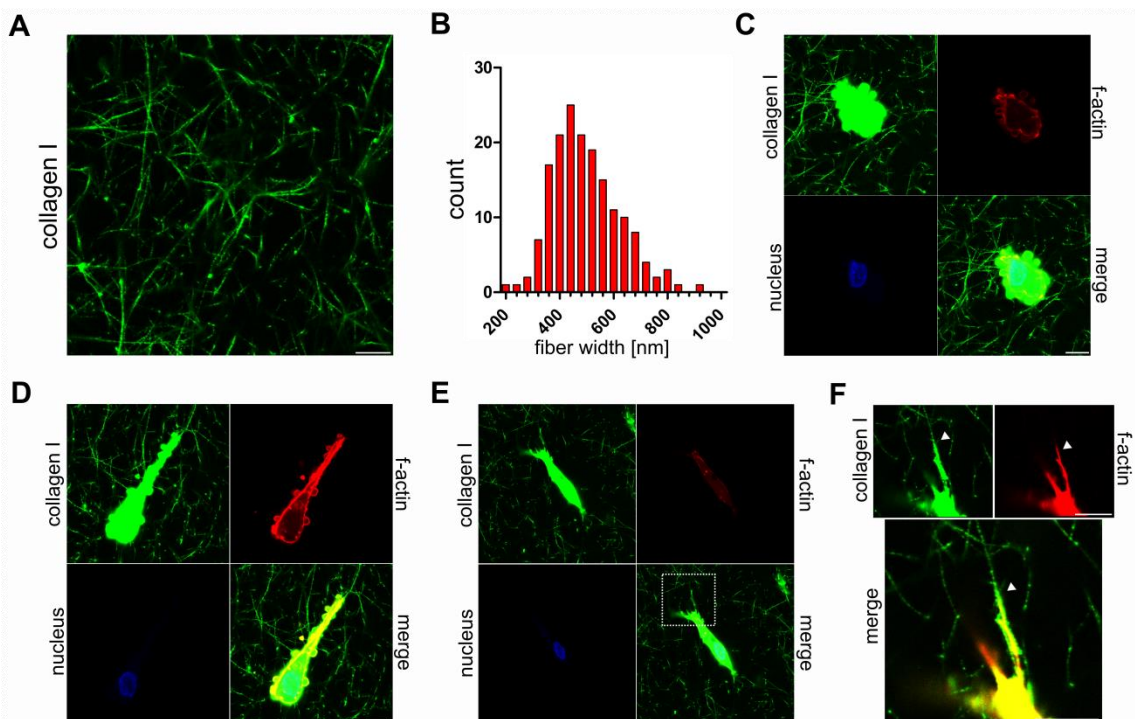
Fig. 3.8 Characterization of collagen I gel and its interaction with HUVECs.
(**A**) Confocal image of immuno-stained collagen I gel. (**B**) Fiber width quantification of immuno-stained collagen I gels. (**C**) Confocal image of a blebbing, non-migrating HUVEC stained for collagen I, nuclei, and f-actin. (**D**) Confocal image of a HUVEC in the retraction/elongation stained for collagen I, nuclei, and f-actin. (**E-F**) Migrating cell in collagen gel. White arrowhead mark actin protrusions. Bars equal 10 μm.

extensions were observed in the elongated morphology of 3D migrating cells. These extensions were clearly overlapping with the collagen I staining [**Fig. 3.8E-F**]. Protrusions of intermediate cell morphologies, presumably in the retraction or elongation process, were sometimes parallel to a collagen I fiber, too [**Fig. 3.8D**].

3.1.8 HUVECs migrating in a fibrillary 3D environment show morphological transitions comparable to HUVECs migrating in 1D.

ECs displayed a bimodal behavior on micro-tracks (see section 3.1.5). Next, it was questioned whether micro-tracks can be used as a tool to predict the impact of
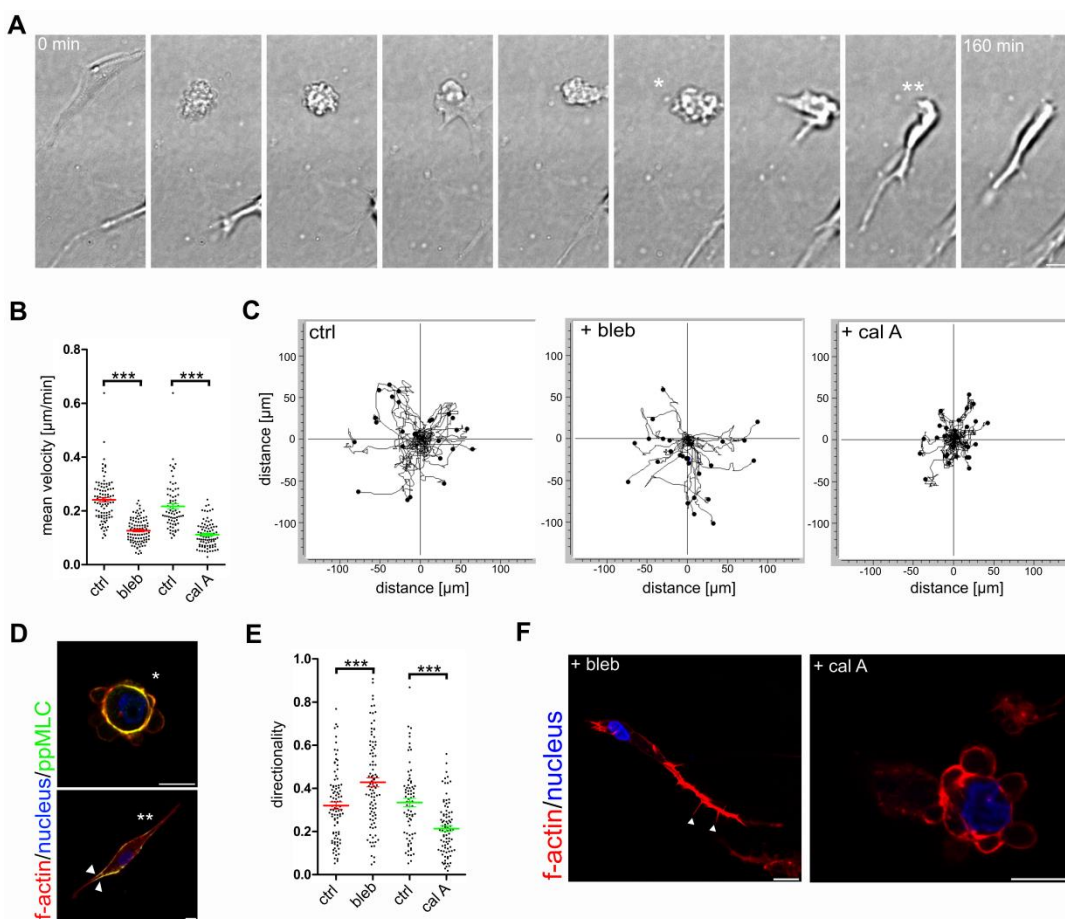
Fig. 3.9 HUVECs migrating in a fibrillary 3D environment show morphological transitions comparable to HUVECs migrating in 1D.
(**A**) Differential interference contrast images of a cell migrating in a collagen I gel revealing switches between bleb (*) and non-bleb (**) based cell morphology. (**B**) Mean velocity analysis of HUVECs migrating in a 1 mg/ml collagen I gel treated with 10 μM Blebbistatin or 500 pM Calyculin A, respectively. (**C**) Representative cell trajectories of cells migrating in a collagen I gel treated with Blebbistatin or Calyculin A. (**D**) HUVECs in collagen I gel stained for phosphorylation of the myosin light chain (ppMLC), f-actin, and nuclei. (*) round, bleb-based morphology, (**) elongated migration morphology. (**E**) Directionality analysis of HUVECs after treatment with 10 μM Blebbistatin and 500 pM Calyculin A, respectively. (**F**) Cells in collagen I gels treated with 10 μM Blebbistatin or 500 pM Calyculin A, respectively, and stained for f-actin and nuclei. White arrowheads mark thin filamentous protrusions. n = 3. Mean ± SEM. t-test; p***<0.001; Bars equal 10 μm.

contractility influencing compounds to cell migration in 3D. Here, mean velocity, directionality, and morphology were considered. Live cell imaging of cells migrating in collagen I gels revealed that switching of the round, bleb-based morphology into the elongated morphology occurs highly dynamic [**Fig. 3.9A**; **Movie S7**]. To differentiate between these two contractile modes, cells in collagen I gels were immuno-stained for the phosphorylated and thus active form of the myosin light chain. Round, blebbing cells possessed a high cortical contractility while elongated cells showed contractility exclusively in the presumable trailing edge [**Fig. 3.9D**] (images provided by Kerstin Kick). In tracking analysis of cells migrating in collagen I gels, a reduced mean velocity with both Blebbistatin and Calyculin A treatment was observed (reduced by 47 % and 48 %, respectively) [**Fig. 3.9B**]. The corresponding trajectories are displayed in **Fig. 3.9C**. Analysis of directionality revealed, that Blebbistatin treatment leads to an increased directionality while Calyculin A treated cells move less persistent [**Fig. 3.9E**]. Upon Blebbistatin treatment, cells reacted with profound elongation of a single cellular protrusion and obtained a very elongated morphology with a few very thin lateral protrusions [**Fig. 3.9F; Movie S8**]. In contrast to this, Calyculin A treated cells failed to elongate along collagen fibers and switched more often into the round bleb-based morphology [**Fig. 3.9F; Movie S9**].

3.1.9 Impact of actin cytoskeleton disruption on cell motility in 2D, 1D, and 3D

The actin cytoskeleton plays a fundamental role in cell migration. Therefore, the impact of actin cytoskeleton influencing compounds was investigated in regard to changes in migration. Cytochalasin D, a compound known to have a disrupting influence on the actin cytoskeleton was applied (Schliwa 1982). Additionally, an inhibitor of Ezrin was used. Ezrin is a member of the Ezrin/Radixin/Moesin (ERM) family and an important linker between actin and the plasma membrane (Gautreau et al. 1999). In order to adjust compound concentrations, scratch assays were performed using various concentrations of the two mentioned inhibitors. Cytochalasin D showed an inhibition of cell migration in a concentration range of 50 to 500 nM within an observation window of 16 hours [**Fig. 3.10A**]. The Ezrin inhibitor NSC668394 displayed an inhibition of migration in a concentration range of 10 to 50 µM within 16 hours, in comparison to the respective DMSO control [**Fig. 3.10B**]. Cytochalasin D treated cells displayed a reduced amount of stress fibers, no clear leading edges, and a completely disrupted actin cytoskeleton architecture [**Fig. 3.10C**]. Trajectory analysis in single cell experiments revealed, that the mean velocity was decreased after treatment with 100 nM Cytochalasin D [**Fig. 3.10D**]. Also the Ezrin inhibitor NSC668394 reduced the mean velocity at a concentration of 25 µM in single cell analysis [**Fig. 3.10E**].
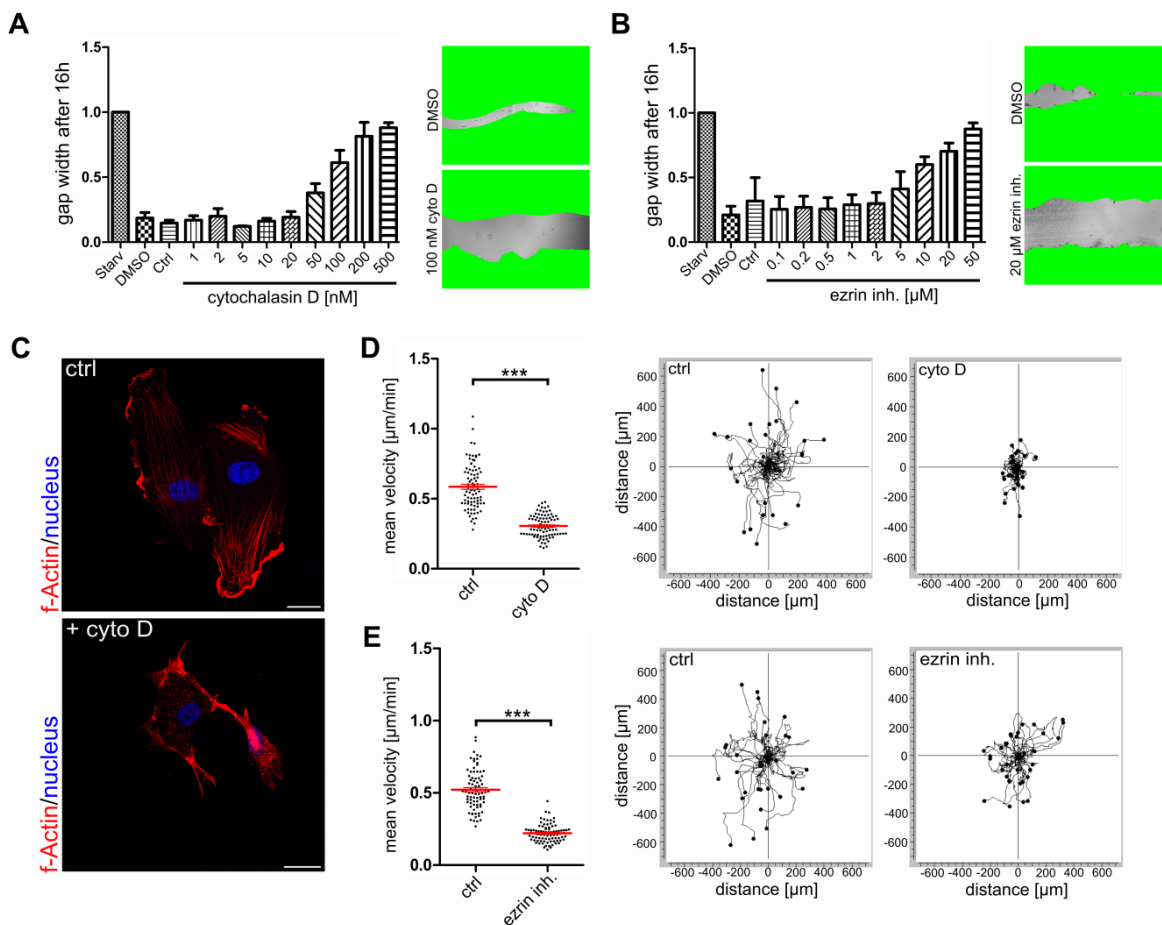
Fig. 3.10 Cytochalasin D and the Ezrin inhibitor NSC668394 reduce motility in 2D.
Scratch assay analysis with (**A**) the actin disrupting agent Cytochalasin D and (**B**) the Ezrin inhibitor NSC668394, respectively. Compounds were applied in various concentrations. Values were normalized to the starvation (starv) control. Images show representative images with cell-covered areas in green. (**C**) HUVECs were treated with 100 nM Cytochalasin D (cyto D) and fixated after 20 hours. Images show representative cells stained for f-actin and nuclei. Mean velocity analysis of cells treated with (**D**) 100 nM Cytochalasin D and (**E**) 25 µM Ezrin inhibitor NSC668394, respectively, with corresponding cell trajectories. n =3. Mean ± SEM. t-test; p***<0.001; Bars equal 20 µm.

Likewise, cells migrating on 3 µm wide tracks reacted to the disruption of the actin cytoskeleton very strongly [**Fig. 3.11**]. Cells treated with 100 nM Cytochalasin D displayed a significantly reduced mean velocity [**Fig. 3.11A**]. However, a stronger effect upon inhibition of Ezrin was observed for cells migrating on micro-tracks compared to the 2D system [**Fig. 3.11B**]. In total, cells were slowed down by 79 %. In **Fig. 3.11C** representative images of a Cytochalasin D treated cells and control cells are shown. In regard to actin morphology, the pronounced cortical actin and the characteristic railroad fibers were disrupted in compound treated cells.

In summary, in line with 2D and 1D, migration in 3D was decreased with both Cytochalasin D and the Ezrin inhibitor NSC668394. Mean velocity was strongly reduced with 100 nM Cytochalasin D [**Fig. 3.12A**] and 25 µM NSC668394 [**Fig. 3.12B**]. In 3D, cells completely failed to elongate along collagen fibers upon both Cytochalasin D and NSC668394 treatment.
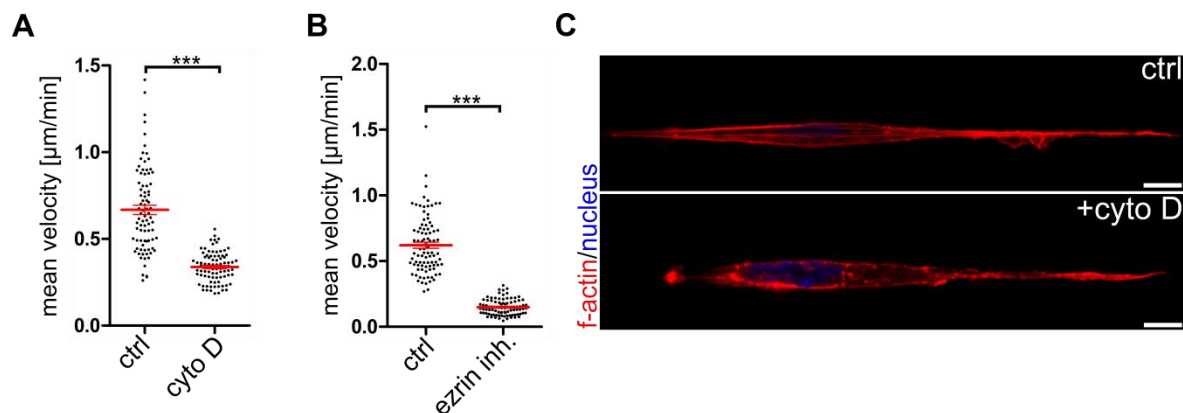
Fig. 3.11 Cytochalasin D and the Ezrin inhibitor NSC668394 reduce motility of HUVECs migrating in a 1D environment.
Mean velocity analysis of cells treated with (**A**) 100 nM Cytochalasin D and (**B**) 25 µM of the Ezrin inhibitor NSC668394, respectively. (**C**) Confocal images of HUVECs treated with Cytochalasin D and corresponding control. Cell were fixated 20 hours after seeing and stained for f-actin and nuclei. n = 3. Mean ± SEM. t-test; p***<0.001; Bars equal 10 µm.
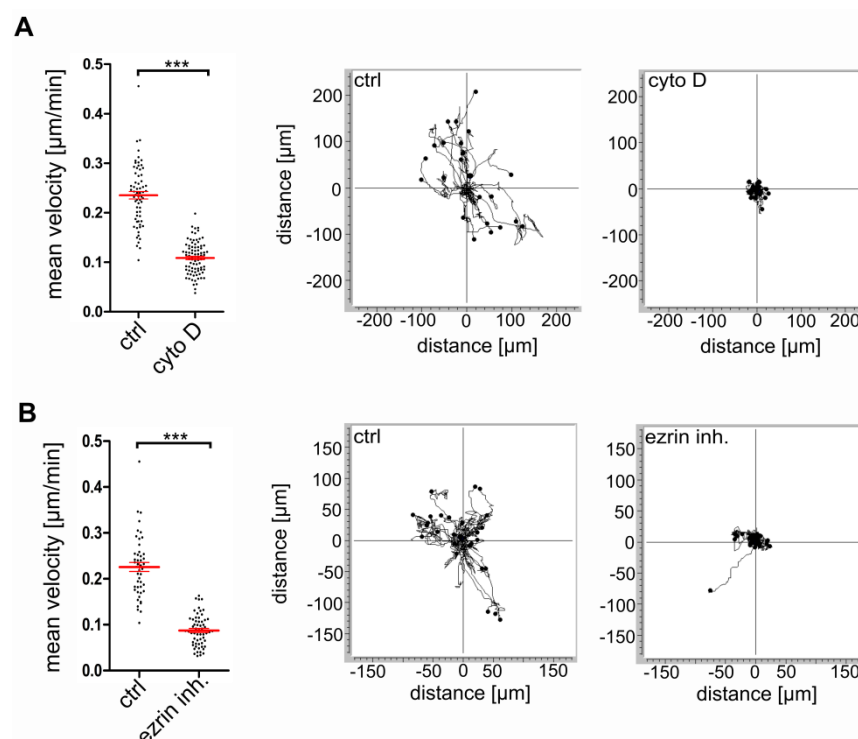
**Fig. 3.12 Cytochalasin D and the Ezrin inhibitor NSC668394 reduce motility of HUVECs migrating in a 3D collagen matrix.** (**A**) Mean velocity analysis of cells treated with 100 nM Cytochalasin D, with corresponding cell trajectories. (**B**) Mean velocity analysis of cells treated with 25 µM of the Ezrin inhibitor NSC668394, with corresponding cell trajectories. Mean ± SEM. t-test; p***<0.001.
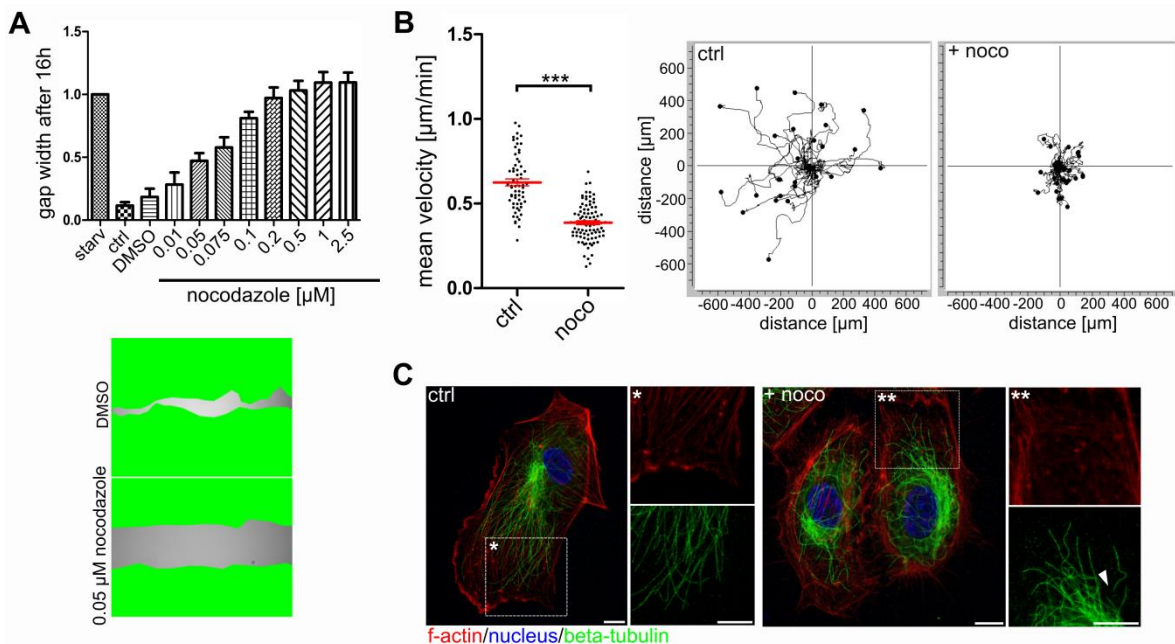
Fig. 3.13 Nocodazole reduces motility of HUVECs migrating in 2D.
(**A**) Scratch assay with the microtubule disrupting agent Nocodazole (noco) applied in various concentrations. Values were normalized to starvation (starv) control. Images show representative images with cell-covered areas in green. (**B**) Mean velocity analysis of single HUVECs treated with 50 nM Nocodazole and corresponding control as well as corresponding cell trajectories (**C**) Representative confocal images of HUVECs treated with Nocodazole and DMSO (ctrl). Cells were fixated 20 hours after treatment with glutaraldehyde after a MT washout assay was performed. Cells were fixated 20 hours after treatment. White arrowhead marks MT rupture. n =3. Mean ± SEM. t-test; p***<0.001. Bars equal 10 µm.

3.1.10 Nocodazole reduces cell motility in 2D and 3D systems but not in the 1D system

Beside actin filaments, also microtubules (MTs) as a component of the cytoskeleton play an important role in cell migration. Thus the importance of MTs in 1D, 2D, and 3D systems was tested by using the disrupting agent Nocodazole (Vasquez et al. 1997). In order to adjust compound concentration, a scratch assay was performed testing the effects of various concentration of Nocodazole [**Fig. 3.13A**]. Cell migration was inhibited in a concentration range of 10 to 200 nM [**Fig. 3.13A**]. Likewise, higher concentrations than 200 nM inhibited cell migration but additionally induced apoptosis. For further experiments, a concentration of 50 nM was used as a pronounced inhibition of migration [**Fig. 3.13A**], but no apoptotic cells were observed. In single cell tracking experiments the mean velocity was significantly reduced by 38 % [**Fig. 3.13B**]. The corresponding trajectories of an exemplary experiment are pictured in **Fig. 3.13B**. Cell morphology changed dramatically upon Nocodazole treatment, resulting in cells displaying a circular and unpolarized phenotype. Immuno-stainings of MTs revealed that 20 hours after Nocodazole treatment, MTs were disrupted in the periphery of the cell [**Fig. 3.13C**].

In the 1D system a disruption of MTs structure was induced in the periphery of the cell, near the leading edge by Nocodazole treatment (data not shown). However, observed effects were not as pronounced as in 2D. Migration experiments carried out on narrow migration tracks (1D) showed no significant effect in regard to mean velocity [**Fig. 3.14A**].

In collagen I gels (3D), treatment with 50 nM Nocodazole led to a decreased mean velocity (by 49 %) [**Fig. 3.14B, left panel**] as visualized by the corresponding cell trajectories [**Fig. 3.14B, right panel**]. After treatment, cells failed to elongate along collagen fibers and displayed an un-polarized, mostly multiaxial phenotype.
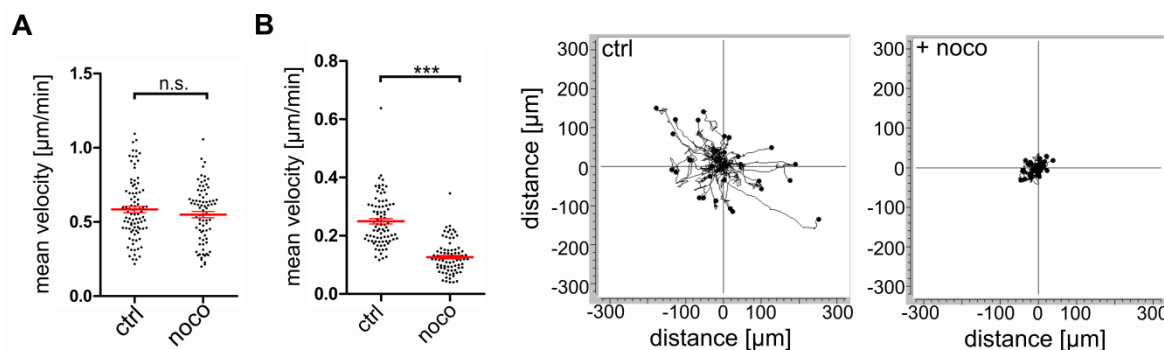
Fig. 3.14 Nocodazole reduces motility of HUVECs migrating in a 3D collagen I matrix but displays no effect on cells migrating in a 1D environment.
(**A**) Mean velocity analysis of HUVECs in 1D after treatment with 50 nM Nocodazole and corresponding control. (**B**) Mean velocity analysis of HUVECs in 3D after treatment with 50 nM Nocodazole and corresponding trajectories from single representative experiment. n = 3. Mean ± SEM. t-test; p***<0.001, n.s. = not significant.

3.1.11 The Rac1 inhibitor NSC23677 reduces motility of cells in 2D, but not in 1D and 3D systems

As Rac1 is one of the most important regulators of cell motility, the Rac1 inhibitor NSC23677 was used in a concentration of 50 µM, in order to elucidate the role of Rac1 in cell migration in 1D, 2D, and 3D systems. HUVECs migrating on flat surfaces (2D) showed a highly significant reduction of mean velocity after treatment with this inhibitor [**Fig. 3.15A**]. The corresponding trajectories from a single experiment are pictured in **Fig. 3.15B**. In contrast to the observation of cells in 2D, the migration behavior of cells in 1D was mildly but consistent altered upon Rac1 inhibition. A slight but significant reduction of mean velocity was observed [**Fig. 3.16A**]. Likewise, the behavior of 3D migrating cells was examined in more detail. In 3D, cells did not react very pronounced to Rac1 inhibition in regard to mean velocity as it was observed for migrating cells in 1D [**Fig. 3.16B**].
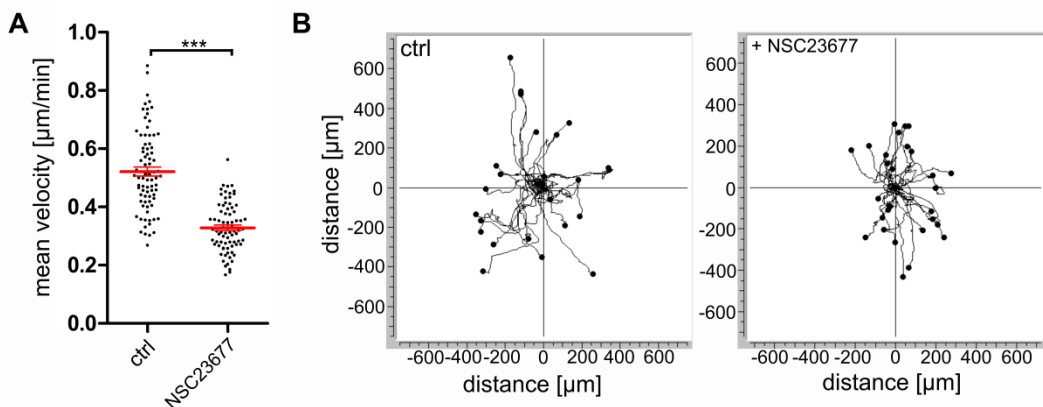
Fig. 3.15 The Rac1 inhibitor NSC23766 reduces motility of HUVECs migrating in 2D.
(**A**) Mean velocity analysis of HUVECs in 2D after treatment with 50 µM NSC23766 and corresponding control. (**B**) Trajectories from a single representative experiment of HUVECs treated with 50 µM NSC23766. n = 3. Mean ± SEM. t-test; p***<0.001.
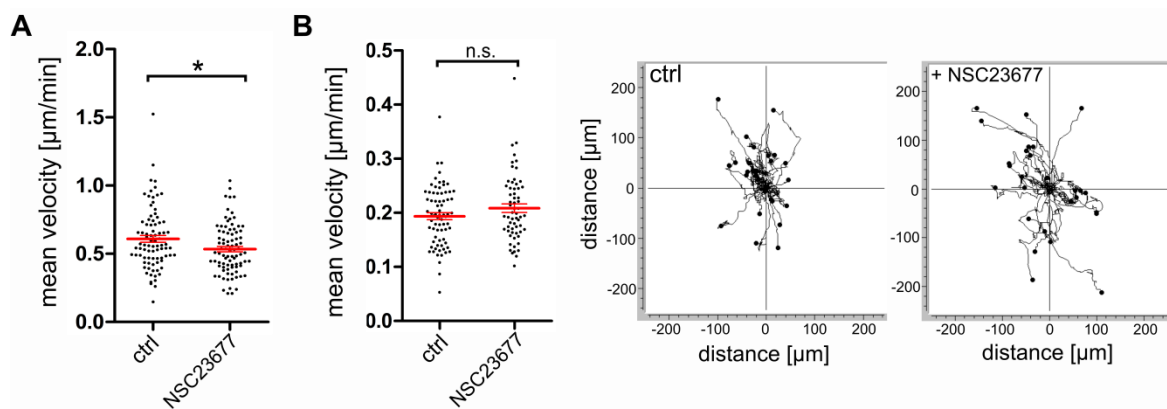
Fig. 3.16 The Rac1 inhibitor NSC23766 does not influence motility of HUVECs in the 1D environment and in a 3D collagen I matrix.
(**A**) Mean velocity analysis of HUVECs in 1D after treatment with 50 µM NSC23766 and corresponding control. (**B**) Mean velocity analysis of HUVECs in 1D after treatment with 50 µM NSC23766 and corresponding control. Trajectories are from a single representative experiment cells. n = 3. Mean ± SEM. t-test; p*<0.001 n.s. = not significant.

3.2 Closing the gap between *in vivo* and *in silico* - a novel approach of tip cell formation studies

3.2.1 The theory of tip cell formation combined with structured surfaces

Beside other factors, in theory, angiogenic sprouting requires the dynamic establishment of tip cells. These cells contain a specific set of receptors on their surface which are necessary to lead a sprout towards a hypoxic area (introduced in section 2.4). Basically, the formation of tip cells depends on the amount of cell-cell contacts, as the regulation of tip cell/stalk cell selection is Notch signaling dependent (Blanco and Gerhardt 2013) [**Fig. 3.17A**]. In this study, specific micro-structures were designed, harboring areas where cells are either able to develop a high amount or a limited number of cell-cell contacts [**Fig. 3.17B**]. Additionally, a branch was included in the geometry, which forces one specific cell to have exclusively one cell-cell contact in contrast to the other cells of the population [**Fig. 3.17B**]. Micro-contact printing was performed with labeled fibronectin in order to estimate and therefore guarantee the quality of the protein patterns [**Fig. 3.17C**]. The aim of this project was the establishment and characterization of a system which closes the gap between theoretic modeling and highly complex *in vivo* experiments. As VEGFR2 (Kdr) is the most prominent marker of tip cells, VEGFR2 regulation was evaluated for a cell population on the previously described pattern.
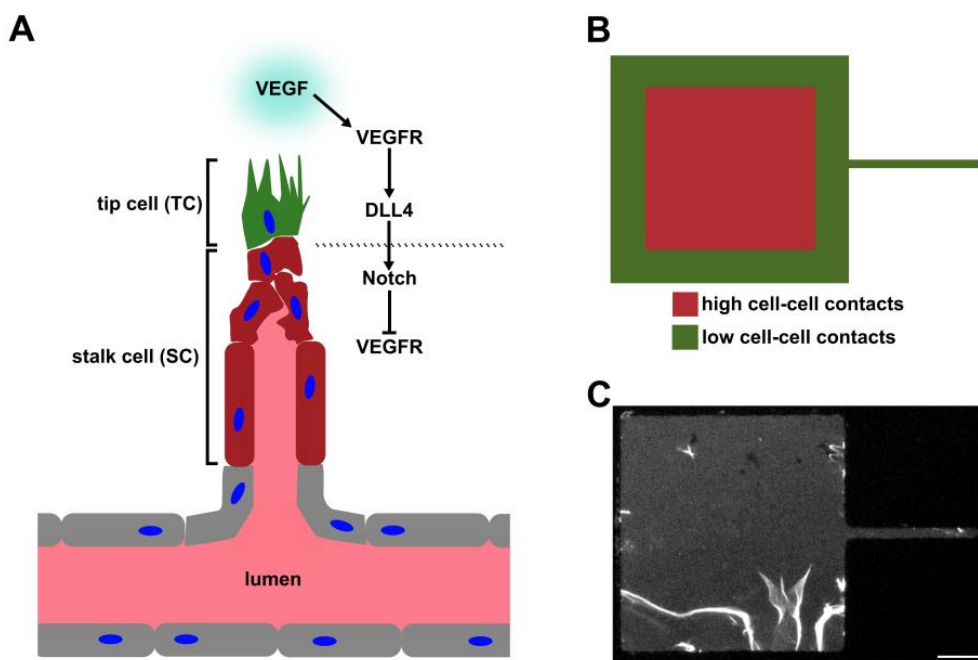
Fig. 3.17 Theory of tip cell formation combined with structured surfaces.
(**A**) Schematic representation of the theoretical background of tip cell formation (**B**) Geometry of the pattern used for tip cell formation studies (**C**) Geometry displayed in (B) brought to a surface by micro contact printing using DyLight488 labeled fibronectin. Bar equals 50 µm.

3.2.2 Regulation of VEGFR2 matches the theoretical background of tip and stalk cell formation

To evaluate the impact of our microstructures on VEGFR2 expression, cells were seeded on the micro-patterns as introduced in **Fig. 3.17**. One day after seeding the VEGFR2 protein level of the cells was variable within the cell population on the micro-pattern [**Fig. 3.18**]. In order to differentiate between cells used for the quantification, cells were stained for VE-cadherin which is mainly localized in the cell-cell contact areas. Cells expressing a high level of VEGFR2 always displayed a high amount of cytosolic VE-cadherin [**Fig. 3.18, left panel**]. It was observed that VEGFR2 expression was quite evenly distributed over the micro-pattern and can be found to a very high extend in the pattern branch [**Fig. 3.18, right panel**]. Seven days after cell cultivation this situation changed drastically, as only few cells possessed a high VEGFR2 level. VEGFR2 expressing cells were predominantly located in the areas allowing for a low number of cell-cell contacts [**Fig. 3.18**].
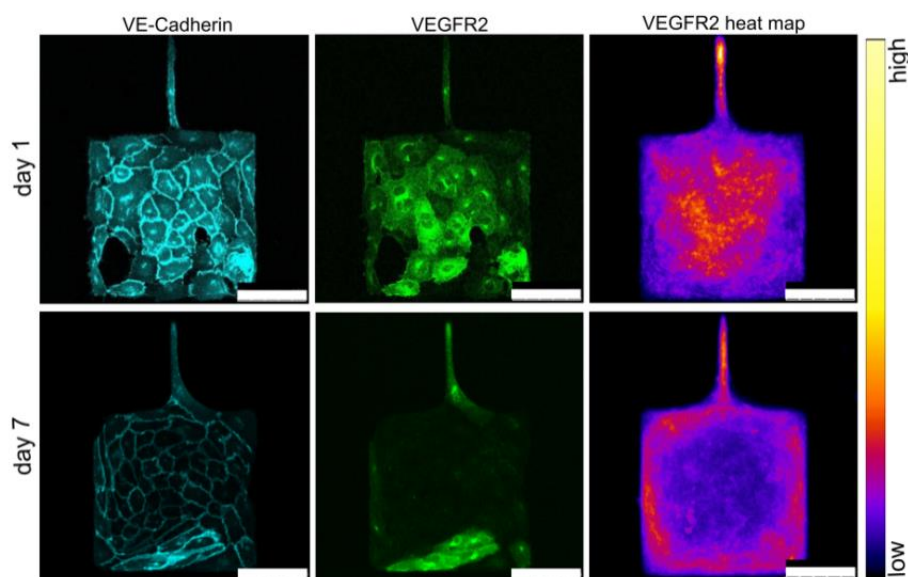
Fig. 3.18 Micro-patterns allow for modification of VEGFR2 expression patterns. Immuno-stainings of HUVECs seeded on micro-patterns (250x250 μm squares with 150 μm long and 10 μm wide branches). VEGFR2 heat map was created by adding up several images of VEGFR2 immuno-stainings. Subsequently, the intensity was encoded in false colors. Images were acquired with a Leica SP8 confocal microscope. Bars equal 100 μm.

3.2.3 VEGFR2 regulation in artificial tip and stalk cells is Notch signaling dependent

As a differential regulation of VEGFR2 expression levels was observed on micro-patterns, depending on the relative cell position, it was investigated if it is possible to block this behavior with the Notch signaling inhibitor dibenzazepine (DBZ). Cells in the tip position, possessing only one cell-cell contact were classified as a tip cell (TC) [**Fig. 3.19A**]. Cells

in direct contact to the tip cell were classified as a stalk cells (SC) [**Fig. 3.19A**]. To differentiate between single cells in intensity quantification, the cell-cell contact marker VE-Cadherin and VEGFR2 were co-stained. Intensity quantification without using DBZ revealed that tip cells expressed higher VEGFR2 levels compared to their corresponding stalk cells (negative value in transformed ratios; value of zero means no difference between tip and stalk cells, positive value means stalk cells possess more VEGFR2 intensity) [**Fig. 3.19B**]. This behavior was blocked by using DBZ, as treated cells showed a nearly equal expression of VEGFR2 between tip and stalk cells [**Fig. 3.19B**]. To prove that Notch signaling was inhibited within the observation time frame of 24 hours, a Western Blot analysis was performed for VEGFR2 and NICD, the cleaved and active form of Notch. The VEGFR2 expression levels in treated and control cells remained equal, while NICD was reduced upon treatment with 10 µM DBZ [**Fig. 3.19C**].
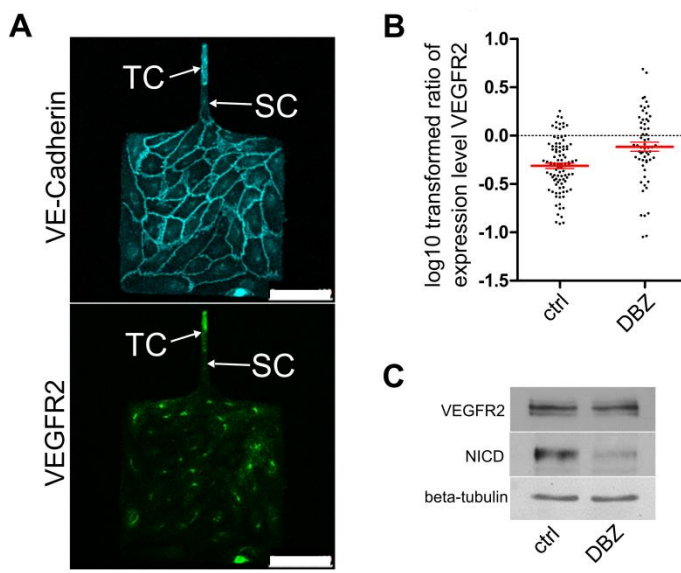
Fig. 3.19 VEGFR2 regulation in artificial tip and stalk cells is dependent on Notch signaling. (**A**) Exemplary images of HUVECs on microstructures stained for VE-Cadherin and VEGFR2. TC = Tip cell; SC = Stalk cell. (**B**) Log10 transformed VEGFR2 expression ratios of TCs and corresponding stalk cells. Ratio > 0 means stalk cells express more VEGFR2. Ratio < 0 means tip cells express more VEGFR2. n = 3 (**C**) Western Blot analysis of HUVECs treated with 10 µM DBZ and analyzed for NICD and VEGFR2. Beta-tubulin served as a loading control

4. Discussion

4.1 Micro-tracks as a model to study endothelial cell migration

4.1.1 Confined protein micro-tracks impact endothelial cell architecture

In all experiments of this study, cell shape and thus the actin cytoskeleton of ECs changed drastically with reduction of micro-track width [**Fig. 3.1B**]. In contrast to the observation of aligned stress fibers on rectangular shaped micro-patterns by others (Roca-Cusachs et al. 2008), cells in the experiments of this study formed pronounced cortical actin fibers and displayed a reduced stress fiber content with decreasing track width (**Fig. 3.1B**). The different observations are probably due to the different micro-pattern dimensions used in both studies. Likely, the reduced stress fiber content affects the g-actin to f-actin ratio within a cell in the 1D system in comparison to cells in 2D, which display a large amount of stress fibers [**Fig. 3.7A**]. The outcome of this ratio alteration might affect gene expression *via* actin sensitive pathways like the myocardin-related transcription factor (MRTF) pathway (Medjkane et al. 2009). Likewise, it is conceivable that stress fibers of cells on narrow tracks are bundled into cortical actin, changing their cellular localization with an increasing degree of confinement. This rearrangement has to be proven and can be investigated by using micro-patterns providing 1D to 2D transitions. The decreased spreading area on 3 µm wide tracks resulted in a more 3D-like morphology of the actin cytoskeleton and a pronounced membrane curvature as verified by cross section analysis [**Fig. 3.8B**]. This might have various molecular effects on the cell. For example it has been shown that GEFs and GAPs containing curvature sensing F-BAR domains (Heath and Insall 2008) are able to modulate Rac1 signaling and thus affect cell spreading and migration (de Kreuk et al. 2011). Moreover, the high amount of cortical actin is potentially induced by membrane curvature through F-BAR domain containing proteins influencing actin polymerization *via* N-WASP (Takano et al. 2008).

The pronounced cortical actin bundles of stretched endothelial cells on 3 µm wide tracks are responsible for nucleus deformation and altered chromatin condensation as described in this study [**Fig. 3.3**] and in a previous one (Versaevel et al. 2012). Nucleus deformation is the limiting factor for migration through confined 3D environments, as it is up to ten times stiffer than the residual components of a cell (Wolf et al. 2013). Both alteration of chromatin condensation as well as the high tensional stress exerted to the nucleus might affect gene transcription in the 1D setting (Pajerowski et al. 2007). Interestingly nuclei of cells on 30 µm wide tracks displayed a slightly stretched morphology as proven by shape factor analysis [**Fig.3.3**]. Nuclei of cells on 30 µm wide tracks are not subject of compression by cortical actin bundles as observed for cells on 3 µm wide tracks.

However, the deformation of the nucleus can possibly be explained through the alignment of actin [**Fig. 3.1B**] or microtubules [**Fig. 3.2**], as both are physically connected to the nucleus (Reinsch and Gönczy 1998; Dupin et al. 2011). In conclusion, micro-patterns are a great and simple tool to address questions of nucleus deformation and to investigate the underlying mechanisms.

The findings about Golgi and centrosome orientation on micro-structures [**Fig. 3.2**] were partly in accordance to other studies. On 30 μm wide tracks, a lateral assembly of the Golgi and the centrosomes was observed, pointing into the direction of the cell repellent surface. Lateral assembly of the Golgi on broad micro-patterns has been described for fibroblasts (Chen et al. 2013), but was still unknown for the centrosome to my knowledge. On 3 μm wide tracks, the position of the Golgi remained laterally to the nucleus, while the centrosome shifted to a sub-terminal position near the trailing edge [**Fig. 3.2**]. This is in contrast to another study performed with Bsc1 cells where the Golgi was also oriented behind the nucleus on thin migration tracks (Pouthas et al. 2008). However, the degree of confinement might play a pivotal role in this aspect as different migration track dimensions where used. The observed changes of centrosome orientation was in line with observations for other cell types like fibroblasts (Doyle et al. 2009) or the previously mentioned Bsc1 cells (Pouthas et al. 2008). In general, centrosomes and Golgi complexes orientate towards the leading edge in cells migrating in 2D environments (Yvon et al. 2002; Etienne-Manneville 2004). The findings of this study strengthened the role of spatial confinement as an important regulator for the orientation of the Golgi complex and centrosomes. It was demonstrated that confinement is more important for subcellular organization than the direction of movement. Moreover, the uncoupling of Golgi and centrosome upon confinement, and their independent spatial positioning as a reaction to confined spaces has not been described before. This provides a new insight into the diverse impacts of confinement on individual cell components.

4.1.2 A matter of adhesion? – Endothelial cells migrate less efficient on narrow micro-tracks

Migration velocity on 3 μm wide micro-tracks was slower in comparison to 2D cell migration and to migration on wider micro-tracks [**Fig. 3.4A**]. This is in contrast to a study using NIH3T3 fibroblasts, where an increased velocity of cells migrating in 1D, compared to cells migrating in 2D, was demonstrated (Doyle et al. 2009). Some studies investigated the migration velocity of ECs upon different migration track widths but are contradictory to each other, either providing evidence for a correlation (Lei et al. 2012) or excluding a possible relation (S Li et al. 2001). However, only few ECs were analyzed in the two

mentioned studies, providing no basis for a good statistic. Additionally, other substrate dimensions were used in both studies. The findings of this study are in line with previous data describing a coupling of cell mean velocity and persistence of a cell (Maiuri et al. 2012; Maiuri et al. 2015). This correlation is seen by the decreasing directionality with decreasing track width [**Fig. 3.4C**]. Since mean velocity is a parameter comprising the persistence of migration, and since frequent changes of run direction were observed on the thin lines, consequently run velocity and persistence times were analyzed with a bimodal change point analysis (in cooperation with Prof. Joachim Rädler, LMU Munich). Both parameters were in line with the conventional trajectory analysis [**Fig. 3.4G-I**], further supporting the assumption of a correlation of cell velocity and persistence of movement.

As a decreased spreading area was observed with decreasing track width [**Fig. 3.4D**], we suggested that a low adhesive environment might contribute to the low persistence of cells on narrow migration tracks. On narrow micro-tracks membrane blebs were observed as a dynamic reaction to the provided environment (mainly on 3 µm wide tracks but also on 10 µm wide tracks). This phenomenon was not observed on 20 µm and 30 µm wide tracks. As membrane blebbing is a reaction to low adhesiveness, the low directionality on thin tracks is likely a consequence of the frequent losses of polarization resulting in frequent changes in direction. These findings were underlined by the recovery of persistence after Blebbistatin treatment. An increased spreading area as well as a significantly higher directionality was observed for these cells [**Fig. 3.6E**]. Kymographic analysis showed that protrusion activity in cells on 3 µm wide tracks was much higher and uncoordinated compared to cells on 30 µm wide tracks [**Fig. 3.4E-F**]. This uncoordinated movement possibly plays a role in the frequent directional changes. Further, the uncoordinated protrusions of cells in 1D provide an indication that focal adhesion dynamics change in response to the 1D environment as it has been described for fibroblasts (Doyle et al. 2012). Further investigations need to be done and will provide more information about protrusion dynamics of ECs in restricted environments.

4.1.3 HUVECs migrating in 1D share morphological similarities with HUVECs migrating in 3D collagen I matrices

The major aim of this study was the comparison of migration behavior between ECs migrating on micro-tracks, with ECs migrating in fibrillary collagen I matrices, and ECs migrating in the classical 2D cell culture system. The most striking similarities were the absence of cytosolic stress fibers and the presence of cells displaying membrane blebs in both 1D and 3D systems [**Fig. 3.7**]. The formation of membrane blebs will be discussed in more detail in section 4.1.5. We assume that stress fibers are not missing in the 3D setup

but built the pronounced cortical actin, a phenomenon that was also observed in the 1D system. Likewise, in 3D environments the g-actin to f-actin ratio in cell is altered in comparison to cells in the 2D system, as previously discussed before for cells in the 1D setting.

During this thesis additional approaches were made to compare cell architecture between 1D, 2D, and 3D systems. Preliminary results showed that Golgi orientation in 3D environments (data not shown) is comparable to the Golgi orientation of cells on 1D micro-structures [**Fig. 3.2**]. This underlines the data that direction of migration is not the essential factor for Golgi positioning in the cell. Taken together, HUVECs migrating in 1D and 3D systems have common characteristics regarding actin cytoskeleton, membrane blebs, and Golgi orientation

4.1.4 Impact of contractility in 2D, 1D, and 3D - Contractility as a fundamental regulator of cellular shape, adhesion, and persistence

Switching between different kinds of cell protrusions (lamellipodia and blebs) is thought to be favorable for cell motility as cells can migrate more efficiently through complex 3D environments (Friedl 2004; Friedl and Wolf 2010; Friedl et al. 2012). However, most of the studies focusing on bleb to lamellipodia transition use Walker 256 carcinosarcoma cells (Bergert et al. 2012), or dictyostelium (Yoshida and Soldati 2006). In ECs, the formation of membrane blebs has exclusively been described in the context of cell death or spreading to date (Norman et al. 2011). Beside cortical tension (Charras and Paluch 2008; Tinevez et al. 2009), loss of cellular adhesion has been discussed as a potential reason for membrane blebbing (Bergert et al. 2012). Moreover, the impact of membrane curvature has been shown to influence bleb formation in dictyostelium (Tyson et al. 2014). All these mentioned parameters could potentially play a role in the experiments of this study, as a reduced spreading area on narrow micro-tracks was observed [**Fig. 3.5C**] as well as a high membrane curvature which was proven by cross section profiles [**Fig. 3.7B**]. Here, membrane blebbing of ECs in 1D and 3D in phases of contraction and orientation was described [**Fig. 3.5; Fig. 3.6; Fig 3.9**]. Thus, at least in the 3D environment, the formation of membrane blebs is interpreted as a dynamic biological reaction to a non-homogenous environment. A summary of the complex connections between adhesion, contractility, persistence, velocity, and cellular shape in 1D, 2D, and 3D settings, based on the experiments in this study, are displayed in **Fig. 4.1**.

Single cell analysis in the 2D system revealed that cells move slightly faster but less persistent upon contractility inhibition with Blebbistatin (**Fig. 3.6D - E**). The low persistence observed in the experiments was caused by the loss of a single lamellipodium and the formation of uncontrolled protrusions in all directions [**Fig. 3.6C; Movie S5**]. Enhancement of contractility by Calyculin A caused a reduction of both velocity and persistence [**Fig. 3.6**], probably through the failure of an efficient coordination of the migration cycle. Cells displayed a more circular phenotype and had been immobile after

A

Migration in 2D (infinite environment)

contractility

cell spreading

low directionality
(low velocity)

high directionality
(medium velocity)

low directionality
(high velocity)

directionality
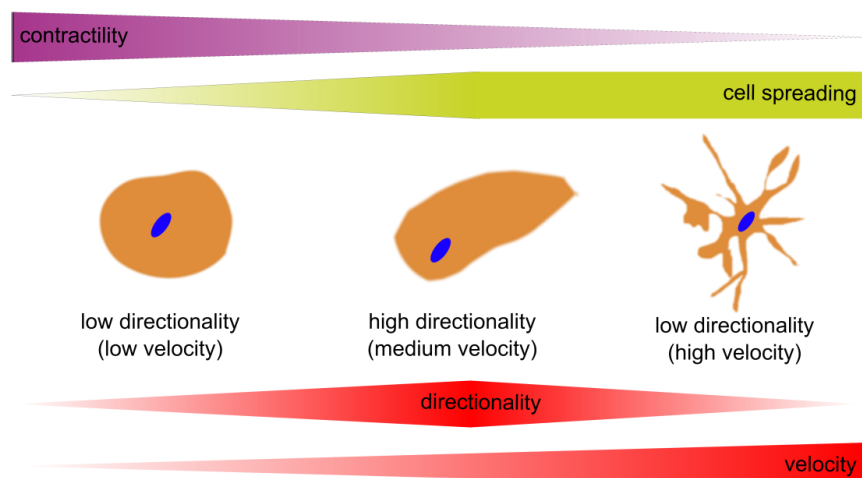
velocity

B

Migration in 1D and 3D (restricted environment)

contractility

cell spreading

immobile
(detachment from matrix)

low directionality
(medium velocity)

high directionality
(low velocity)

directionality
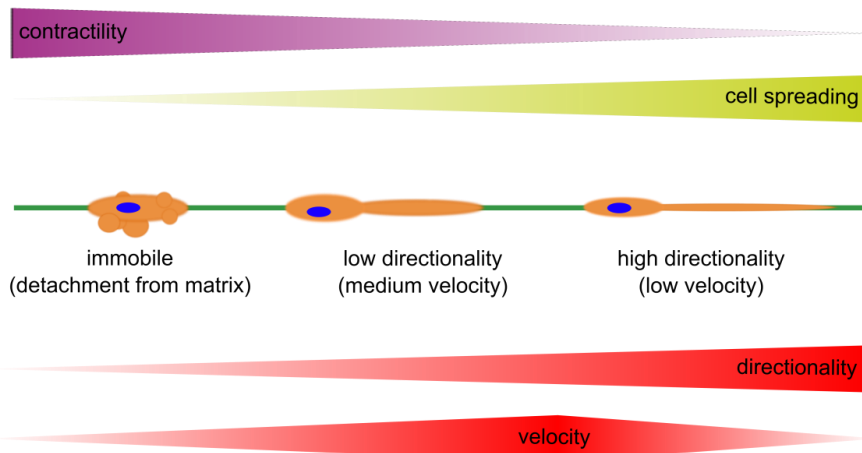
velocity

Fig. 4.1 Schematic overview of the connections between contractility, cell spreading, directionality, and velocity in infinite (2D) and restricted environments (1D and 3D). (**A**) Connection of migration parameters in 2D. The spreading area does not change with lower contractility. Cell shapes changes with the contractility level. (**B**) Connection of migration parameters in 1D and 3D. In contrast to 2D, cell spreading is enhanced with reduction of contractility and cells elongated strongly in both systems. In both 1D and 3D systems, rounded blebbing cells occur in high contractile states, which is in contrast to 2D.

Calyculin A stimulation. Treatment with higher concentrations of Calyculin A led to a loss of adhesion in the 2D system. In contrast Blebbistatin treatment did not affect adhesion in the 2D system [**Fig. 3.6G**]. This was in contrast to the 1D system and presumably likewise to the 3D system, where Blebbistatin lead to an increased adhesion area as discussed later. These observations allow the conclusion that the 2D system is infinite as contractility inhibition, and thus softening of the cell does not promote cell spreading [**Fig. 4.1A**]. Moreover, we concluded that velocity in 2D environments behaves inversely proportional to contractility, while directionality is diminished in both high and low contractile states [**Fig. 4.1A**].

Interestingly, the treatment with Blebbistatin of cells on 3 µm wide tracks influences the universal coupling between cell speed and persistence as described before (Maiuri et al. 2015), as both parameters are regulated separately [**Fig. 3.5**]. The increased persistence achieved with Blebbistatin treatment was associated with an increased spreading area in the 1D system (**Fig. 3.5E**). This allowed the classification of the 1D system as low adhesive (or not infinite) [**Fig. 4.1**]. The lower velocity in the 1D system upon Blebbistatin treatment is explained by inefficient trailing edge retraction or by changes in adhesion dynamics as described before for fibrillary environments (Doyle et al. 2012). To discriminate between these two possibilities, the effect of Blebbistatin on velocity has to be investigated further in future experiments. In contrast to the uncontrolled protrusions observed in 2D, 1D migrating cells elongated strongly upon Blebbistatin treatment [**Fig. 3.5F**]. The lack of lateral protrusions is caused by the lateral restriction which the cells face in the 1D setting. The massive cell elongation might have two different reasons: firstly, myosin II inhibition by Blebbistatin treatment makes the cell softer (Wakatsuki et al. 2003), leading to an increased spreading area and therefore to an elongated phenotype. Secondly, the decreased myosin II activity might inhibit the retraction of the cellular protrusions possibly leading to a disproportion of pushing forces (through actin polymerization) and retracting forces (contractility mediated) and thus resulting in elongated cell protrusions.

The Calyculin A treatment of cells migrating on 3 µm wide tracks caused a reduction of cellular adhesion, and thus an enhancement of blebbing [**Fig. 3.5**]. It was shown that cellular velocity is decreased after Calyculin A treatment in the 1D system, leading to the assumption that velocity is diminished in both high and low contractile states [**Fig. 4.1**]. Analysis of directionality in 1D showed only a slight trend of reduction after Calyculin A treatment, even though a high number of bleb harboring cells were observed in comparison to untreated cells [**Fig. 3.5F**]. However, a contractile response was induced, and cells which were highly contractile and thus low persistent might have been lost due

to loss of adhesion in these experiments [**Fig. 3.5**]. In line with the findings that reduction of track width and thus reduction of spreading area leads to diminished persistence in migration [**Fig. 3.4**], we conclude that directionality and adhesion of ECs is inversely proportional to contractility in the described 1D system. This observation is in contrast to the 2D environment [**Fig. 4.1B**].

ECs migrating in 3D switched between an elongated migration mode and a roundish bleb based orientation mode [**Fig. 3.9; Movie S7**]. Treatment with both Blebbistatin and Calyculin A revealed the same correlation between contractility and velocity/directionality as described for the 1D environment previously [**Fig. 4.1B**]. Treatment with Blebbistatin resulted in massive cell elongation, as seen for the 1D environment, concluding that the adhesion area likewise increases in the 3D setting [**Fig. 3.9F; Movie S8**]. Moreover, as no lateral protrusions were observed upon Blebbistatin treatment, we conclude that the 3D migration along collagen I fibers is laterally restricted, as described for the 1D setting. Cells treated with Blebbistatin moved slower but highly directed in the 3D environment. Based on the observations in 1D the increase of directionality upon contractility inhibition in 3D might be caused by two different factors. Firstly, the missing bleb-based reorientation and thus missing re-elongation along differently oriented fibers stabilizes the direction of migration. Secondly, the stabilization of a uni-axial phenotype by increased spreading and longer protrusions. The stabilization of a uniaxial phenotype is caused by the lateral restricted environment as described for the 1D setting. Likewise, also in the 3D setting an increased spreading area as well as a disproportion of pushing and retracting forces might be the reason for the cell elongation observed in the 3D setting. The decrease of velocity in 3D is probably caused by reduced trailing edge retraction as well as altered focal adhesion dynamics (Doyle et al. 2015). After treatment with Calyculin A, cells reacted with both diminished velocity and directionality. These effects are caused by massive switching to the round blebbing mode with permanent reorientation and adhesion to different fibers [**Fig. 3.9; Movie S9**]. Summed up, in 3D environments directionality and adhesion is inversely proportional to contractility as in the 1D system. In contrast to the observations made for cells migrating in the 2D system, cells moved slower in both high and low contractile states in 3D environments [**Fig 4.1B**].

4.1.5 Impact of microtubule and actin disruption on endothelial cell motility in 1D, 2D, and 3D systems

The inhibitors used in this study were Cytochalasin D, an actin disrupting agent, and the Ezrin inhibitor NSC668394 disrupting actin tethering to the membrane. Cells displayed a good response to both inhibitors in 2D as migration was inhibited in both scratch assays

and single cell experiments upon treatment [**Fig. 3.10**]. Likewise in 1D and 3D, migration was strongly inhibited, as mean velocities were significantly reduced in all settings upon treatment with both inhibitors [**Fig. 3.10; Fig. 3.11**]. These observations displayed the major role of the actin cytoskeleton for EC migration in all three systems. However slight differences were observed between the systems regarding the response of cells to compound treatment. While cells migrating in 2D and 3D responded to both inhibitors in the same way, cells migrating in 1D responded much stronger to the Ezrin inhibitor. This suggests that members of the Ezrin/Radixin/Moesin family (Tsukita and Yonemura 1999) play a pivotal role in migration in restricted environments.

In contrast to this, the microtubule disrupting agent Nocodazole displayed a different impact in 1D, 2D, and 3D settings. In 2D and 3D, mean velocity was significantly reduced [**Fig. 3.13; Fig. 3.14**], while mean velocity of 1D migrating cells was not influenced upon treatment [**Fig. 3.14**]. In the 2D system cells displayed a more rounded morphology and started to tumble after Nocodazole treatment, while cells in 3D failed to elongate along the collagen fibers. The observations for 3D are in line with another study (Doyle et al. 2009). As MTs pay a pivotal role in cell migration (Etienne-Manneville 2013), the cellular reactions in 2D and 3D are plausible. However, the reaction of 1D migrating cell upon MT disruption is less understood. It has been described that MT are responsible for cellular contractility (Kaverina and Straube 2011), and that MT disrupting agents cause a contractile response (Danowski 1989). This contractile response is provoked by the release of the RhoA activating factor GEF-H1 from MTs upon Nocodazole treatment (Chang et al. 2008), and potentially leads to loss of a high contractile cell population in the 1D setting directly after Nocodazole treatment due to loss of adhesion. The same is suspected for Calyculin A treatment. Indeed, cellular reactions of Nocodazole and the contractility inducing agent Calyculin A have been very similar. As the switch between blebbing and non-blebbing mode was found to be contractility-dependent (discussed in section 4.1.6), it would be interesting to know if Nocodazole also induces blebbing and reduces adhesion area in both 1D and 3D systems.

Likewise, it is conceivable that cells migrating in 1D are resistant to the specific concentration of Nocodazole used for 1D migration experiments. Further experiments need to be done using various concentrations of Nocodazole, as well as other MT disrupting agents in order to elucidate the role of MTs in 1D migration.

4.1.6 HUVEC migration is not diminished by Rac1 inhibition in 1D and 3D

Rac1 is an important regulator of cell motility as it is crucial for lamellipodial formation and actin reorganization in general (see section 2.3.1). The Rac1 inhibitor NSC23766 interferes with the binding of Rac1 to its GEFs Trio and Tiam1 (Gao et al. 2004), thereby inhibiting Rac1 activation. However, it has been shown that it does not interfere with Vav (Gao et al. 2004), a GEF which was shown to be activated upon VEGFR2 signaling in endothelial cells promoting Rac1 activation (Garrett et al. 2007). Likewise Trio and Tiam1 have been described as Rac1 regulating factors in endothelial cells (Birukova et al. 2007; Timmerman et al. 2015). Treatment with the Rac1 inhibitor NSC23766 led to completely different results in 1D, 2D and 3D as it inhibited cell migration only in the 2D setting [**Fig. 3.15; Fig. 3.16**]. It is possible that spatial restriction and the low adhesiveness in 1D and 3D led to different expression of the previous described GEFs. For example, a higher level of Vav2 and low levels of Trio and Tiam1 could have led to a cellular resistance towards the inhibitor as it only blocks interaction between Rac1 and Trio/Tiam1. Likewise it is conceivable that Rac1 plays a minor role for cells migrating in the 1D and 3D systems compared to cells migrating in the 2D system. However, the molecular mechanism underlying this observation has to be investigated to certainly explain the observed differences.

4.1.7 Summary– Is 1D migration a sufficient model for 3D migration and an advantage over 2D migration?

The major findings about 1D, 2D, and 3D migration obtained in this study are visually summarized in **Fig 4.2**. Taken together, the migration behavior of cells in 3D has a higher degree of similarity to the cell migration behavior in the 1D environment compared to the migration behavior of cells in the 2D environment. Thus the 1D migration system harbors an advantage over the classical cell culture systems as it displays *in vivo* more closely. HUVECs in all analyzed settings reacted similar to the disruption of the actin cytoskeleton and to inhibition of Ezrin, concluding that actin cytoskeleton integrity is of crucial importance in endothelial cell migration, despite the specific environments. MT disruption had no effect on cells in 1D, but a pronounced effect in 2D and 3D, respectively. Rac1 inhibition exclusively had an effect in the 2D system, but not in 1D and 3D respectively. In line with this, cells migrating in 1D showed a similar actin cytoskeleton morphology as cells migrating in 3D, which was in contrast to the cytoskeleton morphology displayed by cells migrating in 2D.
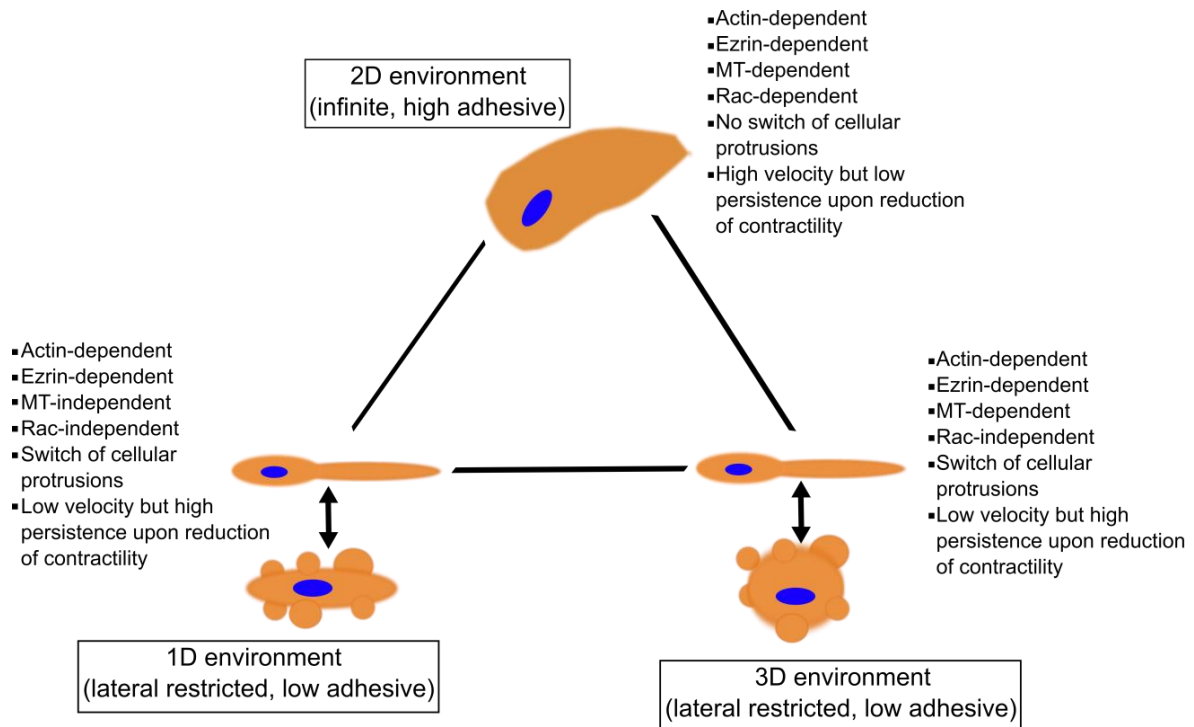
Fig. 4.2 Comprehensive comparison of cellular behavior in 1D, 2D, and 3D environments.
2D systems provide an infinite and highly adhesive environment while 1D and 3D systems provide a low adhesive and lateral restricted environment. While 2D migrating cells display a lamellipodium-based migration without switching protrusions, 1D and 3D migrating cells switch between a lamellipodium-based and a bleb-based morphology. The findings for all three settings are listed next to the schematics of the cellular morphologies. Nuclei are displayed in blue. Explanation of the observations can be found in the text.

The main differences in 1D and 3D systems compared to the 2D system upon changes in contractility were identified in both low and high contractile states. In high contractile states, the morphological transitions (switch of protrusions) in both 1D and 3D systems were the most prominent observation. No drastic differences of the migration parameters velocity and directionality were observed in comparison to the 2D setting [**Fig. 4.1**]. In contrast to this, Blebbistatin treatment and thus the reduction of contractility led to similar changes in migration parameter in 1D and 3D settings and an opposite effect in the 2D setting. This suggests, that studies using traditional 2D cell migration systems, might underestimate reactions of cells in low contractile states as the spreading area is infinite and not laterally restricted in contrast to 1D and 3D [**Fig. 4.1**]. Thus, the migration behavior on micro-tracks mimics the *in vivo* situation better, as it captures the whole dynamic range of morphological transitions, including migration behavior in low contractile states [**Fig. 4.2**].

The technical advantages of a 1D system over a 2D system are a great benefit for cell-based studies as the predictive value is higher for the *in vivo* situation, and thus facilitates the translation to animal experiments. Likewise the possibility to perform high-throughput assays (e.g. with automated tracking), the improved microscopy conditions compared to 3D, as well as the high reproducibility and versatility of this system are favorable for future cell-based studies.

4.1.8 Outlook – Future perspectives

This study paved the way for a reliable 3D migration model even though many unsolved questions remain and several possibilities of optimization exist. A good starting point for further experiments is the investigation of the resistance of 1D and 3D migrating cells towards the Rac1 inhibitor NSC23766. As this inhibitor disrupts the binding to GEFs and not to the effectors it will be interesting if the expression levels of Trio and Tiam1 change upon treatment. Rac1, as a central player in regulation of migration, is expected to be likewise important in 1D and 3D migration systems. However an experimental proof is still missing.

The putative resistance of migrating cells in 1D upon Nocodazole treatment might be due to a high contractile response as described in section 4.1.5. A differential experimental setup with a pre-incubation of the cells with a low concentration of Blebbistatin might counteract these reactions and the impact of microtubules on migration can be analyzed more reliably. However, it has to be taken into account that Blebbistatin influences both contractility and velocity, making it absolutely necessary to analyze both parameters in these experiments very carefully.

Blebbistatin treatment stabilizes the highly directed migration phenotype of cells migrating in the 1D and 3D systems. Quantitative kymographic analyses of cells treated with Blebbistatin will reveal underlying regulatory mechanisms e.g. the disproportion of pushing and retracting forces as proposed in section 4.1.4.

Another question which has not been addressed in this study is the dependency of migration on the ECM protein density on the protein tracks. Due to technical limitations, this parameter cannot be carefully controlled in micro-contact printing. However, this is achievable using other techniques like plasma-induced patterning (Hsieh et al. 2009), where protein concentrations at the surface can be directly influenced.

Another main difference between the current 1D and 3D migration model is the elasticity of the substrate. While the 1D migration experiments were performed on relatively rigid plastic surfaces, 3D migrating cells faced an elastic and deformable collagen environment. To date protein structures can be brought onto soft surfaces like polyacrylamide gels (Yu et al. 2012). This allows the imitation of the elastic environment of 3D systems and its combination with the lateral restriction and low adhesiveness provided by the micro-tracks. As cells spread less on soft substrates (Cui et al. 2015), the cellular reactions in regard to migration but also to morphological switching are of great interest.

Besides the experimental setups, there are some technical possibilities to enhance the model of 3D migration. 3 µm wide patterns were used as the thinnest migration tracks in this study. However, the technical limitation of micro-contact printing is in the range of 500 nm, which is similar to the width of a collagen fiber of the collagen I gels used in this study [**Fig. 3.8**]. A single track of 500 nm might be too less adhesive for cellular attachment, but a network of thin 500 nm tracks on a surface possibly imitates a collagen network very closely. This setup would provide great possibilities for cell migration analyses, for example the investigation of decision-making processes, depending of constraint and homogeneity of the environment.

4.2 Closing the gap between *in vivo* and *in silico* – A novel approach for tip cell formation studies

4.2.1 VEGFR2 expression patterns on structured surfaces match the theoretical background of tip cell formation

Tip cell formation is a process which is mainly dependent on cell-cell contacts (Blanco and Gerhardt 2013). The results of this study demonstrated that expression of VEGFR2, a prominent marker of tip cells is influenced by using micro-structured surfaces. Cells in the area providing a low number of cell-cell contacts, and especially in the branch of the structure displayed higher expression levels of VEGFR2 [**Fig. 3.19**], what is in line with the theoretical expectations for this approach [**Fig. 3.17**]. The differences in VEGFR2 expression levels were blocked with the use of the gamma-secretase inhibitor DBZ, diminishing Notch signaling [**Fig. 3.19**]. This implies that VEGFR2 regulation in our model system is Notch signaling-dependent which is in line with previous *in vivo* observations and modeling approaches *in silico*. However, other diverse factors might contribute to this phenomenon. First of all, cell-cell contacts affect cell proliferation of endothelial cells. The findings in the studies about contact mediated inhibition of proliferation are contradictive to each other, as some groups found an inhibiting effect on proliferation

(e.g. Grazia Lampugnani et al. 2003), while another found an stimulating effect by using micro-patterns (Gray et al. 2008). Notable in the work of Gray and colleagues is the investigation of cell-cell contacts without changing the adhesion area. As adhesion area also affects proliferation of cells (Pirone et al. 2006), this is an important aspect often neglected in comparative studies. The changes in proliferative activity might influence VEGFR2 expression levels, an aspect that has to be investigated further, especially as the effect of VEGFR2 receptor expression differed between day one and day seven of cell cultivation [**Fig. 3.18**]. Another study, where a similar approach with epithelial cells was investigated, postulated a strong influence of intercellular mechano-transduction on the expression patterns of epithelial-mesenchymal transition (EMT) markers (Gomez et al. 2010). This implies that mechanical differences in the inner and outer regions of the pattern potentially influence the expression patterns of VEGFR2 in the experiments of this study.

4.2.2 Outlook – Possible applications for the introduced system

As this system is in an early stage of development there are various possibilities for optimization and remaining open questions to answer. The advantages over current possibilities to investigate tip cell formation, like complex animal models, are enormous. The first step to make this model more straight forward, is the establishment of prospects for the live observations of gene expression. The current analysis of the data is time consuming as it is based on quantification of confocal images of immuno-stained cells. As HUVECs are primary cells, genetic manipulation is hardly feasible as they are short-living. Moreover, the use of immortalized HUVECs is problematic as it cannot be excluded whether they have lost endothelial-specific properties upon immortalization. A quick and easy approach of gene transcription analysis is currently under investigation in our laboratory, using the "Smart Flare®" technology in combination with micro-structured surfaces. This approach will enable the investigation of gene expression by a fluorescence-based microscopy method in a highly time-resolved manner.

The huge advantage of investigating tip cell formation on micro-structures is the versatility of the technique, allowing for manipulation of cellular behavior. First of all, the geometry of the micro-structures is variable, providing high control over cell-cell contact interface of single cells. Cells can be trapped in the branch with molecular ratchets as described before (Mahmud et al. 2009). Thus, persistence of the cells in the tip cell position is controllable. Moreover, other processes are addressable with this system. For example, in our laboratory it was shown that MRTF signaling in endothelial changes drastically with the amount of cell-cell contacts (Florian Gegenfurtner, AK Vollmar, unpublished data).

Other processes, like the epithelial-mesenchymal transition (EMT) are Notch signaling-dependent (Wang et al. 2010) and can be investigated closely with the help of the introduced micro-structures. As micro-structures provide a highly controllable setting, this model in combination with live observations of gene expression will provide a powerful tool to obtain highly time resolved data, allowing to draw conclusions about the *in vivo* situation, and to provide data needed for theoretical modeling approaches.

4.3 Conclusion - Models for angiogenesis on micro-structured surfaces

This study proves that micro-structured surfaces are useful to model certain angiogenesis related processes in a highly controlled manner. Beside the similarities between EC migration in 1D and 3D highlighted in this study, a novel approach for tip cell formation studies revealed promising results. This study leads the way to more sophisticated models for angiogenesis related processes in the future and provides a novel view on endothelial cell biology.

5. Material and Methods

5.1 Material

5.1.1 Primary cells

HUVECs (human umbilical vein endothelial cells) were purchased from PromoCell (Heidelberg, Germany). They are commonly used as primary model cells for the investigation of angiogenesis related processes (Crampton et al. 2007). In advance of every experiment, cells were checked for their morphology, contamination and overall condition with a transmitted light microscope.

5.1.2 Bacteria

Chemo-competent *Escherichia coli* cells

Strain	Genotype	Reference
DH5αF'	F'-, *end*A1, *hsd*R17 (rK-,mK+), *sup*E44,*thi*1-, *recA*-, λ-, *gyr*A96, *rel*A1	(Hanahan 1983)

5.1.3 Devices

Table 1: Devices

Device	Manufacturer (name and headquarters)
Blotting device	BioRad, Hercules, CA, USA
Cell counter Vi-Cell XR	Beckmann & Coulter, Brea, CA, USA
Cell Culture Incubator Hera Cell	Heraeus, Hanau, Germany
Centrifuge Megafuge	Thermo Scientific, Waltham, MA, USA
Centrifuge Mikro 220R	Hettich, Tuttlingen, Germany
Centrifuge Rotina R46	Hettich, Tuttlingen, Germany
Electrophorese chamber	BioRad, Hercules, CA, USA
Gel caster	BioRad, Hercules, CA, USA
Heating Block	Eppendorf, Hamburg, Germany
Heating Cabinet	Memmert, Schwabach, Germany

Incubation chamber microscope 1	Ibidi, Martinsried, Germany
Incubation chamber microscope 2	Okolab, Pozzuoli, Italy
Laminar Flow Hera Safe	Heraeus, Hanau, Germany
Laser writer ProtoLaser	LPKF, Tualatin, OR, USA
microscope incubation system 1	Ibidi, Martinsried, Germany
microscope incubation system 2	Okolab, Pozzuoli, Italy
Nano Drop	Thermo Scientific, Waltham, MA, USA
Photo Developer Curix 60	Afga, Mortsel, Belgium
Plate Reader	Tecan, Männedorf, Switzerland
Shaker Thermoshake (bacteria incubation)	Gerhardt, Königswinter, Germany
Shaker Vibrax (table top device)	Ika, Staufen, Germany
SP8 LSM confocal microscope	Leica, Wetzlar, Germany
Table Centrifuge Galaxy Mini	VWR, Radnor, PA, USA
Ti Eclipse wide-field microscope	Nikon, Tokio, Japan
UV/Ozone-Cleaner	Novascan, Ames, MA, USA
Water bath Haake C10	Thermo Scientific, Waltham, MA, USA

5.1.4 Chemicals and reagents

All chemical used in this study were obtained in the highest purity grade.

Table 2: Chemicals

Chemical	Manufacturer (name and headquarters)
Acrylamide/Bisacrylamide	Carl Roth, Karlsruhe, Germany
Beta-mercaptoethanol	Sigma-Aldrich, St. Louis, MO, USA
Blebbistatin (-/-)	Sigma-Aldrich, St. Louis, MO, USA
Blotto solution	Thermo Scientific, Waltham, MA, USA
Bovine serum albumin (BSA)	Sigma-Aldrich, St. Louis, MO, USA
Bradford reagent	BioRad, Heidelberg, Germany
Calyculin A	CalBiochem, San Diego, CA, USA
Collagen G	Biochrom AG, Berlin, Germany

Complete	Roche, Penzberg, Germany
Cytochalasin D	Sigma-Aldrich, St. Louis, MO, USA
Dimethylsulfoxide (DMSO)	Applichem, Darmstadt, Germany
ECL reagent	GE Lifesciences, Little Chalfont UK
EGTA	Applichem, Darmstadt, Germany
Ezrin Inh. NSC6683894	Merck, Darmstadt, Germany
Fibronectin	Dow Corning, New York, NY, USA
FluorSave mounting medium	CalBiochem, Darmstadt, Germany
Glutaraldehyde	Fluka Biochem, Taufkirchen, Germany
Glycin	Applichem, Darmstadt, Germany
Hoechst 33342	Sigma-Aldrich, St. Louis, MO, USA
Kanamycin	Sigma-Aldrich, St. Louis, MO, USA
LB Agar powder	Invitrogen, Carlsbad, CA, USA
Mr-Dev600	Micro resist technology, Berlin, Germany
$NaBH_4$	Fluka Biochem, Taufkirchen, Germany
Nocodazole	Sigma-Aldrich, St. Louis, MO, USA
Formaline	Applichem, Darmstadt, Germany
Polydimethylsiloxane (PDMS) Sylgard 184	Dow Corning, New York, NY, USA
Poly-L-lysine-(2)-polyethyleneglycol (PLL-(2)-PEG)	Surface Solutions, Dübendorf, Switzerland
Rac1 Inhibitor NSC23766	CalBiochem, Darmstadt, Germany
Rat tail collagen I	Ibidi, Martinsried, Germany
Rhodamine-phalloidin	Sigma-Aldrich, St. Louis, MO, USA
Sodium dodecyl sulfate (SDS)	Carl Roth, Karlsruhe, Germany
Sodium fluoride (NaF)	Merck, Darmstadt, Germany
Sodium orthovanadate (Na_3VO_4)	ICN, Biomedicals, Aurora, OH, USA
SU8 photo resist	MicroChem, Westborough, MA, USA
Tris base	Carl Roth, Karlsruhe, Germany
Tris hydrochloride	Carl Roth, Karlsruhe, Germany
Triton X-100	Sigma-Aldrich, St. Louis, MO, USA
Tween 20	Carl Roth, Karlsruhe, Germany

5.1.5 Composition of solutions and buffers

Table 3: Solutions and buffer composition

Solution/Buffer	Composition
Brinkley buffer 5X	1 mM $MgCl_2$, 1mM EGTA, 80mM PIPES
Cell extraction buffer	20 % Brinkley buffer, 80% ddH_2O, 4 mM EGTA, 0.5 % Triton X-100
Electrophoresis buffer 10x	250 mM Tris, 2M glycine, 10 % SDS
LB Agar	10 g/l Tryptone, 5 g/l NaCl, 5 g/l Yeast extract, 15 g/ml Agar
LB Medium	10 g/l Tryptone, 5 g/l NaCl, 5 g/l Yeast extract
Lysis Buffer	Tris/HCL 50 mM, NaCl 150 mM, 1 % Nonidet NP-40, 0.25 % sodium deoxycholate, 0.1 % SDS, 4 mM complete EDTA
PBS-T	PBS + 0.1% Tween 20
Phosphate buffered saline (PBS)	137 mM NaCl, 2.7 mM KCl, 10 mM Na_2KPO_4, 1,8 mM KH_2PO_4
Phosphate buffered saline with Ca^{2+}/Mg^{2+}	137 mM NaCl, 2.7 mM KCl, 10 mM Na_2KPO_4, 1,8 mM KH_2PO_4, 0.7 mM $CaCl_2$, 0.5 mM $MgCl_2$
Polyacrylamide gels separation gel 10 %	Acrylamamide/Bis 33 %, 375 mM Tris (pH 8.8), 0.1 % SDS, 0.1 %TEMED, 0.05 % APS
Polyacrylamide stacking gel	17 % Acrylamamide/Bis, 125 mM Tris (pH 6.8), 0.1 % SDS, 0.1 % TEMED, 0.05 % APS
SDS sample buffer 5x	20% glycerine, 10% SDS, 10% beta-mercaptoethanol, 0.05% bromphenolblue
Tank buffer 10x	250 mM Tris, 1.92 M glycine

5.1.6 Cell culture medium and components

Table 4: Cell culture media and components

Medium	Manufacturer (name and headquarters)
Amphotericin B	AppliChem, Darmstadt, Germany
DMEM	PAA, Pasching, Austria
Endothelial basal medium 10X (ECBM)	Promocell, Heidelberg, Germany
Endothelial basal medium 1X (ECBM)	Promocell, Heidelberg, Germany
Endothelium growth medium (ECGM)	Promocell, Heidelberg, Germany
Endothelium growth medium (ECGM)	Pelo, Planegg, Germany
Fetal calf serum (FCS)	PAA, Pasching, Austria
M199	PAA, Pasching, Austria
Penicillin/Streptomycin	PAN Biotech, Aidenbach, Germany
Trypsin/EDTA 10x	PAN Biotech, Aidenbach, Germany

5.1.7 Kits

Table 5: Kits

Software	Manufacturer (name and headquarters)
Plasmid preparation kit	Qiagen, Venlo, Netherlands
Protein labeling kit	Thermo Scientific, Waltham, MA, USA
Transfection kit HUVEC	Targeting systems, El Cajon, CA, USA

5.1.8 Antibodies

Table 6: Primary antibodies

Name/Target	Supplier	Used dilutions
Beta-tubulin	#2146 Cell Signaling, Danvers, MA, USA	1:200
Collagen I	#34710 Abcam, Cambridge, UK	1:200
Cortactin	#3503 Cell Signaling, Danvers, MA, USA	1:200
Fibronectin	#73611 Santa Cruz, Dallas, TX, USA	1:200
Gamma-tubulin	#6557 Sigma, St. Louis, MO, USA	1:7000
GM130	#12480 Cell Signaling, Danvers, MA, USA	1:200
Integrin beta 1	#8978 Santa Cruz, Dallas, TX, USA	1:200
NICD (Notch 1cleaved)	#4147 Cell Signaling, Danvers, MA, USA	1:200
Phospho-myosin light chain	#3674 Cell Signaling, Danvers, MA, USA	1:200
VE-Cadherin	#6458 Santa Cruz, Dallas, TX, USA	1:200
VEGFR2	#2479 Cell Signaling, Danvers, MA, USA	1:200

Table 7: Secondary antibodies

Name/Target	Supplier	Used dilutions
Goat anti-rabbit Alexa Fluor488	Invitrogen, Carlsbad, CA, USA	1:400
Goat anti-mouse Alexa Fluor488	Invitrogen, Carlsbad, CA, USA	1:400
Goat anti-rabbit Alexa Fluor680	Invitrogen, Carlsbad, CA, USA	1:400
Goat anti-mouse Alexa Fluor680	Invitrogen, Carlsbad, CA, USA	1:400

5.1.9 Plasmids

Table 8: Plasmids

Name	Reference/Supplier
Cortactin-GFP	Addgene #50728
LifeAct-RFP	Ibidi, Martinried, Germany

5.1.10 Software

Table 9: Software

Software	Origin
GraphPad Prism	GraphPad Software, La Jolla, CA, USA
ImageJ	Open Source
Inkscape	Open Source
LAS X	Leica, Wetzlar, Germany
MATLAB	MathWorks, Natick, MA, USA
NIS-Elements	Nikon, Tokio, Japan

5.2 Methods

5.2.1 Cell culture

5.2.1.1 Cultivation of cells

HUVECs were cultivated under sterile conditions with endothelial cell growth medium (ECGM) obtained from PromoCell or Pelo, supplemented with 1 % penicillin/streptavidin/amphotericin B and 10 % FCS. During this study medium suppliers were changed due to problems of proper cell growth and migration after using a new batch of medium. No changes in cellular behavior have been observed after changing the suppliers. For all experiments, cells were used in one of the passages #2 to #6.

Cells were incubated at constantly at 37 °C under 5 % CO_2 atmosphere. Prior to experiments and passaging, cells were covered with 1x trypsin/EDTA until cells detached. Subsequently, trypsin was inactivated by DMEM supplemented with 10 % fetal calf serum (FCS). Cells were pelleted by centrifugation at 1000 rpm for 5 min (RT). Subsequently the cell pellet was resuspended in ECGM and diluted to the desired cell concentrations for further usage in the various experimental procedures.

5.2.1.2 Cryo-conservation and thawing of cells

Spare HUVECs were frozen in liquid nitrogen and freshly thawed upon need. For cryo-conservation, cells were harvested as described above and diluted in freezing medium (20 % FCS, 10 % DMSO in M199) in a concentration of $2x10^6$ cells/ml. Subsequently, cell solution was transferred into cryo-vials and immediately stored into liquid nitrogen.

To thaw cells, cryo-vials containing the frozen cells were pre-warmed in a water bath to 37 °C and immediately transferred into ECGM, for incubation either in a 25 cm^2 or 75 cm^2 cell culture flask depending on the passage.

5.2.1.3 Cell counting

Cells were counted using a Beckman & Coulter ViCell cell counter. The amount of viable cells was taken for further calculation of desired cell concentrations in the different experimental setups.

5.2.2 Cell biological methods

5.2.2.1 Transient Transfection

HUVECs were seeded in a 6-well plate in a concentration of 0.25 x 10^6/well, 24 hours prior to transfection. For transfection routine, a HUVEC transfection kit (Targeting Systems, El Cajon, CA, USA) was used according to the manufacturers' protocol. The transfection master-mix contained 1.5 µg purified plasmid-DNA, 15 µl peptide enhancer, and 5 µl Targefect in 1 ml DMEM without supplements. The master mix was incubated for 25 minutes at 37 °C prior to transfection. Subsequently, cells were washed gently with pre-warmed PBS (+ Ca^{2+}, Mg^{2+}) twice, and transfection mix was added to the cell layer by pipetting. After 2 hours at 37 °C, the transfection mix was aspirated and cells were gently washed with pre-warmed PBS (+ Ca^{2+}, Mg^{2+}) twice. 16-20 hours after transfection, expression levels of transfected plasmid DNA were sufficient for further experimental procedures.

5.2.2.2 Migration experiments

5.2.2.2.1 Migration experiments on micro-patterns

Structured surfaces for migration experiments were manufactured as described in the soft lithography section (see section 5.2.3). To visualize and therefore to ensure a high printing quality, a mixture containing 40 µg/ml unlabeled fibronectin and 10 µg/ml labeled fibronectin was used for micro contact printing (µCP). Fibronectin was labeled as described in section 5.2.6.5. Cells were seeded at a density of 25 x 10^3 cells per well in 200 µl full growth medium. Subsequently cells were allowed to attach to the micro-patterns for 1.5 to 2 hours. Subsequently, cells were carefully washed with pre-warmed PBS (+ Ca^{2+}, Mg^{2+}) twice in order to remove unattached cells. All experiments were all performed in full growth medium. Prior to each experiment, fluorescence images were taken from all defined positions in order to ensure proper printing quality. Experiments were started 1 hour after treatment with the respective compound/inhibitor.

5.2.2.2.2 Migration experiments on 2D surfaces

2D migration experiments were performed using Ibidi chemotaxis slides without applying a chemotactic gradient or Ibidi 8-well slides. Cells were filled into the observation channel in a density of 3x10^6 cells/ml according to the manufactures instructions or seeded in an 8-well slide in a concentration of 25 x 10^3 cells/well in 200 µl endothelial full growth medium. After 2 hours, cells have been settled down and adhered to the surface and the channel was flushed twice with basal medium. Subsequently, both reservoirs were filled

with full growth medium supplemented with 10 % FCS. In the 8-well slides, cells were carefully washed with pre-warmed PBS (+ Ca^{2+}, Mg^{2+}) twice in order to remove unattached cells, before adding full growth medium. The experiment was started 1 hour after compound/inhibitor treatment.

5.2.2.2.3 Migration experiments in collagen I gels

3D migration experiments were performed using Ibidi chemotaxis slides without applying a chemotactic gradient. Cells were embedded in a Collagen I gel as described in the following. 60 µl of commercially obtained rat Tail collagen I (stock solution 5mg/ml) was mixed with 20 µl of 10x endothelial basal medium (BM). 112 µl ultrapure sterile water, 8 µl $NaHCO_3$ and 50 µl 1x endothelial basal medium. All solutions were constantly incubated on ice during the procedure. 18×10^6 cells/ml were mixed with the gel and filled into the observation channel according to manufactures instructions. For polymerization the gel was incubated at 37 °C, 5 % CO_2 for at least 30 minutes. Upon polymerization, both reservoirs were filled with full growth medium supplemented with 10 % FCS for all experiments. Experiments were started 2 hours after compound/inhibitor treatment, due to the longer diffusion time into the gel.

5.2.2.2 Compound/Inhibitor treatment

Inhibitor treatment of HUVECs was always performed without pre-incubation. Inhibitors were diluted to the desired stock concentrations according to the manufacturers' protocol. The calculation of stock solutions was adjusted for every compound to reach a final solvent concentration of 0.1 % to 0.5 % (DMSO or H_2O). Appropriate concentrations for each experiment were achieved by diluting the stock concentrations in endothelial full growth medium. For migration experiments in 8-well slides, 200 µl of full growth medium with the desired inhibitor concentration was applied to each well and experiments were started 1 hour later. For 3D experiments, both reservoirs were filled with ECGM containing the appropriate inhibitor concentration. 3D experiments were started 2 hours after treatment.

5.2.2.3 Scratch assay (Wound healing assay)

Scratch assays were performed in a 96-well plate format. Cells were seeded in a concentration of 0.45×10^6 cells/ml one day prior to the experiment, in order to achieve a confluent cell layer. After 24 hours, the scratch was applied in all 96 wells simultaneously

using a self-built device. Subsequently, cells were carefully washed with PBS ($+Mg^{2+}$, Ca^{2+}) twice and fresh medium was added, containing the respective compounds/inhibitors in various concentrations. Controls contained the respective DMSO concentrations. As an additional controls, starvation medium (pure DMEM) and pure ECGM medium without DMSO was applied to the cells. For each treatment, the scratch width of three individual wells was quantified after 16 hours of incubation according to a published protocol (Liang, Park, and Guan 2007).

5.2.3 Lithography

5.2.3.1 Master wafer production

Master wafer production of the intended micro patterns was prepared on silicone using photolithography under clean room conditions. An adhesion promoter (TI-Prime) was spin-coated onto a silicon wafer (Si-Mat), firstly by cebtrifugation at 500 rpm for 5 seconds and subsequently 5000 rpm for 30 seconds. Next, the wafer was heated for 2 minutes at 120°C on a hot plate. Subsequently, 15 µm thick layer of negative photoresist SU-8 100 was applied by spin-coating firstly at 500 rpm for 5 seconds and then accelerating the centrifugation speed to 2000 rpm for 35 seconds. After soft-baking the wafer at 65°C for 2 minutes and then at 95°C for 5 minutes, the wafer was exposed to UV-light (spectral lines at 365 nm, 405 nm, 436 nm) through a photo mask (purchased at Zitzmann GmbH) of the intended pattern. Alternatively, a laser lithography device was used to write the desired pattern directly into the photoresist. After exposure, an additional baking step was performed at 95 °C in order to selectively crosslink the UV-exposed portions of the resist. Subsequently, the wafer was placed in the developer solution mr-Dev 600 for approximately 2 minutes. To inhibit crack formation in the photoresist layer, the wafer was heated again for 5 minutes at 95 °C. Finally, the surface was silanized with per-fluoro-tri-chlorosilane by evaporation and then coated with PDMS as described in the next section.

5.2.3.2 Micro contact printing

Silicon masters were covered with Sylgard silicone elastomere 184 (=PDMS) in a 1:10 ratio, and PDMS (=poly dimethyl siloxane) was allowed to polymerize overnight at 60 °C after vacuum-based removal of air bubbles. PDMS stamps were cut out from the silicon wafer and treated in a PSD-UV ozone/UV-cleaner for 20 minutes. Subsequently, PDMS stamps were incubated in a protein solution containing 50 µg/ml fibronectin. After 2 hours of incubation, stamps were removed from the protein solution, washed twice with ultrapure

water, and left in laminar flow for drying. Eight to ten minutes later, stamps were completely dry and ready for further use. 8-well slides were pre-treated with UV/Ozone for 8 minutes and PDMS stamps were positioned into a well with the structured side facing the surface. For proper protein transfer, the stamp was left on the surface for 1 hour. Subsequently, the non-adhesive regions were passivated with 1 mg/ml PLL-(2)-PEG (Poly-L-lysine-(2)-poly ethylene glycol) diluted in PBS for 20 min. Before cell seeding, wells were washed twice with PBS in order to remove unbound PLL-(2)-PEG.

5.2.4 Immunofluorescence staining

5.2.4.1 Staining on surfaces

Immunofluorescence stainings in 1D and 2D settings were performed in identical experimental procedures. 20 hours after cell seeding, cells were washed twice with pre-warmed PBS. Subsequently, cells were fixated with 4 % pFA for 10 minutes. After an additional washing step with PBS, cells were permeabilized for 10 minutes using 0.2 % Triton X-100 in PBS. Prior to staining procedure, samples were blocked with 1 % BSA in PBS for 30 minutes. Subsequently, primary antibodies were added, diluted in PBS containing 1 % BSA. After incubation at 4 °C over night, samples were washed three times with PBS containing 0.2 % BSA. Then secondary antibodies, as well as 0.5 µg/ml Hoechst 33342 1:400 rhodamine-phalloidin were diluted in PBS + 0.2 % BSA and added to the wells. After 30 minutes, cells were washed three times with PBS + 0.2 % BSA for 5 minutes and covered with Save Flour Reagent and a coverslip.

5.2.4.2 Staining in Collagen I gels

HUVEC in Collagen I gels were fixed with 4 % pFA for 40 minutes and washed with PBS twice for 20 min each time. Subsequently, cells were permeabilized for 20 minutes using 0.5 % Triton X-100 in PBS. Then, samples were washed with PBS for 30 minutes and blocked with 1 % BSA in PBS overnight. Primary antibodies were diluted to the intended concentrations in PBS/1 % BSA. Staining solution was filled in both reservoirs and incubated at 4 °C for 72 hours. After incubation, samples were washed twice with PBS for 30 minutes and secondary antibodies were added in the appropriate concentrations for 48 hours. In general, applied primary and secondary antibody concentrations were twice as high as for 1D and 2D immuno-stainings Subsequently, gels were washed twice with PBS for 30 minutes and stained for 40 min with 0.5 µg/ml Hoechst 33342 and rhodamine-phalloidin, diluted 1:400 in PBS. Subsequently samples were washed again for

30 minutes with PBS. For immuno-stainings of collagen I in collagen gels, gels were fixed with 0.2 % glutaraldehyde instead of 4 % pFA

5.2.4.3 Tubulin washout

20 hours after seeding HUVECs in an 8-well slide, cells were washed twice with PBS (+ Ca^{2+}/Mg^{2+}). Monomeric tubulin was extracted by adding 270 µl cell extraction buffer into each well. After 10 seconds, samples were fixed by adding 0.5 % glutaraldehyde to the cell extraction buffer for 10 minutes. Subsequently, 270 µl of 0.1 % $NaBH_4$ solution was added for 7 min, in order to quench the auto-fluorescence of glutaraldehyde. Subsequent immune-staining was performed as described in section 5.2.4.1.

5.2.5 Microscopy

5.2.5.1 Laser scanning confocal microscopy

Laser scanning confocal microscopy was performed using a Leica SP8 LSM microscope. Pinhole size was at 1.0 airy unit for all experiments. The following excitation laser wave lengths were used: 405 nm, 488 nm, 561 nm, 647 nm. The detectors were individually adjusted to the specific spectrums of the fluorescence dyes. To avoid cross-talk between the channels only sequential scans of single channels were made in all experiments. In order to reduce background noise, an average of four frames was obtained for every channel. Scanning frequency was at 400 Hz for most of the experiments. For fast cellular processes scan frequency was set to 1400 Hz or to 7000 Hz (resonance scanner). Objectives used in this study: 63x oil, 40x oil, 63x water, 20x multi immersion, 10x air.

Images used for densitometry analysis, were recorded with a consistent resolution (usually 1024 x 1024 pixels), detector gain, laser intensity and zoom factor. Moreover, lasers were pre-warmed for at least 1 hour to avoid changes in signal intensity over time. To avoid information loss due to over exposure, images were checked for local signal intensities with false color transformation.

5.2.5.2 Wide field microscopy

Wide field microscopy was performed using a Nikon Ti Eclipse inverted microscope. Fluorescence microscopy was performed using preset excitation and extinction filter sets for the corresponding wavelength.

5.2.5.3 Live cell imaging

Live cell imaging with the LSM SP8 confocal microscope was performed using an Okolab bold line incubation system. For the Nikon Ti Eclipse, a complete incubation system from Ibidi was used. Cells were kept under 37 °C, 80 % humidity and 5 % CO_2 during the entire experiment.

5.2.6 Protein-biochemical methods

5.2.6.1 Preparation of lysates

24 hours after treatment, cells were washed once with ice-cold PBS. For 6 well plates, 180 µl of lysis buffer was added to each well and cells were frozen at -80 °C for at least 20 minutes. Lysates were thawed on ice and transferred into reaction tubes. Subsequently, lysates were centrifuged for 10 minutes at 4 °C and 14.000 rpm. 5 µl of the supernatant were used to determine the protein content with a Bradford protein assay. The residual samples were mixed with 5x sample buffer, and heated to 95 °C for 5 minutes. Samples were kept frozen at -20 °C until further usage.

5.2.6.2 Bradford assay

Bradford assay was performed in a 96-well plate format. Protein samples and BSA standards were mixed with 1x Bradford solution in triplicates and incubated on a shaker for 5 minutes. Subsequently, samples were measured using a plate reader and protein concentration of the samples was determined by extrapolation to a BSA standard solution.

5.2.6.3 SDS-PAGE

Prior to experiment, samples were adjusted to the same protein concentration using 1x sample buffer. SDS-PAGE (sodium dodecyl sulfate polyacrylamide gel electrophoresis) was performed using 10 % or 12 % polyacrylamide gels. 40 µl of each sample was loaded in the pockets of the gel and electrophoresis was performed in running buffer at a constant voltage of 100 V for 1 hour.

5.2.6.4 Western Blot analysis

Proteins were transferred using a wet blotting system. Nitrocellulose membranes were cut to adequate size and equilibrated in tank buffer for at least 20 minutes. Protein transfer was performed at 100 V for 1.5 hours. Subsequently, the membrane was blocked with

5 % Blotto for 2 hours at RT and primary antibodies were added at 4°C over night. After washing four times with PBS-T under agitation, HRP-coupled secondary antibodies were added and the membrane was incubated for 2 hours at RT. Unbound antibodies were removed by washing the membrane four times with PBS-T. Photo sensitive films were developed using an Agfa Curix 60 developer after 1 minute incubation with Amersham ECL reagent.

5.2.6.5 Protein labeling

Protein labeling of fibronectin was performed using an antibody labeling kit from pierce (DyLight488). A volume of 500 µl with a fibronectin concentration of 2 mg/ml (in H_2O supplemented with borate puffer obtained from the kit) was added to the vial containing the dye for 60 min under light exclusion. Subsequently, labeled proteins were purified according to the manufacturer's instructions. Finally, labeled protein concentration was determined using a Nano Drop device.

5.2.7 Molecular biological methods

5.2.7.1 E.coli cultivation

Escherichia coli bacteria were cultivated in liquid LB-Medium under strong agitation or on LB containing agar plate at 37 °C. For selection 50 µg/ml ampicillin or kanamycin was added depending on the bacterial resistance on the respective plasmid.

5.2.7.2 Transformation

100 µl of competent *E.coli* cells (DH5αF strain) were thawed on ice and mixed carefully with 0.5 – 1.5 µl DNA (depending on DNA concentration and quality). Bacteria were incubated on ice for 30 minutes and heat-shocked at 42 °C for 1 minute and 15 seconds. After an additional incubation time on ice for 2 min, bacteria were plated on LB plates (containing the respective antibiotics) and incubated at 37 °C overnight. On the next day a single colony was picked with a sterile pipette tip and transferred into LB-medium for plasmid preparation.

5.2.7.3 Plasmid preparation

Plasmid preparation was performed using a Quiagen Maxi Preparation Kit according to manufacturer` instructions. Final plasmid concentration was determined using a Nano Drop device.

5.2.8 Theoretical methods

5.2.8.1 Image and movie processing

Image and movie processing was performed using the open source software ImageJ or Fiji. Figures were made using the open source vector based graphic program Inkscape.

5.2.8.2 Statistical analysis

Statistical analysis was performed using GraphPad Prism.

5.2.8.3 Densitometry analysis

Densitometry analysis was performed using the open source software ImageJ. Images were converted into 8-bit greyscale images and pixel intensity was quantified using the measure tool. For comparison of different regions always a same sized region of interest was chosen.

5.2.8.4 Analysis of length and shapes

Measurement of length and shapes was performed using ImageJ or the Leica related program LAS X. In ImageJ, pixel size was adjusted using the information provided by the microscope associated programs LAS X or NIS-elements.

5.2.8.5 Analysis of mean velocity

Mean velocity of cell trajectories was determined using the open source software chemotaxis & migration tool from Ibidi according to the manufacturers' instructions. Pixel size information for coordinate transformation was taken from the microscope associated programs LAS X or NIS-elements.

5.2.8.6 Analysis of Directionality

Directionality of cell trajectories was determined using the open source software chemotaxis & migration tool from Ibidi according to the manufacturers' instructions. Pixel size information for coordinate transformation was taken from the microscope associated programs LAS X or NIS-elements.

5.2.8.7 Change point (bimodal) analysis of migration tracks

The bimodal analysis was performed in cooperation with Felix Segerer, Christoph Schreiber and Joachim Rädler of the physics department of the LMU Munich.

In order to evaluate the transition points between the two different migration regimes (run and rest states), we implemented an iterative change point analysis based on classical cumulative sum (CUSUM) statistics in combination with a motion classification via a fit on the mean squared displacement (MSD).

To this end, in order to find characteristic changes in the cellular motion pattern, we first calculated the CUSUM of the velocity $v(t)$ (i.e. the moving distance between two consecutive frames divided by the time period between two frames within a track) for each time *t* within a track.

$$S_t = \sum_{i=1}^{t} (v_i - \bar{v})$$

Here, $\bar{v}$ denotes the average velocity within the tracking interval t = 0,…,T. To evaluate whether a change point occurred within the interval, we estimate a confidence level for the change point existence via a bootstrap analysis. Therefore, we define the estimator for the magnitude of the change as

$$S_{diff} = (\max_{t=0,\ldots,T} S_t) - (\min_{t=0,\ldots,T} S_t)$$

which is calculated for the actually measured velocity CUSUM as well as for a set of bootstrapped CUSUMs where the consecutive order of $v_t : - \, t \in \{0, \ldots, T\}$ is permutated randomly. The confidence level for at least one change point occurrence within the interval is now calculated as:

$$L_{conf} = \frac{N_{(S_{diff} < S_{diff}^0)}}{N_{perm}}$$

Here $N_{(S_{diff} < S_{diff}^0)}$ denotes the number of bootstrap CUSUMs for which S_{diff} is smaller than the estimator of the original CUSUM S_{diff}^0 and N_{perm} denotes the total number of bootstrap samples. If not denoted otherwise, $N_{perm} = 10000$ was chosen. If L_{conf} is above a certain threshold level L_{th} we evaluated the position of the change point via the CUSUM estimator:

$$S_{CP} = \max_{t=0,\ldots,T} |S_t|$$

As a trade-off between accuracy and liability to small fluctuation in cell motion, $L_{th} = 0.7$ was chosen. If a change point was detected with confidence $L_{conf} > L_{th}$, this procedure was repeated iteratively for the two resulting intervals adjacent to the change point until no further change points with a confidence level $L_{conf} > L_{th}$ were detected.

In the next step, to determine if an interval is part of the running or resting period of a cell, the time averaged MSD was calculated for each interval between two consecutive change points via:

$$MSD(t) = \frac{1}{T - t + 1} \sum_{\tau=0}^{T-t} [\varphi(\tau + t) - \varphi(\tau)]^2$$

The MSD was now fitted by a fitting function $(t) = a \cdot t^b$, were the fitting exponent b indicates whether a motion pattern shows normal ($b = 1$) or anomalous diffusion ($b \neq 1$). Here, a value of $b = 2$ would correspond to ballistic motion. In order to dissect periods where the cells show directional persistent motion, a threshold of $b_{th} = 1.75$ was chosen, classifying all intervals where $b < b_{th}$ as non ballistic and therefore rest states and all intervals where $b > b_{th}$ as ballistic and consequently run state periods. Note that for very short intervals (*T*< 60min), were only a very limited set of data points is accessible, the fit of the MSD is not a very robust measure. Hence for such short intervals, the criterion such that if v_t is strictly increasing or decreasing within the interval was chosen, the interval was considered a run state, while it was considered a rest state if this condition is not met. Finally, all change points between two rest state periods or two run state periods going in the same direction were removed.

6. References

Abaci, Hasan Erbil, Yu-I Shen, Scott Tan, and Sharon Gerecht. 2014. "Recapitulating Physiological and Pathological Shear Stress and Oxygen to Model Vasculature in Health and Disease." *Scientific Reports* 4 (January). Nature Publishing Group: 4951. doi:10.1038/srep04951.

Arnaoutova, Irina, and Hynda K Kleinman. 2010. "In Vitro Angiogenesis: Endothelial Cell Tube Formation on Gelled Basement Membrane Extract." *Nature Protocols* 5 (4). Nature Publishing Group: 628–35. doi:10.1038/nprot.2010.6.

Arnold, Marco, Elisabetta Ada Cavalcanti-Adam, Roman Glass, Jacques Blümmel, Wolfgang Eck, Martin Kantlehner, Horst Kessler, and Joachim P Spatz. 2004. "Activation of Integrin Function by Nanopatterned Adhesive Interfaces." *Chemphyschem : A European Journal of Chemical Physics and Physical Chemistry* 5 (3): 383–88. doi:10.1002/cphc.200301014.

Artavanis-Tsakonas, S, M D Rand, and R J Lake. 1999. "Notch Signaling: Cell Fate Control and Signal Integration in Development." *Science (New York, N.Y.)* 284 (5415): 770–76. http://www.ncbi.nlm.nih.gov/pubmed/10221902.

Baker, Marianne, Stephen D Robinson, Tanguy Lechertier, Paul R Barber, Bernardo Tavora, Gabriela D'Amico, Dylan T Jones, Boris Vojnovic, and Kairbaan Hodivala-Dilke. 2012. "Use of the Mouse Aortic Ring Assay to Study Angiogenesis." *Nature Protocols* 7 (1). Nature Publishing Group, a division of Macmillan Publishers Limited. All Rights Reserved.: 89–104. doi:10.1038/nprot.2011.435.

Bentley, Katie, Giovanni Mariggi, Holger Gerhardt, and Paul A Bates. 2009. "Tipping the Balance: Robustness of Tip Cell Selection, Migration and Fusion in Angiogenesis." *PLoS Computational Biology* 5 (10): e1000549. doi:10.1371/journal.pcbi.1000549.

Bergert, M., S. D. Chandradoss, R. A. Desai, and E. Paluch. 2012. "Cell Mechanics Control Rapid Transitions between Blebs and Lamellipodia during Migration." *Proceedings of the National Academy of Sciences*. doi:10.1073/pnas.1207968109.

Birukova, Anna A, Irina Malyukova, Arsen Mikaelyan, Panfeng Fu, and Konstantin G Birukov. 2007. "Tiam1 and betaPIX Mediate Rac-Dependent Endothelial Barrier Protective Response to Oxidized Phospholipids." *Journal of Cellular Physiology* 211 (3): 608–17. doi:10.1002/jcp.20966.

Blanco, Raquel, and Holger Gerhardt. 2013. "VEGF and Notch in Tip and Stalk Cell Selection." *Cold Spring Harbor Perspectives in Medicine* 3 (1): a006569. doi:10.1101/cshperspect.a006569.

Burridge, Keith, and Renee Doughman. 2006. "Front and Back by Rho and Rac." *Nature Cell Biology* 8 (8). Nature Publishing Group: 781–82. doi:10.1038/ncb0806-781.

Carmeliet, P, and R K Jain. 2000. "Angiogenesis in Cancer and Other Diseases." *Nature* 407 (6801): 249–57. doi:10.1038/35025220.

Chang, Yuan-Chen, Perihan Nalbant, Jörg Birkenfeld, Zee-Fen Chang, and Gary M Bokoch. 2008. "GEF-H1 Couples Nocodazole-Induced Microtubule Disassembly to Cell Contractility via RhoA." *Molecular Biology of the Cell* 19 (5): 2147–53. doi:10.1091/mbc.E07-12-1269.

Charras, G. T., C.-K. Hu, M. Coughlin, and T. J. Mitchison. 2006. "Reassembly of Contractile Actin Cortex in Cell Blebs." *The Journal of Cell Biology* 175 (3): 477–90. doi:10.1083/jcb.200602085.

Charras, Guillaume, and Ewa Paluch. 2008. "Blebs Lead the Way: How to Migrate without Lamellipodia." *Nature Reviews. Molecular Cell Biology* 9 (9): 730–36. doi:10.1038/nrm2453.

Charras, Guillaume T, Justin C Yarrow, Mike A Horton, L Mahadevan, and T J Mitchison. 2005. "Non-Equilibration of Hydrostatic Pressure in Blebbing Cells." *Nature* 435 (7040). Macmillian Magazines Ltd.: 365–69. doi:10.1038/nature03550.

Chen, Bo, Girish Kumar, Carlos C Co, and Chia-Chi Ho. 2013. "Geometric Control of Cell Migration." *Scientific Reports* 3: 2827. doi:10.1038/srep02827.

Coleman, M L, E A Sahai, M Yeo, M Bosch, A Dewar, and M F Olson. 2001. "Membrane Blebbing during Apoptosis Results from Caspase-Mediated Activation of ROCK I." *Nature Cell Biology* 3 (4): 339–45. doi:10.1038/35070009.

Crampton, Steve P, Jaeger Davis, and Christopher C W Hughes. 2007. "Isolation of Human Umbilical Vein Endothelial Cells (HUVEC)." *Journal of Visualized Experiments : JoVE*, no. 3 (January): 183. doi:10.3791/183.

Cui, Yidan, Feroz M Hameed, Bo Yang, Kyunghee Lee, Catherine Qiurong Pan, Sungsu Park, and Michael Sheetz. 2015. "Cyclic Stretching of Soft Substrates Induces Spreading and Growth." *Nature Communications* 6 (January). Nature Publishing Group: 6333. doi:10.1038/ncomms7333.

D'Alessio, Alessio, Francesco Moccia, Jie-Hui Li, Alessandra Micera, and Themis R Kyriakides. 2015. "Angiogenesis and Vasculogenesis in Health and Disease." *BioMed Research International* 2015 (January): 126582. doi:10.1155/2015/126582.

Dahl, Kris Noel, Alexandre J S Ribeiro, and Jan Lammerding. 2008. "Nuclear Shape, Mechanics, and Mechanotransduction." *Circulation Research*. doi:10.1161/CIRCRESAHA.108.173989.

Danowski, B A. 1989. "Fibroblast Contractility and Actin Organization Are Stimulated by Microtubule Inhibitors." *Journal of Cell Science* 93 (Pt 2) (June): 255–66. http://www.ncbi.nlm.nih.gov/pubmed/2482296.

Davis, George E, and Donald R Senger. 2005. "Endothelial Extracellular Matrix: Biosynthesis, Remodeling, and Functions during Vascular Morphogenesis and Neovessel Stabilization." *Circulation Research* 97 (11): 1093–1107. doi:10.1161/01.RES.0000191547.64391.e3.

De Kreuk, Bart-Jan, Micha Nethe, Mar Fernandez-Borja, Eloise C Anthony, Paul J Hensbergen, Andre M Deelder, Markus Plomann, and Peter L Hordijk. 2011. "The F-BAR Domain Protein PACSIN2 Associates with Rac1 and Regulates Cell Spreading and Migration." *Journal of Cell Science* 124 (Pt 14): 2375–88. doi:10.1242/jcs.080630.

Del Toro, Raquel, Claudia Prahst, Thomas Mathivet, Geraldine Siegfried, Joshua S Kaminker, Bruno Larrivee, Christiane Breant, et al. 2010. "Identification and Functional Analysis of Endothelial Tip Cell-Enriched Genes." *Blood* 116 (19): 4025–33. doi:10.1182/blood-2010-02-270819.

Dike, L E, C S Chen, M Mrksich, J Tien, G M Whitesides, and D E Ingber. 1999. "Geometric Control of Switching between Growth, Apoptosis, and Differentiation during Angiogenesis Using Micropatterned Substrates." *In Vitro Cellular & Developmental Biology. Animal* 35 (8): 441–48. doi:10.1007/s11626-999-0050-4.

Djonov, V, M Schmid, S A Tschanz, and P H Burri. 2000. "Intussusceptive Angiogenesis: Its Role in Embryonic Vascular Network Formation." *Circulation Research* 86 (3): 286–92. doi:10.1161/01.RES.86.3.286.

Doggrell, Sheila A. 2005. "Pegaptanib: The First Antiangiogenic Agent Approved for Neovascular Macular Degeneration." *Expert Opinion on Pharmacotherapy* 6 (8): 1421–23. doi:10.1517/14656566.6.8.1421.

Donovan, D., N. J. Brown, E. T. Bishop, and C. E. Lewis. 2001. "Comparison of Three in Vitro Human 'Angiogenesis' Assays with Capillaries Formed in Vivo." *Angiogenesis* 4 (2): 113–21. doi:10.1023/A:1012218401036.

Doyle, A. D., M. L. Kutys, M. A. Conti, K. Matsumoto, R. S. Adelstein, and K. M. Yamada. 2012. "Micro-Environmental Control of Cell Migration - Myosin IIA Is Required for Efficient Migration in Fibrillar Environments through Control of Cell Adhesion Dynamics." *Journal of Cell Science*. doi:10.1242/jcs.098806.

Doyle, Andrew D., Nicole Carvajal, Albert Jin, Kazue Matsumoto, and Kenneth M. Yamada. 2015. "Local 3D Matrix Microenvironment Regulates Cell Migration through Spatiotemporal Dynamics of Contractility-Dependent Adhesions." *Nature Communications* 6 (November). Nature Publishing Group: 8720. doi:10.1038/ncomms9720.

Doyle, Andrew D., Francis W. Wang, Kazue Matsumoto, and Kenneth M. Yamada. 2009. "One-Dimensional Topography Underlies Three-Dimensional Fi Brillar Cell Migration." *Journal of Cell Biology* 184 (4): 481–90. doi:10.1083/jcb.200810041.

Dupin, Isabelle, Yasuhisa Sakamoto, and Sandrine Etienne-Manneville. 2011. "Cytoplasmic Intermediate Filaments Mediate Actin-Driven Positioning of the Nucleus." *Journal of Cell Science* 124 (Pt 6): 865–72. doi:10.1242/jcs.076356.

Edwards, D C, L C Sanders, G M Bokoch, and G N Gill. 1999. "Activation of LIM-Kinase by Pak1 Couples Rac/Cdc42 GTPase Signalling to Actin Cytoskeletal Dynamics." *Nature Cell Biology* 1 (5): 253–59. doi:10.1038/12963.

Etienne-Manneville, Sandrine. 2004. "Cdc42--the Centre of Polarity." *Journal of Cell Science* 117 (Pt 8): 1291–1300. doi:10.1242/jcs.01115.

Etienne-Manneville, Sandrine. 2013. "Microtubules in Cell Migration." *Annual Review of Cell and Developmental Biology* 29 (1). Annual Reviews: 471–99. doi:10.1146/annurev-cellbio-101011-155711.

Fackler, Oliver T, and Robert Grosse. 2008. "Cell Motility through Plasma Membrane Blebbing." *The Journal of Cell Biology* 181 (6): 879–84. doi:10.1083/jcb.200802081.

Folkman, J. 1971. "Tumor Angiogenesis: Therapeutic Implications." *The New England Journal of Medicine* 285 (21): 1182–86. doi:10.1056/NEJM197111182852108.

Folkman, J. 1995. "Angiogenesis in Cancer, Vascular, Rheumatoid and Other Disease." *Nature Medicine* 1 (1): 27–31. doi:10.1038/nm0195-27.

Friedl, Peter. 2004. "Prespecification and Plasticity: Shifting Mechanisms of Cell Migration." *Current Opinion in Cell Biology* 16 (1): 14–23. doi:10.1016/j.ceb.2003.11.001.

Friedl, Peter, Erik Sahai, Stephen Weiss, and Kenneth M. Yamada. 2012. "New Dimensions in Cell Migration." *Nature Reviews Molecular Cell Biology*. doi:10.1038/nrm3459.

Friedl, Peter, and Katarina Wolf. 2010. "Plasticity of Cell Migration: A Multiscale Tuning Model." *Journal of Cell Biology*. doi:10.1083/jcb.200909003.

Gagnon, Edith, Paola Cattaruzzi, May Griffith, Lea Muzakare, Katell LeFlao, Robert Faure, Richard Béliveau, Sabah N Hussain, Michael Koutsilieris, and Charles J Doillon. 2002. "Human Vascular Endothelial Cells with Extended Life Spans: In Vitro Cell Response, Protein Expression, and Angiogenesis." *Angiogenesis* 5 (1-2): 21–33. http://www.ncbi.nlm.nih.gov/pubmed/12549857.

Gao, Yuan, J Bradley Dickerson, Fukun Guo, Jie Zheng, and Yi Zheng. 2004. "Rational Design and Characterization of a Rac GTPase-Specific Small Molecule Inhibitor." *Proceedings of the National Academy of Sciences of the United States of America* 101 (20): 7618–23. doi:10.1073/pnas.0307512101.

Gardel, Margaret L, Benedikt Sabass, Lin Ji, Gaudenz Danuser, Ulrich S Schwarz, and Clare M Waterman. 2008. "Traction Stress in Focal Adhesions Correlates Biphasically with Actin Retrograde Flow Speed." *The Journal of Cell Biology* 183 (6): 999–1005. doi:10.1083/jcb.200810060.

Garrett, Tiana A, Jaap D Van Buul, and Keith Burridge. 2007. "VEGF-Induced Rac1 Activation in Endothelial Cells Is Regulated by the Guanine Nucleotide Exchange Factor Vav2." *Experimental Cell Research* 313 (15): 3285–97. doi:10.1016/j.yexcr.2007.05.027.

Gautreau, A, P Poullet, D Louvard, and M Arpin. 1999. "Ezrin, a Plasma Membrane-Microfilament Linker, Signals Cell Survival through the Phosphatidylinositol 3-kinase/Akt Pathway." *Proceedings of the National Academy of Sciences of the United States of America* 96 (13): 7300–7305. http://www.pubmedcentral.nih.gov/articlerender.fcgi?artid=22080&tool=pmcentrez&rendertype=abstract.

Gerhardt, Holger, Matthew Golding, Marcus Fruttiger, Christiana Ruhrberg, Andrea Lundkvist, Alexandra Abramsson, Michael Jeltsch, et al. 2003. "VEGF Guides Angiogenic Sprouting Utilizing Endothelial Tip Cell Filopodia." *The Journal of Cell Biology* 161 (6): 1163–77. doi:10.1083/jcb.200302047.

Glade-Bender, Julia, Jessica J Kandel, and Darrell J Yamashiro. 2003. "VEGF Blocking Therapy in the Treatment of Cancer." *Expert Opinion on Biological Therapy* 3 (2): 263–76. doi:10.1517/14712598.3.2.263.

Gomez, Esther W, Qike K Chen, Nikolce Gjorevski, and Celeste M Nelson. 2010. "Tissue Geometry Patterns Epithelial-Mesenchymal Transition via Intercellular Mechanotransduction." *Journal of Cellular Biochemistry* 110 (1): 44–51. doi:10.1002/jcb.22545.

Gray, Darren S, Wendy F Liu, Colette J Shen, Kiran Bhadriraju, Celeste M Nelson, and Christopher S Chen. 2008. "Engineering Amount of Cell-Cell Contact Demonstrates Biphasic Proliferative Regulation through RhoA and the Actin Cytoskeleton." *Experimental Cell Research* 314 (15): 2846–54. doi:10.1016/j.yexcr.2008.06.023.

Grazia Lampugnani, Maria, Adriana Zanetti, Monica Corada, Takamune Takahashi, Giovanna Balconi, Ferruccio Breviario, Fabrizio Orsenigo, et al. 2003. "Contact Inhibition of VEGF-Induced Proliferation Requires Vascular Endothelial Cadherin, Beta-Catenin, and the Phosphatase DEP-1/CD148." *The Journal of Cell Biology* 161 (4): 793–804. doi:10.1083/jcb.200209019.

Gridelli, C., P. Maione, F. Del Gaizo, G. Colantuoni, C. Guerriero, C. Ferrara, D. Nicolella, D. Comunale, A. De Vita, and A. Rossi. 2007. "Sorafenib and Sunitinib in the Treatment of Advanced Non-Small Cell Lung Cancer." *The Oncologist* 12 (2): 191–200. doi:10.1634/theoncologist.12-2-191.

Grossier, Jean-Philippe, Georgia Xouri, Bruno Goud, and Kristine Schauer. 2014. "Cell Adhesion Defines the Topology of Endocytosis and Signaling." *The EMBO Journal* 33 (1): 35–45. doi:10.1002/embj.201385284.

Guo, D Q, L W Wu, J D Dunbar, O N Ozes, L D Mayo, K M Kessler, J A Gustin, et al. 2000. "Tumor Necrosis Factor Employs a Protein-Tyrosine Phosphatase to Inhibit Activation of KDR and Vascular Endothelial Cell Growth Factor-Induced Endothelial Cell Proliferation." *The Journal of Biological Chemistry* 275 (15): 11216–21. http://www.ncbi.nlm.nih.gov/pubmed/10753929.

Hanahan, D. 1983. "Studies on Transformation of Escherichia Coli with Plasmids." *Journal of Molecular Biology* 166 (4): 557–80. doi:10.1016/S0022-2836(83)80284-8.

Heath, Robert J W, and Robert H Insall. 2008. "F-BAR Domains: Multifunctional Regulators of Membrane Curvature." *Journal of Cell Science* 121 (Pt 12): 1951–54. doi:10.1242/jcs.023895.

Higuchi, Maiko, Rina Kihara, Tomohiko Okazaki, Ichiro Aoki, Shiro Suetsugu, and Yukiko Gotoh. 2013. "Akt1 Promotes Focal Adhesion Disassembly and Cell Motility through Phosphorylation of FAK in Growth Factor-Stimulated Cells." *Journal of Cell Science* 126 (Pt 3): 745–55. doi:10.1242/jcs.112722.

Holmqvist, Kristina, Michael J Cross, Charlotte Rolny, Robert Hägerkvist, Nader Rahimi, Taro Matsumoto, Lena Claesson-Welsh, and Michael Welsh. 2004. "The Adaptor Protein Shb Binds to Tyrosine 1175 in Vascular Endothelial Growth Factor (VEGF) Receptor-2 and Regulates VEGF-Dependent Cellular Migration." *The Journal of Biological Chemistry* 279 (21): 22267–75. doi:10.1074/jbc.M312729200.

Hsieh, Shuchen, Yue-An Cheng, Chiung-Wen Hsieh, and YiLen Liu. 2009. "Plasma Induced Patterning of Polydimethylsiloxane Surfaces." *Materials Science and Engineering: B* 156 (1-3): 18–23. doi:10.1016/j.mseb.2008.10.036.

Huot, J., F. Houle, F. Marceau, and J. Landry. 1997. "Oxidative Stress Induced Actin Reorganization Mediated by the p38 Mitogen-Activated Protein Kinase/Heat Shock Protein 27 Pathway in Vascular Endothelial Cells." *Circulation Research* 80 (3): 383–92. doi:10.1161/01.RES.80.3.383.

Ishihara, H, H Ozaki, K Sato, M Hori, H Karaki, S Watabe, Y Kato, N Fusetani, K Hashimoto, and D Uemura. 1989. "Calcium-Independent Activation of Contractile Apparatus in Smooth Muscle by Calyculin-A." *The Journal of Pharmacology and Experimental Therapeutics* 250 (1): 388–96.

Jakobsson, Lars, Claudio A Franco, Katie Bentley, Russell T Collins, Bas Ponsioen, Irene M Aspalter, Ian Rosewell, et al. 2010. "Endothelial Cells Dynamically Compete for the Tip Cell Position during Angiogenic Sprouting." *Nature Cell Biology* 12 (10): 943–53. doi:10.1038/ncb2103.

James, Jane, Edgar D Goluch, Huan Hu, Chang Liu, and Milan Mrksich. 2008. "Subcellular Curvature at the Perimeter of Micropatterned Cells Influences Lamellipodial Distribution and Cell Polarity." *Cell Motility and the Cytoskeleton* 65 (11): 841–52. doi:10.1002/cm.20305.

Jiang, Xingyu, Derek A Bruzewicz, Amy P Wong, Matthieu Piel, and George M Whitesides. 2005. "Directing Cell Migration with Asymmetric Micropatterns." *Proceedings of the National Academy of Sciences of the United States of America* 102 (4): 975–78. doi:10.1073/pnas.0408954102.

Kaipainen, A, J Korhonen, T Mustonen, V W van Hinsbergh, G H Fang, D Dumont, M Breitman, and K Alitalo. 1995. "Expression of the Fms-like Tyrosine Kinase 4 Gene Becomes Restricted to Lymphatic Endothelium during Development." *Proceedings of the National Academy of Sciences of the United States of America* 92 (8): 3566–70. http://www.pubmedcentral.nih.gov/articlerender.fcgi?artid=42208&tool=pmcentrez&rendertype=abstract.

Kaverina, Irina, and Anne Straube. 2011. "Regulation of Cell Migration by Dynamic Microtubules." *Seminars in Cell & Developmental Biology* 22 (9): 968–74. doi:10.1016/j.semcdb.2011.09.017.

Kidoaki, Satoru, and Takehisa Matsuda. 2007. "Shape-Engineered Vascular Endothelial Cells: Nitric Oxide Production, Cell Elasticity, and Actin Cytoskeletal Features." *Journal of Biomedical Materials Research. Part A* 81 (3): 728–35. doi:10.1002/jbm.a.31112.

Kilian, Kristopher A, Branimir Bugarija, Bruce T Lahn, and Milan Mrksich. 2010. "Geometric Cues for Directing the Differentiation of Mesenchymal Stem Cells." *Proceedings of the National Academy of Sciences of the United States of America* 107 (11): 4872–77. doi:10.1073/pnas.0903269107.

Kitzing, Thomas M, Arul S Sahadevan, Dominique T Brandt, Helga Knieling, Sebastian Hannemann, Oliver T Fackler, Jörg Grosshans, and Robert Grosse. 2007. "Positive Feedback between Dia1, LARG, and RhoA Regulates Cell Morphology and Invasion." *Genes & Development* 21 (12): 1478–83. doi:10.1101/gad.424807.

Kovács, Mihály, Judit Tóth, Csaba Hetényi, András Málnási-Csizmadia, and James R. Seller. 2004. "Mechanism of Blebbistatin Inhibition of Myosin II." *Journal of Biological Chemistry* 279 (34): 35557–63. doi:10.1074/jbc.M405319200.

Kroll, J, and J Waltenberger. 1999. "A Novel Function of VEGF Receptor-2 (KDR): Rapid Release of Nitric Oxide in Response to VEGF-A Stimulation in Endothelial Cells." *Biochemical and Biophysical Research Communications* 265 (3): 636–39. doi:10.1006/bbrc.1999.1729.

Lamalice, Laurent, François Houle, and Jacques Huot. 2006. "Phosphorylation of Tyr1214 within VEGFR-2 Triggers the Recruitment of Nck and Activation of Fyn Leading to SAPK2/p38 Activation and Endothelial Cell Migration in Response to VEGF." *The Journal of Biological Chemistry* 281 (45): 34009–20. doi:10.1074/jbc.M603928200.

Lamalice, Laurent, François Houle, Guillaume Jourdan, and Jacques Huot. 2004. "Phosphorylation of Tyrosine 1214 on VEGFR2 Is Required for VEGF-Induced Activation of Cdc42 Upstream of SAPK2/p38." *Oncogene* 23 (2): 434–45. doi:10.1038/sj.onc.1207034.

Lamalice, Laurent, Fabrice Le Boeuf, and Jacques Huot. 2007. "Endothelial Cell Migration during Angiogenesis." *Circulation Research* 100 (6): 782–94. doi:10.1161/01.RES.0000259593.07661.1e.

Lämmermann, Tim, Bernhard L. Bader, Susan J. Monkley, Tim Worbs, Roland Wedlich-Söldner, Karin Hirsch, Markus Keller, et al. 2008. "Rapid Leukocyte Migration by Integrin-Independent Flowing and Squeezing." *Nature* 453 (7191): 51–55. doi:10.1038/nature06887.

Lampugnani, Maria Grazia, Fabrizio Orsenigo, Maria Cristina Gagliani, Carlo Tacchetti, and Elisabetta Dejana. 2006. "Vascular Endothelial Cadherin Controls VEGFR-2 Internalization and Signaling from Intracellular Compartments." *The Journal of Cell Biology* 174 (4): 593–604. doi:10.1083/jcb.200602080.

Le Boeuf, Fabrice, François Houle, and Jacques Huot. 2004. "Regulation of Vascular Endothelial Growth Factor Receptor 2-Mediated Phosphorylation of Focal Adhesion Kinase by Heat Shock Protein 90 and Src Kinase Activities." *The Journal of Biological Chemistry* 279 (37): 39175–85. doi:10.1074/jbc.M405493200.

Lei, Yifeng, Omar F. Zouani, Murielle Rémy, Cédric Ayela, and Marie Christine Durrieu. 2012. "Geometrical Microfeature Cues for Directing Tubulogenesis of Endothelial Cells." *PLoS ONE* 7 (7). doi:10.1371/journal.pone.0041163.

Li, S, S Bhatia, Y L Hu, Y T Shiu, Y S Li, S Usami, and S Chien. 2001. "Effects of Morphological Patterning on Endothelial Cell Migration." *Biorheology* 38 (2-3): 101–8. http://www.ncbi.nlm.nih.gov/pubmed/11381168.

Li, Song, Ngan F Huang, and Steven Hsu. 2005. "Mechanotransduction in Endothelial Cell Migration." *Journal of Cellular Biochemistry* 96 (6): 1110–26. doi:10.1002/jcb.20614.

Liang, Chun-Chi, Ann Y Park, and Jun-Lin Guan. 2007. "In Vitro Scratch Assay: A Convenient and Inexpensive Method for Analysis of Cell Migration in Vitro." *Nature Protocols* 2 (2): 329–33. doi:10.1038/nprot.2007.30.

Lin, Xiefan, and Brian P Helmke. 2009. "Cell Structure Controls Endothelial Cell Migration under Fluid Shear Stress." *Cellular and Molecular Bioengineering* 2 (2): 231–43. doi:10.1007/s12195-009-0060-z.

Madonna, Rosalinda, and Raffaele De Caterina. 2009. "VEGF Receptor Switching in Heart Development and Disease." *Cardiovascular Research* 84 (1): 4–6. doi:10.1093/cvr/cvp270.

Mahmud, Goher, Christopher J. Campbell, Kyle J. M. Bishop, Yulia A. Komarova, Oleg Chaga, Siowling Soh, Sabil Huda, Kristiana Kandere-Grzybowska, and Bartosz A. Grzybowski. 2009. "Directing Cell Motions on Micropatterned Ratchets." *Nature Physics* 5 (8). Nature Publishing Group: 606–12. doi:10.1038/nphys1306.

Maiuri, Paolo, Jean-François Rupprecht, Stefan Wieser, Verena Ruprecht, Olivier Bénichou, Nicolas Carpi, Mathieu Coppey, et al. 2015. "Actin Flows Mediate a Universal Coupling between Cell Speed and Cell Persistence." *Cell* 161 (2). Elsevier: 374–86. doi:10.1016/j.cell.2015.01.056.

Maiuri, Paolo, Emmanuel Terriac, Perrine Paul-Gilloteaux, Timothée Vignaud, Krista McNally, James Onuffer, Kurt Thorn, et al. 2012. "The First World Cell Race." *Current Biology*. doi:10.1016/j.cub.2012.07.052.

Makanya, Andrew N., Ruslan Hlushchuk, and Valentin G. Djonov. 2009. "Intussusceptive Angiogenesis and Its Role in Vascular Morphogenesis, Patterning, and Remodeling." *Angiogenesis* 12 (2): 113–23. doi:10.1007/s10456-009-9129-5.

Málnási-Csizmadia, András, and Mihály Kovács. 2010. "Emerging Complex Pathways of the Actomyosin Powerstroke." *Trends in Biochemical Sciences* 35 (12): 684–90. doi:10.1016/j.tibs.2010.07.012.

Maniatis, Nikolaos A, Viktor Brovkovych, Scott E Allen, Theresa A John, Ayesha N Shajahan, Chinnaswamy Tiruppathi, Stephen M Vogel, Randal A Skidgel, Asrar B Malik, and Richard D Minshall. 2006. "Novel Mechanism of Endothelial Nitric Oxide Synthase Activation Mediated by Caveolae Internalization in Endothelial Cells." *Circulation Research* 99 (8): 870–77. doi:10.1161/01.RES.0000245187.08026.47.

Mattila, Pieta K, and Pekka Lappalainen. 2008. "Filopodia: Molecular Architecture and Cellular Functions." *Nature Reviews. Molecular Cell Biology* 9 (6). Nature Publishing Group: 446–54. doi:10.1038/nrm2406.

Medjkane, Souhila, Cristina Perez-Sanchez, Cedric Gaggioli, Erik Sahai, and Richard Treisman. 2009. "Myocardin-Related Transcription Factors and SRF Are Required for Cytoskeletal Dynamics and Experimental Metastasis." *Nature Cell Biology* 11 (3): 257–68. doi:10.1038/ncb1833.

Morales-Ruiz, M, D Fulton, G Sowa, L R Languino, Y Fujio, K Walsh, and W C Sessa. 2000. "Vascular Endothelial Growth Factor-Stimulated Actin Reorganization and Migration of Endothelial Cells Is Regulated via the Serine/threonine Kinase Akt." *Circulation Research* 86 (8): 892–96. http://www.ncbi.nlm.nih.gov/pubmed/10785512.

Murrell, Michael, Patrick W Oakes, Martin Lenz, and Margaret L Gardel. 2015. "Forcing Cells into Shape: The Mechanics of Actomyosin Contractility." *Nature Reviews. Molecular Cell Biology* 16 (8): 486–98. doi:10.1038/nrm4012.

Nimnual, Anjaruwee S, Laura J Taylor, and Dafna Bar-Sagi. 2003. "Redox-Dependent Downregulation of Rho by Rac." *Nature Cell Biology* 5 (3). Nature Publishing Group: 236–41. doi:10.1038/ncb938.

Norman, Leann, Kheya Sengupta, and H. Aranda-Espinoza Helim. 2011. "Blebbing Dynamics during Endothelial Cell Spreading." *European Journal of Cell Biology* 90 (1): 37–48. doi:10.1016/j.ejcb.2010.09.013.

Ohta, Yasutaka, John H. Hartwig, and Thomas P. Stossel. 2006. "FilGAP, a Rho- and ROCK-Regulated GAP for Rac Binds Filamin A to Control Actin Remodelling." *Nature Cell Biology* 8 (8). Nature Publishing Group: 803–14. doi:10.1038/ncb1437.

Okochi, Norihiko, Takuya Okazaki, and Hideshi Hattori. 2009. "Encouraging Effect of Cadherin-Mediated Cell-Cell Junctions on Transfer Printing of Micropatterned Vascular Endothelial Cells." *Langmuir : The ACS Journal of Surfaces and Colloids* 25 (12): 6947–53. doi:10.1021/la9006668.

Olsson, Anna-Karin, Anna Dimberg, Johan Kreuger, and Lena Claesson-Welsh. 2006. "VEGF Receptor Signalling - in Control of Vascular Function." *Nature Reviews. Molecular Cell Biology* 7 (5): 359–71. doi:10.1038/nrm1911.

Ozerdem, U, K A Grako, K Dahlin-Huppe, E Monosov, and W B Stallcup. 2001. "NG2 Proteoglycan Is Expressed Exclusively by Mural Cells during Vascular Morphogenesis." *Developmental Dynamics : An Official Publication of the American Association of Anatomists* 222 (2): 218–27. doi:10.1002/dvdy.1200.

Pajerowski, J David, Kris Noel Dahl, Franklin L Zhong, Paul J Sammak, and Dennis E Discher. 2007. "Physical Plasticity of the Nucleus in Stem Cell Differentiation." *Proceedings of the National Academy of Sciences of the United States of America* 104 (40): 15619–24. doi:10.1073/pnas.0702576104.

Paluch, Ewa, Cécile Sykes, Jacques Prost, and Michel Bornens. 2006. "Dynamic Modes of the Cortical Actomyosin Gel during Cell Locomotion and Division." *Trends in Cell Biology* 16 (1). Elsevier: 5–10. doi:10.1016/j.tcb.2005.11.003.

Parsons, J Thomas, Alan Rick Horwitz, and Martin A Schwartz. 2010. "Cell Adhesion: Integrating Cytoskeletal Dynamics and Cellular Tension." *Nature Reviews. Molecular Cell Biology* 11 (9). Nature Publishing Group, a division of Macmillan Publishers Limited. All Rights Reserved.: 633–43. doi:10.1038/nrm2957.

Pelosi, Elvira, Germana Castelli, and Ugo Testa. 2014. "Endothelial Progenitors." *Blood Cells, Molecules, and Diseases*. doi:10.1016/j.bcmd.2013.11.004.

Phng, Li-Kun, Fabio Stanchi, and Holger Gerhardt. 2013. "Filopodia Are Dispensable for Endothelial Tip Cell Guidance." *Development (Cambridge, England)* 140 (19): 4031–40. doi:10.1242/dev.097352.

Pirone, Dana M, Wendy F Liu, Sami Alom Ruiz, Lin Gao, Srivatsan Raghavan, Christopher A Lemmon, Lewis H Romer, and Christopher S Chen. 2006. "An Inhibitory Role for FAK in Regulating Proliferation: A Link between Limited Adhesion and RhoA-ROCK Signaling." *The Journal of Cell Biology* 174 (2): 277–88. doi:10.1083/jcb.200510062.

Pouthas, François, Philippe Girard, Virginie Lecaudey, Thi Bach Nga Ly, Darren Gilmour, Christian Boulin, Rainer Pepperkok, and Emmanuel G Reynaud. 2008. "In Migrating Cells, the Golgi Complex and the Position of the Centrosome Depend on Geometrical Constraints of the Substratum." *Journal of Cell Science* 121 (Pt 14): 2406–14. doi:10.1242/jcs.026849.

Pugh, Christopher W, and Peter J Ratcliffe. 2003. "Regulation of Angiogenesis by Hypoxia: Role of the HIF System." *Nature Medicine* 9 (6): 677–84. doi:10.1038/nm0603-677.

Reinsch, S, and P Gönczy. 1998. "Mechanisms of Nuclear Positioning." *Journal of Cell Science* 111 (Pt 1 (August): 2283–95. http://www.ncbi.nlm.nih.gov/pubmed/9683624.

Ribatti, Domenico, and Enrico Crivellato. 2012. "'Sprouting Angiogenesis', a Reappraisal." *Developmental Biology* 372 (2): 157–65. doi:10.1016/j.ydbio.2012.09.018.

Riento, Kirsi, and Anne J Ridley. 2003. "Rocks: Multifunctional Kinases in Cell Behaviour." *Nature Reviews. Molecular Cell Biology* 4 (6): 446–56. doi:10.1038/nrm1128.

Roca-Cusachs, Pere, Jordi Alcaraz, Raimon Sunyer, Josep Samitier, Ramon Farré, and Daniel Navajas. 2008. "Micropatterning of Single Endothelial Cell Shape Reveals a Tight Coupling between Nuclear Volume in G1 and Proliferation." *Biophysical Journal* 94 (12): 4984–95. doi:10.1529/biophysj.107.116863.

Rolli, Claudio G, Hidekazu Nakayama, Kazuo Yamaguchi, Joachim P Spatz, Ralf Kemkemer, and Jun Nakanishi. 2012. "Switchable Adhesive Substrates: Revealing Geometry Dependence in Collective Cell Behavior." *Biomaterials* 33 (8): 2409–18. doi:10.1016/j.biomaterials.2011.12.012.

Ruprecht, Verena, Stefan Wieser, Andrew Callan-Jones, Michael Smutny, Hitoshi Morita, Keisuke Sako, Vanessa Barone, et al. 2015. "Cortical Contractility Triggers a Stochastic Switch to Fast Amoeboid Cell Motility." *Cell* 160 (4): 673–85. doi:10.1016/j.cell.2015.01.008.

Schliwa, M. 1982. "Action of Cytochalasin D on Cytoskeletal Networks." *The Journal of Cell Biology* 92 (1): 79–91. http://www.pubmedcentral.nih.gov/articlerender.fcgi?artid=2112008&tool=pmcentrez&rendertype=abstract.

Shao, Jianbo, Lei Wu, Jianzhang Wu, Yunhuan Zheng, Hui Zhao, Qinghui Jin, and Jianlong Zhao. 2009. "Integrated Microfluidic Chip for Endothelial Cells Culture and Analysis Exposed to a Pulsatile and Oscillatory Shear Stress." *Lab on a Chip* 9 (21): 3118–25. doi:10.1039/b909312e.

Sheetz, M P, D Felsenfeld, C G Galbraith, and D Choquet. 1999. "Cell Migration as a Five-Step Cycle." *Biochemical Society Symposium* 65 (January): 233–43. http://www.ncbi.nlm.nih.gov/pubmed/10320942.

Shen, Qiang, Robert R Rigor, Christopher D Pivetti, Mack H Wu, and Sarah Y Yuan. 2010. "Myosin Light Chain Kinase in Microvascular Endothelial Barrier Function." *Cardiovascular Research* 87 (2): 272–80. doi:10.1093/cvr/cvq144.

Siemerink, Martin J, Ingeborg Klaassen, Ilse M C Vogels, Arjan W Griffioen, Cornelis J F Van Noorden, and Reinier O Schlingemann. 2012. "CD34 Marks Angiogenic Tip Cells in Human Vascular Endothelial Cell Cultures." *Angiogenesis* 15 (1): 151–63. doi:10.1007/s10456-011-9251-z.

Sit, Soon-Tuck, and Ed Manser. 2011. "Rho GTPases and Their Role in Organizing the Actin Cytoskeleton." *Journal of Cell Science* 124 (Pt 5): 679–83. doi:10.1242/jcs.064964.

Spring, Herbert, Thomas Schüler, Bernd Arnold, Günter J Hämmerling, and Ruth Ganss. 2005. "Chemokines Direct Endothelial Progenitors into Tumor Neovessels." *Proceedings of the*

National Academy of Sciences of the United States of America 102 (50): 18111–16. doi:10.1073/pnas.0507158102.

Staton, Carolyn A, Malcolm W R Reed, and Nicola J Brown. 2009. "A Critical Analysis of Current in Vitro and in Vivo Angiogenesis Assays." *International Journal of Experimental Pathology* 90 (3): 195–221. doi:10.1111/j.1365-2613.2008.00633.x.

Strasser, Geraldine A, Joshua S Kaminker, and Marc Tessier-Lavigne. 2010. "Microarray Analysis of Retinal Endothelial Tip Cells Identifies CXCR4 as a Mediator of Tip Cell Morphology and Branching." *Blood* 115 (24): 5102–10. doi:10.1182/blood-2009-07-230284.

Takano, Kazunori, Kazunari Takano, Kiminori Toyooka, and Shiro Suetsugu. 2008. "EFC/F-BAR Proteins and the N-WASP-WIP Complex Induce Membrane Curvature-Dependent Actin Polymerization." *The EMBO Journal* 27 (21): 2817–28. doi:10.1038/emboj.2008.216.

Terranova, V P, R DiFlorio, R M Lyall, S Hic, R Friesel, and T Maciag. 1985. "Human Endothelial Cells Are Chemotactic to Endothelial Cell Growth Factor and Heparin." *The Journal of Cell Biology* 101 (6): 2330–34. http://www.pubmedcentral.nih.gov/articlerender.fcgi?artid=2114007&tool=pmcentrez&rendertype=abstract.

Théry, Manuel. 2010. "Micropatterning as a Tool to Decipher Cell Morphogenesis and Functions." *Journal of Cell Science* 123 (Pt 24): 4201–13. doi:10.1242/jcs.075150.

Théry, Manuel, Anne Pépin, Emilie Dressaire, Yong Chen, and Michel Bornens. 2006. "Cell Distribution of Stress Fibres in Response to the Geometry of the Adhesive Environment." *Cell Motility and the Cytoskeleton* 63 (6): 341–55. doi:10.1002/cm.20126.

Timmerman, Ilse, Niels Heemskerk, Jeffrey Kroon, Antje Schaefer, Jos van Rijssel, Mark Hoogenboezem, Jakobus van Unen, et al. 2015. "A Local VE-Cadherin and Trio-Based Signaling Complex Stabilizes Endothelial Junctions through Rac1." *Journal of Cell Science* 128 (16): 3041–54. doi:10.1242/jcs.168674.

Tinevez, Jean-Yves, Ulrike Schulze, Guillaume Salbreux, Julia Roensch, Jean-François Joanny, and Ewa Paluch. 2009. "Role of Cortical Tension in Bleb Growth." *Proceedings of the National Academy of Sciences of the United States of America* 106 (44): 18581–86. doi:10.1073/pnas.0903353106.

Tojkander, Sari, Gergana Gateva, and Pekka Lappalainen. 2012. "Actin Stress Fibers--Assembly, Dynamics and Biological Roles." *Journal of Cell Science* 125 (Pt 8): 1855–64. doi:10.1242/jcs.098087.

Tonnesen, M G, X Feng, and R A Clark. 2000. "Angiogenesis in Wound Healing." *The Journal of Investigative Dermatology. Symposium Proceedings / the Society for Investigative Dermatology, Inc. [and] European Society for Dermatological Research* 5 (1): 40–46. doi:10.1046/j.1087-0024.2000.00014.x.

Tsukita, S., and S. Yonemura. 1999. "Cortical Actin Organization: Lessons from ERM (Ezrin/Radixin/Moesin) Proteins." *Journal of Biological Chemistry* 274 (49): 34507–10. doi:10.1074/jbc.274.49.34507.

Tyson, R. A., E. Zatulovskiy, R. R. Kay, and T. Bretschneider. 2014. "How Blebs and Pseudopods Cooperate during Chemotaxis." *Proceedings of the National Academy of Sciences* 111 (32): 11703–8. doi:10.1073/pnas.1322291111.

Vartanian, Keri B, Michelle A Berny, Owen J T McCarty, Stephen R Hanson, and Monica T Hinds. 2010. "Cytoskeletal Structure Regulates Endothelial Cell Immunogenicity Independent of Fluid Shear Stress." *American Journal of Physiology. Cell Physiology* 298 (2): C333–41. doi:10.1152/ajpcell.00340.2009.

Vasquez, R J, B Howell, A M Yvon, P Wadsworth, and L Cassimeris. 1997. "Nanomolar Concentrations of Nocodazole Alter Microtubule Dynamic Instability in Vivo and in Vitro." *Molecular Biology of the Cell* 8 (6): 973–85. http://www.pubmedcentral.nih.gov/articlerender.fcgi?artid=305707&tool=pmcentrez&rendertype=abstract.

Versaevel, Marie, Thomas Grevesse, and Sylvain Gabriele. 2012. "Spatial Coordination between Cell and Nuclear Shape within Micropatterned Endothelial Cells." *Nature Communications* 3 (January): 671. doi:10.1038/ncomms1668.

Vicente-Manzanares, Miguel, Xuefei Ma, Robert S Adelstein, and Alan Rick Horwitz. 2009. "Non-Muscle Myosin II Takes Centre Stage in Cell Adhesion and Migration." *Nature Reviews. Molecular Cell Biology* 10 (11): 778–90. doi:10.1038/nrm2786.

Volkmann, N, K J Amann, S Stoilova-McPhie, C Egile, D C Winter, L Hazelwood, J E Heuser, R Li, T D Pollard, and D Hanein. 2001. "Structure of Arp2/3 Complex in Its Activated State and in Actin Filament Branch Junctions." *Science (New York, N.Y.)* 293 (5539): 2456–59. doi:10.1126/science.1063025.

Wakatsuki, Tetsuro, Robert B Wysolmerski, and Elliot L Elson. 2003. "Mechanics of Cell Spreading: Role of Myosin II." *Journal of Cell Science* 116 (Pt 8): 1617–25. http://www.ncbi.nlm.nih.gov/pubmed/12640045.

Wang, Zhiwei, Yiwei Li, Dejuan Kong, and Fazlul H Sarkar. 2010. "The Role of Notch Signaling Pathway in Epithelial-Mesenchymal Transition (EMT) during Development and Tumor Aggressiveness." *Current Drug Targets* 11 (6): 745–51. http://www.pubmedcentral.nih.gov/articlerender.fcgi?artid=3084452&tool=pmcentrez&rendertype=abstract.

Welch, Heidi C.E., W.John Coadwell, Len R. Stephens, and Phillip T. Hawkins. 2003. "Phosphoinositide 3-Kinase-Dependent Activation of Rac." *FEBS Letters* 546 (1): 93–97. doi:10.1016/S0014-5793(03)00454-X.

Willett, Christopher G, Yves Boucher, Emmanuelle di Tomaso, Dan G Duda, Lance L Munn, Ricky T Tong, Daniel C Chung, et al. 2004. *Direct Evidence That the VEGF-Specific Antibody Bevacizumab Has Antivascular Effects in Human Rectal Cancer. Nature Medicine*. Vol. 10. doi:10.1038/nm988.

Wolf, Katarina, Irina Mazo, Harry Leung, Katharina Engelke, Ulrich H von Andrian, Elena I Deryugina, Alex Y Strongin, Eva-B Bröcker, and Peter Friedl. 2003. "Compensation Mechanism in Tumor Cell Migration: Mesenchymal-Amoeboid Transition after Blocking of Pericellular Proteolysis." *The Journal of Cell Biology* 160 (2): 267–77. doi:10.1083/jcb.200209006.

Wolf, Katarina, Mariska Te Lindert, Marina Krause, Stephanie Alexander, Joost Te Riet, Amanda L Willis, Robert M Hoffman, Carl G Figdor, Stephen J Weiss, and Peter Friedl. 2013. "Physical Limits of Cell Migration: Control by ECM Space and Nuclear Deformation and Tuning by Proteolysis and Traction Force." *The Journal of Cell Biology* 201 (7): 1069–84. doi:10.1083/jcb.201210152.

Yang, J T, H Rayburn, and R O Hynes. 1993. "Embryonic Mesodermal Defects in Alpha 5 Integrin-Deficient Mice." *Development (Cambridge, England)* 119 (4): 1093–1105.

Yoshida, Kunito, and Thierry Soldati. 2006. "Dissection of Amoeboid Movement into Two Mechanically Distinct Modes." *Journal of Cell Science* 119 (Pt 18): 3833–44. doi:10.1242/jcs.03152.

Yu, Haiyang, Sijing Xiong, Chor Yong Tay, Wen Shing Leong, and Lay Poh Tan. 2012. "A Novel and Simple Microcontact Printing Technique for Tacky, Soft Substrates And/or Complex Surfaces in Soft Tissue Engineering." *Acta Biomaterialia* 8 (3): 1267–72. doi:10.1016/j.actbio.2011.09.006.

Yvon, Anne-Marie C, Jonathan W Walker, Barbara Danowski, Carey Fagerstrom, Alexey Khodjakov, and Patricia Wadsworth. 2002. "Centrosome Reorientation in Wound-Edge Cells Is Cell Type Specific." *Molecular Biology of the Cell* 13 (6): 1871–80. doi:10.1091/mbc.01-11-0539.

7. Appendix

7.1 Movie descriptions

Movies are on the compact disc attached to this thesis.

Movie S1 HUVEC migrating straight over a 3 µm wide micro-track without changing direction.

Movie S2 HUVEC migrating over a 3 µm wide micro-track, with frequent changes of directions. During contraction and reorientation, the cell starts to bleb at the whole cell body.

Movie S3 HUVEC on a 3 µm wide micro-track transfected with LifeAct-RFP (displayed in red) and Cortactin-GFP (displayed in green). Cell is in a lamellipodium-based migration mode without displaying membrane blebs.

Movie S4 HUVEC on a 3 µm wide micro-track transfected with LifeAct-RFP (displayed in red) and Cortactin-GFP (displayed in green). Cell is in a phase of contraction and reorientation and displays pronounced membrane blebs.

Movie S5 HUVEC migrating on a planar 2D, fibronectin coated plastic surface. Cell was treated with 10 µM Blebbistatin.

Movie S6 HUVECs migrating on a planar 2D, fibronectin coated plastic surface

Movie S7 HUVEC migrating in collagen gel switches between morphological modes.

Movie S8 HUVEC migrating in a collagen I gel after Blebbistatin treatment (10 µM).

MovieS9 HUVEC migrating in a collagen I gel after Calyculin A treatment (500 pM).

7.2 List of Figures

7.3 List of Tables

7.4 Abbreviations

µl	Microliter
µM	Micromolar
µm	Micrometer
1D	One dimensional
2D	Two dimensional
3D	Three Dimensional
ATP	Adenosine triphosphate
BSA	Bovine serum albumin
CAM	Chorio-allantoic membrane
CTRL	Control
Cyto D	Cytochalasin D
DBZ	Dibenzazepine
DLL4	Delta like ligand 4
DMSO	Dimethyl sulfoxide
DNA	Desoxy ribonucleotid acid
EC	Endothelial cell
ECBM	Endothelial basal medium
ECGM	Endothelial growth medium
ECM	Extracellular matrix
ELC	Essential light chain
EMT	Epithelial mesenchymal transition
EPC	Endothelial progenitor cell
FCS	Fetal calf serum
GAF	GTPase activating protein
GEF	Guanine nucleotide exchange factor
HIF	Hypoxia inducible factor
HUVEC	Human umbilical vein endothelial cells
kDA	Kilo Dalton
LB	Lysogeny broth
M	Molar
MAPK	Mitogen activated protein kinase
ml	Milliliter
MLC	Myosin light chain
MLCK	Myosin light chain kinase
MLCP	Myosin light chain phosphatase

mM	Millimolar
MRTF	Myocardin related transcription factor
MT	Micotubule
NICD	Notch intracellular domain
nM	Nanomolar
nm	Nanometer
NO	Nitric oxide
Noco	Nocodazole
PBS	Phosphate buffered saline
PDMS	Poly dimethyl siloxane
pFA	Para formaldehyde
PKB	Protein kinase B
PLGF	Placenta growth factor
PLL-PEG	Poly-L-lysine poly ethylene glycol
pM	Pico molar
RLC	Regulatory light chain
ROCK	Rho associated kinase
Rpm	Rotations per minute
RT	Room temperature
SC	Stalk Cell
SDS	Sodium dodecyl sulfate
SEM	Standard error of the mean
Ser	Serin
siRNA	Short interference ribonucleotide acid
TC	Tip Cell
Thr	Threonin
VEGF	Vascular endothelial growth factor
VEGFR	Vascular endothelial growth factor receptor

7.5 Publications

Parts of this work are subject of the following publication (submitted):

<u>Morphological switching of endothelial cells on micro-tracks mimics aspects of 3D migration in collagen gels</u>

Simon L. Schuster[1], Felix J. Segerer[2], Kerstin Kick[1], Florian A. Gegenfurtner[1], Christoph Schreiber[2], Max Albert[2], Angelika M. Vollmar[1], Joachim O. Rädler[2] and Stefan Zahler[1]

[1]Department of Pharmacy, Pharmaceutical Biology, Ludwig-Maximilians-Universität, Butenandtstraße 5-13, D-81377 Munich, Germany

[2]Faculty of Physics and Center for NanoScience, Ludwig-Maximilians-Universität, Geschwister-Scholl-Platz 1, D-80539 Munich, Germany

In cooperation with Prof Joachim Rädler the following co-authorship was achieved during this work (submitted):

<u>A versatile method for fabrication of multifunctional micropatterns</u>

F. J. Segerer[1], P. J. F. Röttgermann[1], **S. Schuster**[2], A. Piera-Alberola[1], Stefan Zahler[2] and J. O. Rädler[1]

[1]*Faculty of Physics and Center for NanoScience Ludwig-Maximilians-Universität München, Geschwister-Scholl-Platz 1, D-80539 Munich, Germany*

[2]*Department of Pharmacy - Center for Drug Research, Pharmaceutical Biology, Ludwig-Maximilians-Universität München, Butenandtstr. 5-13, D-81377 Munich, Germany*

7.6 Poster presentations

International Physics of Living Systems Network, July 21 -24 2014 Munich Germany

Models for Angiogenesis on micro-structured surfaces

Simon L. Schuster [1], Kerstin Pflieger [1], Florian Gegenfurtner [1], Max Albert[2], Felix Segerer[2], Joachim Rädler[2], Angelika M. Vollmar [1] and Stefan Zahler [1]

[1]Department of Pharmacy, Pharmaceutical Biology, Ludwig-Maximilians-Universität, Butenandtstraße 5-13, D-81377 Munich, Germany

[2]Faculty of Physics and Center for NanoScience, Ludwig-Maximilians-Universität, Geschwister-Scholl-Platz 1, D-80539 Munich, Germany

Physics of Cancer, October 2 -5 2014, Leipzig, Germany

Models for Angiogenesis on micro-structured surfaces

Simon L. Schuster [1], Kerstin Pflieger [1], Florian Gegenfurtner [1], Max Albert[2], Felix Segerer[2], Joachim Rädler[2], Angelika M. Vollmar [1] and Stefan Zahler [1]

[1]Department of Pharmacy, Pharmaceutical Biology, Ludwig-Maximilians-Universität, Butenandtstraße 5-13, D-81377 Munich, Germany

[2]Faculty of Physics and Center for NanoScience, Ludwig-Maximilians-Universität, Geschwister-Scholl-Platz 1, D-80539 Munich, Germany

7.7 Scientific talks

SFB 1032 Retreat, February 24 – 25 2014, Frauenchiemsee, Germany

Artificial Angiogenesis – Set the Stage for new models

8. Acknowledgements

Ich danke Frau Prof. Dr. Angelika Vollmar und Herrn Prof. Dr. Stefan Zahler für die Möglichkeit an diesem vielseitigen Projekt zu arbeiten sowie für die fachliche Betreuung während meiner Promotion. Des Weiteren danke ich für die vielen Freiheiten bei der Gestaltung des Projektes und die Möglichkeit zur wissenschaftlichen Selbstverwirklichung während meiner Zeit in Ihrem Labor.

Zudem danke ich Herrn Prof. Dr. Joachim Rädler für die tolle wissenschaftliche Zusammenarbeit und die zahlreichen konstruktiven Diskussionen.

Ein besonderer Dank geht an alle Mitarbeiter des AK Vollmar, insbesondere Kerstin Kick, Florian Gegenfurtner und Jana Peliskova.

Den Mitarbeitern des Lehrstuhls für Physik, insbesondere Felix Segerer, Christoph Schreiber, Peter Röttgermann und Max Albert danke ich für zahlreichen anregenden Diskussionen und die fachliche Unterstützung.

Meinen Eltern sowie meinen Geschwistern danke ich für die moralische Unterstützung.

Meiner Liebe Carmen danke ich für ihre verständnisvolle Art, für ihr gutmütiges und liebevolles Wesen sowie für den Rückhalt in schwierigen Zeiten.